Title
Near-Field Based Communication and Electrical Systems

Author
Azad, Umar

Publication Date
2013

Peer reviewed|Thesis/dissertation

UNIVERSITY OF CALIFORNIA

Los Angeles

Near-Field Based Communication and Electrical Systems

A dissertation submitted in partial satisfaction of the

requirements for the degree Doctor of Philosophy

in Electrical Engineering

by

Umar Azad

2013

ABSTRACT OF THE DISSERTATION

Near-Field Based Communication and Electrical Systems

by

Umar Azad

Doctor of Philosophy in Electrical Engineering

University of California, Los Angeles, 2013

Professor Yuanxun Wang, Chair

A near-field power transfer equation for an inductively coupled near-field system is derived based on the equivalent circuit model of the coupled resonant loops. Experimental results show that the proposed near-field coupling equation is trustworthy as it correctly predicts the transferred power versus distance relationship for different values of loaded quality factors at the transmitter and the receiver.

Capacity performance of near-field communication (NFC) links is analyzed for noise limited and interference limited scenarios based on information theory. The analytical results provide guidelines for design of inductively coupled antenna systems as the power and capacity budget of the link is carried out. Examples of inductively coupled VLF NFC links are evaluated for different operating scenarios, demonstrating the efficacy and importance of the proposed near-field link budget.

However, in a conventional setup of inductively coupled NFC link, the power coupled through and the bandwidth must be traded off. Direct Antenna Modulation (DAM) is a feasible scheme to break this dilemma. With DAM utilized in NFC link, the power and bandwidth product limit in a high Q system can be circumvented because the non-linear/time-varying nature of the operation allows high speed modulations decoupled from the charging and discharging process of the high-Q resonator. In this work, the theory of NFC link with DAM on the transmitter is presented and validated with an experimental setup. Improvement in reception of the high-speed modulation information is observed in the experiment, implying that a superior capacity performance of a NFC link is achieved through DAM versus the traditional scheme.

The resonant coupling efficiency is limited by the product of the quality factors *Q*, of the transmitter and receiver and the coupling coefficient *k*. We observe that in order to achieve maximum efficiency, the ratio of the load-to-loss impedances at both the source and load should be equal to a prescribed value. This is the same condition that yields simultaneous impedance matching at source and load. The efficiency limit is then calculated for single transmitter and two uncoupled receivers. In that case, optimal efficiency is obtained when the load-to-loss impedance ratio is equal to the same prescribed value for all devices simultaneously. However, this condition does not provide for simultaneous matching at the source and loads, which turns out to be impossible. The analysis is then generalized for a single transmitter and N uncoupled receivers and we find that as the number of receivers increases, the total efficiency limit also increases. Finally, we present the efficiency limits and optimal conditions for a system consisting of single and multiple repeaters between transmitter and receiver, which have been shown previously to relay power to larger distances.

The dissertation of Umar Azad is approved

Tatsuo Itoh

Kung Yao

Troy Carter

Yuanxun Wang, Committee Chair

University of California, Los Angeles

2013

DEDICATION

To my family from where I draw my motivation. Without them, nothing is meaningful.

Table of Contents

ACKNOWLEDGEMENT

I would like to take this opportunity to express my gratitude to Professor Yuanxun Wang for his guidance, mentorship and support throughout my stay at UCLA. I would also like to thank Professor Tatsuo Itoh, Professor Kung Yao, and Professor Troy Carter for taking the time to serve on my dissertation committee.

VITA

2003 HSSC Pre-Engineering

Federal Board of Intermediate and Secondary Education (FBISE)

- 1st position out of 35,000 candidates
- Gold medal and Merit scholarship by FBISE
- Gold medal by F.G. Sirsyed College
- Academic distinction award by President of Pakistan

2007 B.E. Electrical Engineering

College of Electrical and Mechanical Engineering

National University of Sciences and Technology, Pakistan

- 23rd position out of 50,000 candidates in Admission test
- 2nd position holder in Electrical Engineering Department
- Scholarship every semester for scoring GPA above 3.5

2008 Research Engineer

Microwave Lab

College of Electrical and Mechanical Engineering, Pakistan

2010 M.S. Electrical Engineering

University of California, Los Angeles

- Departmental Fellowship for Winter and Spring 2009
- Dimitris N. Chorafas Foundation Award 2010

2011 Summer Antenna Design Intern

Sony Ericsson, Redwood City, California, USA

2012 Summer Intern at Standards Research Lab

Samsung Telecommunications, Richardson, Texas, USA

PUBLICATIONS AND PATENTS

Umar Azad, and Y.E. Wang, "Analysis and experimental results for an inductively coupled near-field power transmission system", *IEEE International Workshop on Antenna Technology (IWAT)*, pp 157-160, 5-7 March 2012.

Umar Azad, and Y.E. Wang, "Direct antenna modulation scheme for enhanced capacity performance of near-field communication link ", *IEEE International Workshop on Antenna Technology (IWAT)*, pp 88-91, 5-7 March 2012.

Umar Azad, H.C. Jing, and Y.E. Wang, "Link budget and capacity performance of inductively coupled resonant loops", *IEEE Transactions on Antennas and Propagation*, vol. 60, no. 5, pp 2453-2461, May 2012.

Umar Azad, and Y.E. Wang, "Capacity performance of an inductively coupled near-field communication link ", *IEEE International Symposium on Antennas and Propagation*, July 2012.

Umar Azad, and Y.E. Wang, "Impact of receiver coil misalignment on near-field communication system performance", *IEEE International Symposium on Antennas and Propagation*, July 2012.

Umar Azad, Ioannis Tzanidis, and Sridhar Rajagopal, "Method and apparatus for optimizing wireless power transfer efficiency in a network consisting of multiple transmitters, receivers and repeaters", *Provisional Patent,* Sept. 2012.

Umar Azad, and Ioannis Tzanidis, "Resonant coupling efficiency limits for multiple receivers in a wireless power transfer system", *accepted by IEEE International Symposium on Antennas and Propagation (APS),* 2013.

Umar Azad, and Y.E. Wang, "Transmitter configuration to improve resonant coupling efficiency of a wireless power transfer system consisting of misaligned coils", *accepted by IEEE International Symposium on Antennas and Propagation (APS)*, 2013.

Umar Azad, and Ioannis Tzanidis, "Resonant coupling efficiency limits for single and multiple receives in a wireless power transfer system", *submitted to IEEE Transactions on Antennas and Propagation.*

Umar Azad, and Y.E. Wang, "Improvement in capacity performance of NFC Link offered by direct antenna modulation scheme over traditional modulation scheme", *submitted to IEEE Transactions on Circuits and Systems.*

CHAPTER 1

Introduction

1.1 ADVANTAGES OF NEAR-FIELD BASED SYSTEMS

Inductively coupled near-field system is a short-range wireless technology which allows the devices to communicate through the coupling of magnetic field rather than the energy radiation-interception process in far-field based systems. The near-field system is a promising alternative to transmit information through challenging communication environments such as underground and underwater scenarios, where the propagation medium is no longer air but soil, rock and water. In such environments, traditional wireless communication techniques using electromagnetic waves suffer high path loss. However, these mediums cause little variation to attenuation rate of magnetic field in air since the magnetic permeabilities of each of these mediums are similar. Near-field systems offer advantages of low cost, high efficiency, and are not affected by large propagation delays, multipath propagation and fading. Furthermore a NFC system has better immunity to eavesdropping because of its low range, can provide short-range connectivity between mobile terminals and is less likely to interfere with other systems operating outside its operational range.

1.2 APPLICATION AREAS FOR NEAR-FIELD BASED SYSTEMS

Inductively coupled near-field based systems have been used or proposed in many application areas such as for wireless power transfer using self-resonant coils in the strongly

coupled regime over distances up to eight times the radius of the coils [1-2], contactless power and information transmission in drill machines and other professional tools subjected to rough working conditions like water and dust where it becomes essential to avoid electrical contacts as much as possible [3], telemetric powering of difficult-to-access sensor systems especially bio-medical implants and neural prosthetic implants offering advantages like no skin penetrating wires and absence of harmful materials which are often used in batteries [4-7], wireless-powered drug release system designed to deliver drug doses in a controlled manner over an extended time [8], a neuro-stimulus chip for retinal prosthetic device in which intraocular system receives data and wireless power transfer from extraocular system via telemetric inductive link [9], RFID allowing tagged items to be individually identified by a reader [10], health monitoring by allowing short range connectivity between health monitoring devices and mobile terminals due to advantages of low price and lesser probability to interfere with another RF system operating outside the operational range of the near-field system compared to other wireless technologies like bluetooth and IrDA [11], real time location system by exploiting the phase difference information between electric field and magnetic field in the near-field regime [12], inductively coupled electric highway system in which energy is electromagnetically transferred from powered roadway to moving vehicles [13], seamless coverage of littoral mine warfare operations in shallow water, surf and beach zones [14], and under-ground communications [15].

1.3 PREVIOUS WORK AND ORGANIZATION OF DISSERTATION

The inductively coupled near-field wireless power transfer (WPT) system consisting of a single transmitter and single receiver has been analyzed by various research groups. A power transfer efficiency (PTE) expression has been derived for an inductively coupled near-field

power transfer system using coupled-mode theory [1-2], and it is observed that resonance plays an essential role in power transfer mechanism and improves the efficiency over the case of inductively coupled non-resonant objects. A near-field power transfer equation is also proposed in [16] in which the path loss concept is introduced to incorporate different rates of path loss of the electromagnetic field in a near-field system. Experimental setups are used to find the optimum condition for wireless power transmission through resonant coupling and it is observed that maximum PTE is achieved in the presence of both the drive loop and the load loop in addition to the transmitter and receiver coil [17]. The voltage gain expression for a magnetically resonant wireless power transfer system consisting of a transmitter coil and drive loop, and receiver coil and load loop, is derived based on the equivalent circuit model [18-19] of the WPT system. It is observed that maximizing the coil's quality factor as well as the proper loading of drive and load loops can result in improved range and efficiency. In chapter 3 a simplified wireless system, consisting of transmitter and receiver coils connected via appropriate impedance matching network to source and load respectively, is analyzed to address how the properties of antennas and impedance terminations impact on the performance of such a system. This is achieved by deriving the power transfer relationship of inductively coupled resonant loops based on its equivalent circuit model. It leads to a concise formulation called near-field power transfer equation, which expresses the transferred power as a function of distance between the loops, dimension and intrinsic quality factors of the loops and terminating impedances at both the transmitter and the receiver. The results for both strong and weak coupling case have been reported in [20-22]. With insights gained from the near-field power transfer equation, a comprehensive discussion is carried out for both the strong coupling and the weak coupling cases, aiming for applications in wireless power transfer systems, and near-field communication

systems respectively. It is observed that in the strong coupling case, for a given distance, an optimal load termination condition exists which maximizes the power transfer efficiency. For the weak coupling case, the received power always reaches its maximum under the conjugate matching condition; it falls off inversely with the sixth power of the distance between the coils, and increases with improving the quality factor of the transmitting and receiving antenna. The experimental results in Chapter 3 validate the proposed near-field power transfer equation.

The received power increases with improving quality factors of the transmitting and receiving antennas in weakly coupled near-field communication (NFC) link. However, the benefit brought by the use of high quality factor coils to the capacity of a NFC system is limited as increasing quality factor eventually limits the bandwidth of the communication system. In general, a loaded quality factor other than the conjugate matching may provide the best tradeoff between the received power and communication bandwidth for the maximum capacity. The capacity performance of a NFC link is discussed in Chapter 4 based on Shannon's information theory [23] for both thermal noise and natural interference limited scenarios. A VLF/ULF NFC link in air is used as an example and its information capacity versus distance is analyzed with numerical simulations for different setups of impedance matching at frequencies 1kHz and 3kHz. The NFC link operates at VLF/ULF since attenuation in conductive media due to eddy currents is small at low frequencies. Antennas with diameters less than 2 meters that can fit easily on those platforms (sub-marines, air-crafts etc) are used. Power supply required is also affordable (less than 250 W for small aerial platforms). It concludes that there is an optimum loaded quality factor selection for both transmitting and receiving loops that results in the maximum capacity for a certain distance of communication for both noise and natural interference limited scenarios [24-25]. Compact Air-Air NFC link provides coverage of an area of one square miles and is

impossible to be intercepted beyond that range. Data rates higher than 1kbps are achieved within the coverage area.

Propagation model and link budget of a NFC system is presented in [26], propagation characteristics such as path loss, bit error rate, communication bandwidth and capacity of magneto-inductive communication channel versus distance are considered for wireless underground sensor networks [15,27] and underwater communication networks [28,29]. The ultimate performance index for any communication system is its capacity bound, which depends on both the received power and bandwidth according to Shannon's law [23]. The study of NFC link in Chapter 4 [22] concludes that the optimal capacity of the link requires a trade-off between the received power and bandwidth, due to the fact that coils with high quality factors increase the received power, but reduce the bandwidth of communication. In Chapter 5, it will be demonstrated that involving non-linear, time-varying operation in a NFC transmitter can achieve capacity performance beyond the conventional limit resulting from the above trade-off. The so-called direct antenna modulation scheme (DAM) technique has been envisioned for efficient radiation of broadband pulses through high-Q electrically small dipole antennas [30-33]. The bandwidth of high-Q antennas is often limited due to the great amount of reactive energy stored inside the antenna or in the adjacent area of the antenna, which needs to be charged and discharged along with the modulation. The essential concept of DAM is to change the path of the current flow in real time so that the current through the antenna can be modulated in a switching mode, independent of the stored energy in the antenna. In addition, the stored energy is preserved approximately as a constant while the modulation is performed at a faster speed than what is allowed in the conventional linear mode. If the switching timing is selected properly, broadband, efficient transmission of digitally modulated data can be achieved. Chapter 5 presents a discussion

on the conventional capacity performance of an inductively coupled NFC link and how to improve the capacity performance through the DAM scheme. Then the transient behavior of the transmitter and receiver resonators is analyzed to prove that DAM offers broadband transmission capability no longer under the limit set by the antenna quality factor. Finally, the experimental results are presented to validate the proposed theory.

High power transfer efficiency is desired in inductively coupled NFC links [1-15] in order to minimize the transmitted power and thus the interference with other electronic devices in the vicinity, keep electric and magnetic fields within human exposure safety limits [34-35] and avoid excessive heat generation at the transmitter. It was recently shown that there exists an upper bound on the resonant coupling efficiency (RCE) (hereinafter simply referred to as "efficiency") calculated for a wireless power transfer system consisting of a single transmitter and receiver using the coupled mode theory [1-2], equivalent circuit model [18,36], and Z-parameters describing the interaction between two small antennas in terms of TE10/TM10 spherical modes [37]. Previously, the condition for optimum efficiency was derived for the load impedance only [18,38-43]. It was observed that impedance matching is important to achieve optimum efficiency. However, a critical aspect of wireless power transfer system design is the knowledge of the optimal source and load impedances that lead to maximum efficiency, and their variation with coupling. This is useful for designing the impedance matching networks at source and load, assessing the impact on power amplifier efficiency (due to input impedance variations) at the transmitter. The scope of Chapter 6 is to present analytical expressions for the transmitter and receiver impedances that lead to maximum efficiency. That is given two or more resonators with specific quality factors and coupling coefficients between them, we predict the maximum achievable efficiency of the WPT system. First, we derive the efficiency limit for a 2-coil

configuration based on the equivalent circuit model. We observe that in order to achieve maximum efficiency, the ratio of the load-to-loss impedances at both the source (R_S/R_{L1}) and load (R_L/R_{L2}) should be equal to the same prescribed value. This turns out to be the same condition that yields simultaneous impedance matching at source and load. This RCE limit agrees well with that previously derived based on the coupled mode theory [1-2]. Then, we consider the more practical case of a single transmitter and two receivers. This case was also studied in [44], but analytical expressions for the source and load resistances to achieve optimal efficiency performance were not presented. It is observed that for a wireless power transfer system consisting of single transmitter and two receivers, impedance matching at the source and both loads, simultaneously, is not possible. The ratio of source-to-loss resistance (R_S/R_{L1}) is observed to be same as that of the loads to their respective coil losses i.e., (R_2/R_{L2}) and (R_3/R_{L3}). This analysis is generalized for a single transmitter and multiple non-coupled receivers.

In Chapter 7, the optimal source and load impedances that yield maximum efficiency are derived for a transmitter, receiver and a repeater (as well as N-repeaters), which can be used to relay power to longer distances [45].

The RCE depends on quality factor of coils and coupling between the coils. The quality factor of a coil placed on a PEC platform such as cell phone or laptop etc., drops effectively reducing RCE. The coupling between two coils placed on a PEC platform also decreases, further reducing RCE. The impact of a PEC platform on the RCE of a WPT system is studied in Chapter 8. Coupling between the coils is not only a function of dimension of the coils and distance between them, but it also depends on the relative orientation of the coils. The receiver coil in applications [1-15] needs not be perfectly aligned (co-axially aligned) with the transmitter coil, effectively reducing the coupling between coils, and therefore the RCE. Coils in the same plane

with their centers displaced are said to be laterally misaligned while coils with coinciding axis, whose planes are tilted to form an angle are said to be angularly misaligned. The coupling between any two circular conductors has been calculated by snow but the formulas are very complicated and there are problems about convergence of the series involved [46]. Mutual inductance values for laterally displaced coils have been computed and presented in graphical form for laterally misaligned coils in [47]. The coupling values are obtained in an analytical form for co-axial coils and coils with lateral and angular misalignment over the complete elliptic integrals of the first and second kind and Heuman's Lambda function [48-50], and for co-axial coils in terms of Bessel functions [51-52]. In Chapter 8, a simple expression for coupling coefficient is derived using the magnetic field expressions in the near-field of a small loop antenna. Special cases of perfectly aligned coils, axially placed angularly misaligned coils, laterally displaced coils, and co-planar laterally displaced coils are discussed. Finally, a transmitter configuration consisting of orthogonal coils is proposed to solve the problem of drop in RCE due to receiver coil misalignment.

CHAPTER 2

Near-Field versus Far-Field Power Transmission

2.1 HISTORY OF WIRELESS POWER TRANSFER

Power transmission by radio waves dates back to the early work of James Clerk Maxwell, who predicted that power could be transmitted from one point to another by electromagnetic waves (1873~1889) [53]. Heinrich Hertz experimentally demonstrated the electromagnetic wave propagation in free space [54]. Nikola Tesla endeavored to transmit power through space, and wrote in a letter to George Westinghouse in 1906, “The transmission of power without wires will very soon create an industrial revolution and such as the world has never seen before” [55]. He erected a 200 feet tall tower, as shown in Fig. 2.1, and wanted to use it for wirelessly transmitting not just signals but also useful amount of electrical power to such things as airships in flights and automobiles on the move. However, he failed because his efforts were decades ahead of the necessary technology (1899-1910) [56].

2.2 CLASSIFICATION OF WIRELESS POWER TRANSFER TECHNIQUES

Wireless power transfer techniques can be broadly classified into two categories

1. Far-field based power transfer.
    i. Directional far-field power transfer

ii. Omni-directional power transfer

2. Inductively coupled near-field based power transfer.

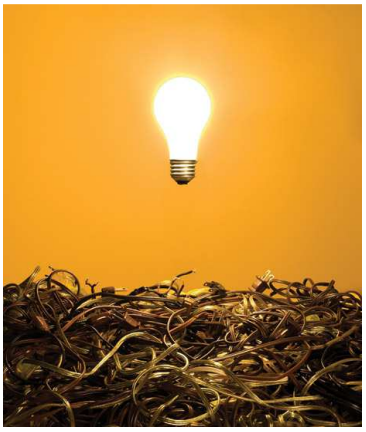

(a)

(b)

Fig 2.1 (a) Promise offered by wireless power transfer technology to cut the last wire
(b) Nikola Tesla planned to use this immense tower to transmit power wirelessly

2.2.1 Far-Field Based Power Transfer

The modern history of free-space power transmission evolved with the projects of developing microwave-powered aircraft and solar-powered satellites [57-58]. These projects used propagating electromagnetic waves to transfer energy in the same way as radio waves transmit signals. This far-field wireless power transmission (WPT) technique can be used to transfer wind energy from sea to land, solar energy from a desert area to an urban area, and to remotely power UAV (Unmanned air vehicle) etc., but it requires sophisticated tracking equipment and line-of-sight connection. Alternatively, RF broadcast methods, which transmit power with an omni-directional pattern, allow for power transmission anywhere in the coverage area. In this case the mobility is maintained, however, power density decreases with square of the distance implying a drop in power transfer efficiency (PTE), as the distance between transmitter and receiver increases.

The microwave-powered helicopter was successfully demonstrated in 1964 [57], as shown in Fig. 2.2.

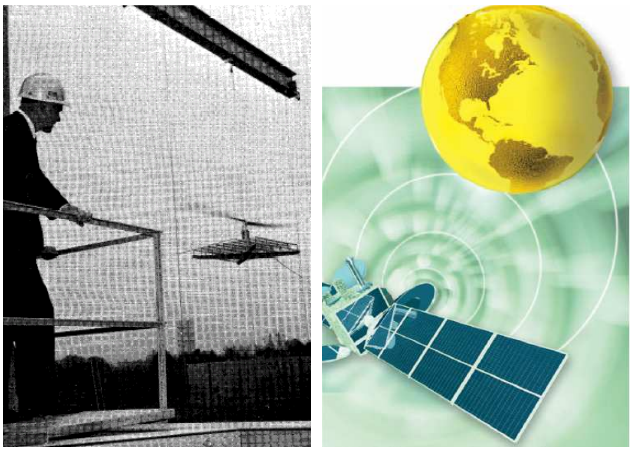

Fig 2.2 Microwave-powered helicopter and solar-powered satellite

2.2.2 Inductively Coupled Near-Field Based Power Transfer

Wireless power transfer can also be achieved by inductive coupling. Unlike the typical RF-links operating at distance of many wavelengths, near-field links usually operate at distances much smaller than the wavelength. The interest in inductively coupled WPT systems rejuvenated after a research group in MIT successfully transferred power over distance four times the radius of the coil [1-2] as shown in Fig. 2.3.

Fig 2.3 Intel's wireless power system (Left) inspired by MIT's (Right)

A practical wireless power transfer scenario involving multiple transmitters, receivers and repeaters is shown in Fig. 2.4. The transmitter coils are made large in order to have more coupling range. Orthogonal coils for transmitter are used to charge receivers with different orientations. Receiver coils are small in size since they have to fit inside the device e.g., cell phone or laptop. Due to small size of receiver coils, mutual coupling between them can be ignored. In this dissertation several interesting scenarios involving single transmitter and single receiver, single transmitter and multiple receivers, single and multiple repeaters between a transmitter and a receiver, and single transmitter consisting of orthogonal coils and a misaligned receiver coil are discussed.

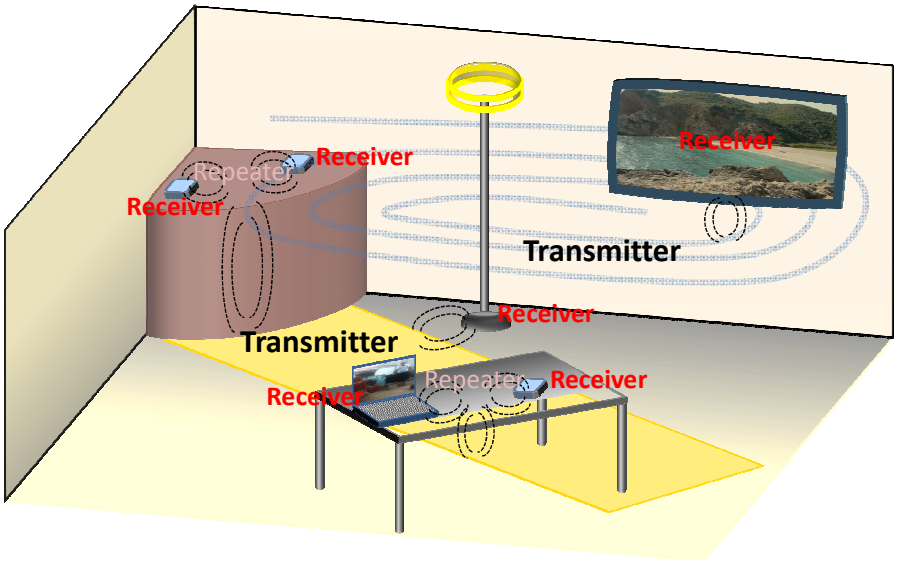

Fig. 2.4 An inductively coupled WPT system consisting of multiple transmitters, repeaters and receivers

2.3 NEAR-FIELD VERSUS FAR-FIELD

The electric and magnetic field components of an infinitesimal magnetic dipole of length l and constant magnetic current I_m at a distance r from it, as shown in Fig. 2.5, are given by [59]

$$E_r = E_\theta = H_\phi = 0 \tag{2-1}$$

$$E_{\phi} = -\frac{I_m l \beta^2}{4\pi} e^{-j\beta r}\left[\frac{j}{\beta r} + \frac{1}{(\beta r)^2}\right]\sin\theta \tag{2-2}$$

$$H_r = \frac{I_m l \beta^2}{2\pi\eta} e^{-j\beta r}\left[\frac{1}{(\beta r)^2} - \frac{j}{(\beta r)^3}\right]\cos\theta \tag{2-3}$$

$$H_{\theta} = \frac{I_m l \beta^2}{4\pi\eta} e^{-j\beta r}\left[\frac{j}{\beta r} + \frac{1}{(\beta r)^2} - \frac{j}{(\beta r)^3}\right]\sin\theta \tag{2-4}$$

where $\beta=2\pi/\lambda$ is the propagation constant, and η is the wave impedance. A magnetic dipole of magnetic moment $I_m l$ is equivalent to a small electric loop of radius a and constant electric current I_o such that

$$I_m l = jS\omega\mu I_o \tag{2-5}$$

where $S = \pi a^2$ is the area of the loop, μ is the permeability of medium and ω is the angular frequency.

Near-field of an antenna refers to distances r for which $\beta r << 1$, such that $\frac{1}{(\beta r)^3} >> \frac{1}{(\beta r)^2} >> \frac{1}{(\beta r)^1}$. Applying near-field approximation to (2-2), (2-3) and (2-4), it is observed that only the magnetic field exists in the near-field regime of an electrically small loop antenna, given by

$$H_r = \frac{(SI_o)}{2\pi}\left[\frac{1}{(r)^3}\right]\cos\theta \tag{2-6}$$

$$H_{\theta} = \frac{(SI_o)}{4\pi}\left[\frac{1}{(r)^3}\right]\sin\theta \tag{2-7}$$

The magnetic field carries the energy in near-field regime of a small loop antenna, unlike the far-field link in which energy is carried by an electromagnetic wave. Furthermore, the path loss in near-field regime is $\propto \frac{1}{r^6}$ compared to path loss $\propto \frac{1}{r^2}$ in the far-field.

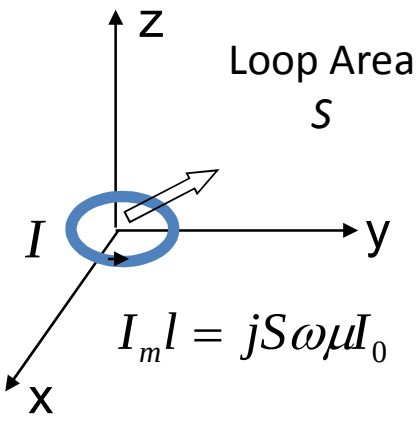

Fig. 2.5 An electrically small loop antenna

CHAPTER 3

An Inductively Coupled Power Transmission System – The Principle and Experimental Results

A near-field system consisting of inductively coupled resonant loops is shown in Fig.3.1 (a). Two circular coils, $coil_1$ and $coil_2$, of radii r_1 and r_2 are centered on a single axis at transmitter and receiver respectively and separated by a distance R. The coils consist of N_1 and N_2 closely wound turns and carry currents I_1 and I_2 respectively. As the dimension of coils and distance between the two coils under consideration are much smaller than the wavelength of the electromagnetic wave, magnetostatic approximations can thus be applied, which lead to the equivalent circuit model in Fig.3.1 (b). R_{L1} and R_{L2} are the resistances of the coils at the operating frequency and include the ohmic loss resistance, radiation resistance and other losses such as the absorption by the surroundings. L_1, L_2 are the self-inductances of the coils and C_1, C_2 are the capacitors to make the transmitter's and receiver's coil resonate at an identical frequency ω_o in order to create the maximum coupling sensitivity. R_S and R_L are the source and load impedances respectively.

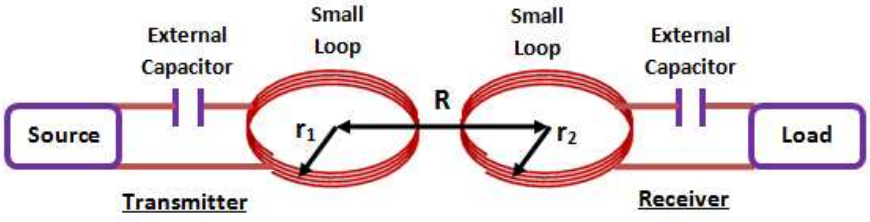

(a)

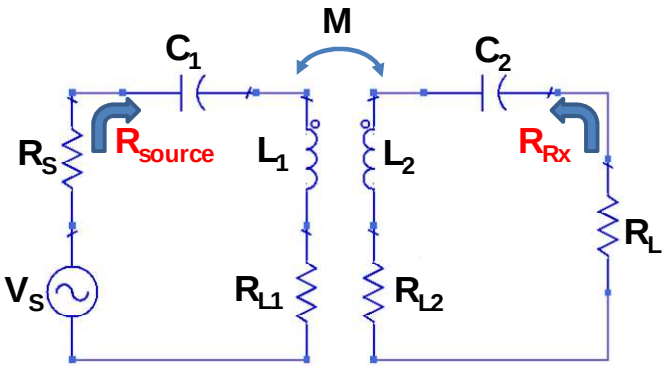

(b)

Fig 3.1 (a) Inductively coupled near-field communication system (b) Equivalent circuit model

3.1 SELF-INDUCTANCE, MUTUAL-INDUCTANCE AND COUPLING COEFFICIENT

Under the assumption of infinitesimal thickness of the coil, the property of inside homogeneous magnetic field in a solenoid is used as a coarse approximation to the field distribution of a loop antenna. The accuracy of these approximations is to be examined against COMSOL simulation results in Chapter 4. An analytical approach for calculating the self-inductance of planar multi-layer rectangular shaped coils is given in [60]. Curves have been plotted for mutual-inductance between coils with parallel planes for a variety of spacing between them in [47]. More accurate expressions for mutual impedance for various configurations, shapes of single-layer and multi-layer coils, laterally displaced coils, and angularly misaligned coils are given in [48,61-64].

The self-inductance of transmitter and receiver coils and the mutual-inductance between the two coils in free space (See Appendix) are given by

$$L_1 = \frac{\mu_o N_1^2 \pi r_1}{2} \quad , \quad L_2 = \frac{\mu_o N_2^2 \pi r_2}{2} \tag{3-1}$$

$$M = \begin{cases} \dfrac{\mu_o \pi N_1 N_2 \, r_1^{\,2} r_2^{\,2}}{2\left(\sqrt{R^2 + r_1^{\,2}}\right)^3}, & r_2 \le r_1 \\ \dfrac{\mu_o \pi N_1 N_2 \, r_1^{\,2} r_2^{\,2}}{2\left(\sqrt{R^2 + r_2^{\,2}}\right)^3}, & r_1 \le r_2 \end{cases} \tag{3-2}$$

For comparison, the exact expression for mutual-inductance given in [63] is

$$M = 2\mu_o \, p^{-1} (r_1 r_2)^{\frac{1}{2}} \left[\left(1 - \frac{1}{2} p^2\right) K - E \right] \tag{3-3}$$

where

$$p^2 = 4 r_1 r_2 \left[(r_1 + r_2)^2 + R^2 \right]^{-1} \tag{3-4}$$

K and *E* are the complete elliptic integrals of the first and the second kind.

Mutual-inductance between two coils having same radius (2 cm each) and different radius (2 cm and 10 cm) aligned along the same axis is evaluated for distance varying from 2 cm to 50 cm using the derived mutual-inductance expression (3-2) and exact mutual-inductance expression (3-3). The results are plotted in Fig. 3.2, which shows good agreement until the two coils are very close to each other.

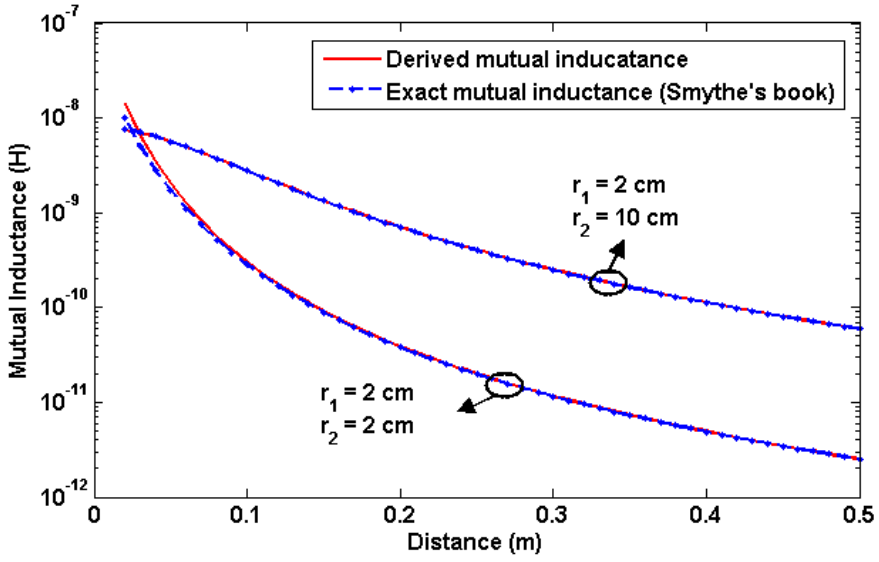

Fig. 3.2 Mutual inductance between two coils using the approximate derived expression (3-2) and exact expression (3-3) in the literature

To quantify the strength of the coupling between the coils, the coupling coefficient k is defined as it is in [10]

$$k = \frac{M}{\sqrt{L_1 L_2}} \tag{3-5}$$

where M is the mutual-inductance induced by the inductive coupling between the two coils. Substituting (3-1) and (3-2) into (3-5), the coupling coefficient between the two coils in free space is yielded as

$$k = \begin{cases} \left(\sqrt{\dfrac{r_1 r_2}{R^2 + r_1^{\,2}}} \right)^3, & r_2 \le r_1 \\ \left(\sqrt{\dfrac{r_1 r_2}{R^2 + r_2^{\,2}}} \right)^3, & r_1 \le r_2 \end{cases} \tag{3-6}$$

$$k = \left(\frac{\sqrt{r_1 r_2}}{R} \right)^3, \quad R >> r_1, r_2 \tag{3-7}$$

It shows that the coupling coefficient between two conductor coils in free space is frequency independent and varies with inverse cube of the distance i.e., $1/R^3$ when the distance between transmitter and receiver is much larger than the radius of transmitter and receiver coils i.e., $R >> r_1$, r_2. This coincides with the near-field of an infinitesimal loop, which is in the order of $1/R^3$. In a homogeneous lossy medium, the attenuation effect of the lossy material on the coupling coefficient needs to be included. The coupling coefficient between the two coils in a lossy medium is then modified to be,

$$k = e^{-\alpha R} \left(\frac{\sqrt{r_1 r_2}}{R} \right)^3, \quad R >> r_1, r_2 \tag{3-8}$$

where, α is the attenuation constant of the medium. For antennas other than loops, coupling coefficient may take different forms but will in general be in the same magnitude unless higher order resonant modes [65] are used, in which case, a more directive coupling but a faster attenuation rate versus distance is expected as predicted by the spatial distribution of the near field of those higher order modes.

3.2 NEAR-FIELD POWER TRANSFER EQUATION

To setup the inductively coupled resonant loops, one must use capacitors C_1 and C_2 to resonate with the self-inductances L_1 and L_2 of the coils at the same frequency $\omega_o = 1/\sqrt{L_1 C_1} = 1/\sqrt{L_2 C_2}$ in both transmitter and receiver respectively. In general, the mutual coupling between two coils affects the impedance seen from both the transmitter and the receiver side. As the self-reactance of the coils is cancelled out by that of the resonating capacitors, the currents i_1 and i_2 flowing at the transmitter and receiver satisfy the following relationship,

$$\begin{aligned} -V_S + i_1 R_S + i_1 R_{L1} - j\omega_o M i_2 &= 0 \\ -j\omega_o M i_1 + i_2 R_L + i_1 R_{L2} &= 0 \end{aligned} \tag{3-9}$$

where V_S is the source voltage. Simultaneously solving the two equations in (3-9) yields the current in receiver coil

$$i_2 = \frac{j\omega_o M V_S}{(R_S + R_{L1})(R_L + R_{L2}) + (\omega_o M)^2} \tag{3-10}$$

Consequently the generalized expression for received power is

$$P_r = \frac{1}{2}|i_2|^2 R_L = P_t \left[\frac{2\omega_o M}{(R_S + R_{L1})(R_L + R_{L2}) + (\omega_o M)^2} \right]^2 R_S R_L \tag{3-11}$$

where $P_t=V_s^2/8R_s$ is the available power from the source at the transmitter. In Fig.3.1(b), applying the definition of quality factors to both the transmitting and receiving resonators yields

$$Q_1 = \frac{\omega_o L_1}{R_S + R_{L1}} \quad , \quad Q_2 = \frac{\omega_o L_2}{R_L + R_{L2}} \quad , \quad Q_{1,\text{int}} = \frac{\omega_o L_1}{R_{L1}} \quad , \quad Q_{2,\text{int}} = \frac{\omega_o L_2}{R_{L2}} \tag{3-12}$$

where Q_1 and Q_2 are the loaded quality factors of the transmitter and the receiver; $Q_{1,\text{int}}$ and $Q_{2,\text{int}}$ are the intrinsic quality factors of the transmitting and receiving antennas. Substituting (3-12) into (3-11), the received power can thus be written as a function of the quality factors,

$$P_r = P_t \left(\frac{2}{1 + k^2 Q_1 Q_2} \right)^2 k^2 Q_1 Q_2 \left(1 - \frac{Q_1}{Q_{1,\text{int}}} \right) \left(1 - \frac{Q_2}{Q_{2,\text{int}}} \right) \tag{3-13}$$

Equation (3-13) is so-called near-field power transfer equation, which reveals the impact of impedance terminations, antenna quality factors and the coupling coefficient on near-field power transfer. Though the equation was derived based on the equivalent circuit of coupled resonant loops, one can generalize this relationship for other resonators coupled through near-field. The intrinsic quality factors of antennas are limited by the loss at the coils including both radiation and conduction loss. As typically antennas with extremely small electrical sizes are used in near-field systems, their radiation loss can often be ignored and the intrinsic quality factors are limited by the ohmic loss of the coils, which is determined by the conductivity and the cross-section of the wire [5].

3.3 POWER TRANSFER UNDER STRONG COUPLING ASSUMPTION

When $k^2Q_1Q_2$ is close to one, e.g., $(\omega_o M)^2$ is comparable to $(R_s+R_{L1})(R_L+R_{L2})$, it implies the coupling is strong enough to have a non-negligible effect on the impedance match on either the transmitter or the receiver. This is so-called strong coupling region [1-2] in which wireless

power transfer often operates. It is evident from (3-13) that a high power transfer efficiency requires the use of high Q coils such that $Q_{1,\text{int}} >> Q_1$ and $Q_{2,\text{int}} >> Q_2$. Equation (3-13) thus reduces to

$$P_r = P_t \left(\frac{2}{1 + k^2 Q_1 Q_2} \right)^2 k^2 Q_1 Q_2 \tag{3-14}$$

It concludes from (3-14) that the received power is maximized when $k^2 Q_1 Q_2 = 1$, yielding a perfect power transfer efficiency η_R, e.g.,

$$\eta = \frac{P_r}{P_t} = 100\% \tag{3-15}$$

Theoretically 100% efficient power transfer for lossless coils can be obtained for any distance by appropriate impedance transformation such that $k^2 Q_1 Q_2 = 1$. This optimum matching condition requires adjusting the source or load impedance for different distances, which may be realized by inserting variable ratio voltage transformers between the transmitter/receiver and the coils. For coils with finite quality factors, the maximum power transfer efficiency $\eta_{\max}$ can be approximately given by substituting the above mentioned maximum power transfer condition $k^2 Q_1 Q_2 = 1$ into (3-13),

$$\eta_{\max} = \left(1 - \frac{Q_1}{Q_{1,\text{int}}} \right) \left(1 - \frac{Q_2}{Q_{2,\text{int}}} \right) \tag{3-16}$$

3.4 POWER TRANSFER UNDER WEAK COUPLING ASSUMPTION

For the case of weak coupling, the effect of the mutual coupling between the two coils on the impedance seen from the transmitter side can be ignored. The currents i_1 and i_2 at the transmitter and the receiver respectively at the resonant frequency are given by,

$$i_1 = \frac{V_S}{(R_S + R_{L1})}$$
$$i_2 = \frac{j\omega_o k\sqrt{L_1 L_2}}{(R_L + R_{L2})} i_1 \quad (3\text{-}17)$$

The received power under weak coupling assumption is

$$P_r = \frac{1}{2}|i_2|^2 R_L = 4P_t k^2 Q_1 Q_2 \left(1 - \frac{Q_1}{Q_{1,\text{int}}}\right)\left(1 - \frac{Q_2}{Q_{2,\text{int}}}\right) \quad (3\text{-}18)$$

The weak coupling case implies $k^2Q_1Q_2 << 1$, as $(\omega_o M)^2 << (R_s+R_{L1})(R_L+R_{L2})$ and as expected the generalized power transfer equation (3-13) reduces to (3-18) by applying this approximation.

Near-field power transfer equation under weak-coupling assumption shows that the received power through inductive coupling in near-field communication system is proportional to the square of the coupling coefficient k^2, the loaded quality factors Q_1, Q_2 and it rolls off at the rate of $1/R^6$, in contrast to the far-field power rolling off in the order of $1/R^2$. This rapid rolling off behavior provides near-field system more advantages for communications in short range as it is less likely to interfere with other systems outside a certain range [11].

The termination efficiency at the transmitter and receiver is characterized by the coupling factor 1- $Q_1/Q_{1,\text{int}}$ and 1- $Q_2/Q_{2,\text{int}}$, respectively. To maximize the received power through the coupling, the critical coupling condition [66] should be selected both at the transmitter and at the receiver, e.g. $Q_1=Q_{1,\text{int}}/2$ and $Q_2=Q_{2,\text{int}}/2$ and the received power under this condition is thus,

$$P_r = P_t k^2 Q_1 Q_2 = P_t k^2 \frac{Q_{1,\text{int}} Q_{2,\text{int}}}{4} \quad (3\text{-}19)$$

It is evident that $Q_{1,\text{int}}$ and $Q_{2,\text{int}}$ should be made as high as possible to maximize the power coupled through under both the strong and weak coupling assumption.

3.5 EXPERIMENTAL VALIDATION OF NEAR-FIELD POWER TRANSFER EQUATION

In order to validate the near-field power-transfer equation, two coils of 5cm radius and 24 tightly packed turns are built using a copper wire of 1mm radius. The self-inductance of the coil computed using (3-1) is 58.4μH while the measured value of the self-inductance using the HP 4342A Q-meter is 60μH. With 330pf capacitors attached to both the coils, the resonant frequency is observed at 1.06MHz. The quality factor of both the coils at 1.06MHz measured using the HP 4342A Q-meter is 59. Therefore the transmitter and receiver coil resistance calculated is 6.75Ω. The transmitter is a signal generator with the standard 50Ω output impedance and the receiver is a digital oscilloscope with 50Ω input impedance. The source voltage is 10 volts peak-to-peak and therefore the maximum available power from the transmitter is 0.25 watts. The experimental setup of the near-field power transfer is shown in Fig.3.3. Two coils are placed normal to each other with centers aligned in one line, which are connected to the transmitter and the receiver respectively through voltage transformers.

Fig 3.3 Experimental setup for near-field power transfer measurements

By selecting the turn ratio of the voltage transformer among 8:3, 1:1 and 3:8, one can obtain source and load terminations with three different loaded quality factors of 29.5, 7 and 1.1 respectively. The received power is measured for different distances and compared with the

calculated received power in Fig. 3.4. The three groups of curves plotted in Fig. 3.4 in different colors correspond to high-Q, medium-Q and low-Q terminations, respectively.

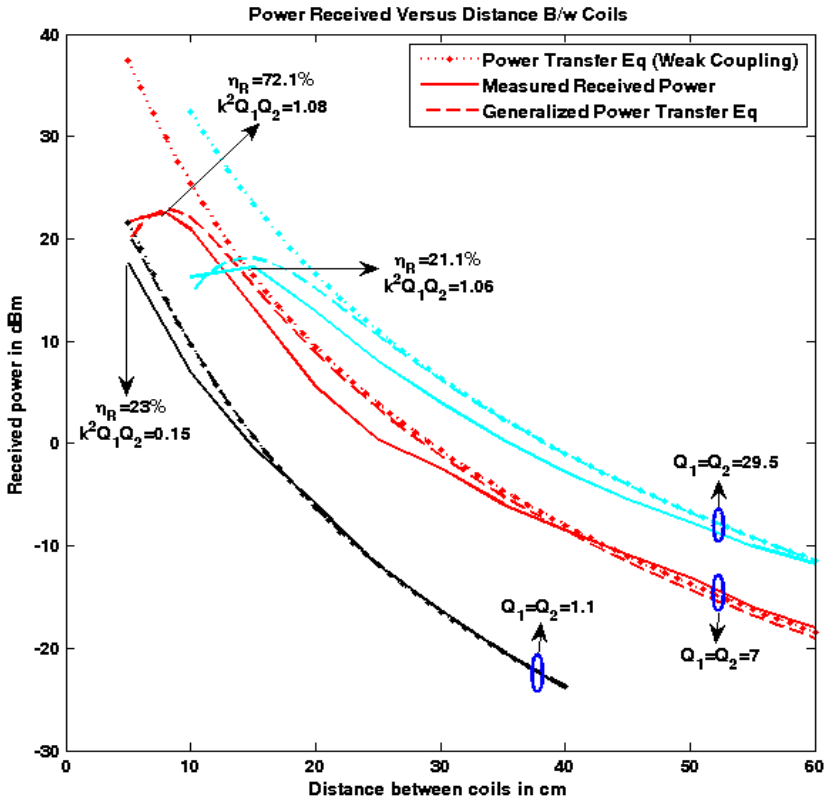

Fig. 3.4. Measured and calculated received power (dBm) plotted using generalized power transfer equation (3-13) and power transfer equation derived under weak coupling assumption (3-18) versus distance between same coils (cm) for different values of loaded Q of transmitter and receiver

Within each group, solid lines, dashed lines and dotted lines are representing the measured received power, the calculated received power using the generalized near-field power-transfer equation (3-13), and calculated received power using the power-transfer equation (3-18) derived under the weak coupling assumption. In general, all the curves within each group converge at far distances when coupling is weak. The discrepancy between the dotted curves and other curves at close distances can be attributed to the weak coupling assumption used in deriving (3-18), as the measured result agrees well with the calculated result without such an assumption even at close distances. The coupled power increases monotonically when distance

draws closer until the coupling is strong enough to affect the impedance matching so that the condition of $k^2Q_1Q_2 << 1$ no longer holds. It is observed that the coupled power indeed reaches to the peak at the proximity of the distance satisfying $k^2Q_1Q_2 = 1$ for all cases except the low-Q case where the distance satisfying such a condition is out of the measured range.

Among the three groups of curves, lower power is observed for lower Q case at far distances, while the high-Q case exhibits the highest received power as it operates at the critical coupling condition. However, the medium-Q case has greater measured power transfer efficiency than that in the high-Q case at close distances as the strong coupling condition kicks in. The measured maximum power transfer efficiency for any distance is 72.1% for the medium-Q case and 21.1% for the high-Q case versus the theoretical predictions of 77.7% and 25% respectively given by Eq. (3-16).

3.6 APPENDIX

3.6.1 Derivation of Expression for Self-Inductance of a Coil

When the radius of a coil is much smaller than the wavelength and its length, one can assume the magnetic field inside the coil is uniformly distributed (solenoid approximation). The self-inductance of a coil is defined as the ratio of magnetic flux linkage to the current through the coil [67]

$$L_1 = \frac{\phi_1}{I_1} = \frac{B_1(z=0).N_1S_1}{I_1} \tag{A-1}$$

where φ_1 is the magnetic flux through coil$_1$ having N_1 turns, and each turn area is S_1. The magnetic flux density at the center of the coil is B_1(z=0) due to current I_1 flowing through the coil.

Magnetic flux density at a point on the axis of the coil carrying current I_1 is given by [67]

$$B_1(z) = \hat{z}\frac{\mu_o N_1 I_1 r_1^{\,2}}{2\left(\sqrt{z^2 + r_1^{\,2}}\right)^3} \tag{A-2}$$

At the center of the coil (z = 0),

$$B_1(z=0) = \hat{z}\frac{\mu_o N_1 I_1}{2r_1} \tag{A-3}$$

Substitute (A-3) and $S_1 = \hat{z}\pi r_1^2$ into (A-1), the self-inductance of the coil L is given by

$$L_1 = \frac{\mu_o N_1^{\,2} \pi\, r_1}{2} \tag{A-4}$$

3.6.2 Derivation of Expression for Mutual-Inductance between Coils

The mutual-inductance M_{21} between coil$_1$ and coil$_2$ is defined as the ratio of flux linkage φ_{21} to coil$_2$ due to current I_1 in coil$_1$ [67]

$$M_{21} = \frac{\phi_{21}}{I_1} = \frac{B_1(z=R).N_2 S_2}{I_1} \tag{A-5}$$

where, coil$_2$ has N_2 turns, and area of each turn is S_2. B_1 (z = R), which can be obtained from (A-2), is the magnetic flux density at the center of the coil$_2$. It should be noted that the magnetic flux density through the area S_2 is assumed to be uniform and identical to the one at the center in (A-5). This condition may only be true when either the coil$_2$ is much smaller than coil$_1$ or the distance R is far greater than the radius of the coil$_1$. Substitute (A-2) and $S_2 = \hat{z}\pi r_2^2$ into (A-5), the mutual-inductance M_{21} under the assumption of infinitesimal thickness of the coil and the homogeneity of the magnetic field in the area of coil$_2$ is given by

$$M_{21} = \frac{\mu_o \pi N_1 N_2 r_1^{\,2} r_2^{\,2}}{2\left(\sqrt{R^2 + r_1^{\,2}}\right)^3} = M_{12} \tag{A-6}$$

Notice that (A-6) does not satisfy symmetry in its expression due to the smaller $coil_2$ assumption made when (A-5) is derived. Taking consideration of symmetry between the coils, a more general form of mutual inductance between two coils is yielded as follows:

$$M = \begin{cases} \dfrac{\mu_o \pi N_1 N_2 r_1^{\,2} r_2^{\,2}}{2\left(\sqrt{R^2 + r_1^{\,2}}\right)^3}, & r_2 \le r_1 \\ \dfrac{\mu_o \pi N_1 N_2 r_1^{\,2} r_2^{\,2}}{2\left(\sqrt{R^2 + r_2^{\,2}}\right)^3}, & r_1 \le r_2 \end{cases} \tag{A-7}$$

CHAPTER 4

Capacity Performance of an Inductively Coupled Near-Field Communication Link

The Shannon-Hartley theorem [23] defines the capacity of a digital communication system

$$C = B_w \log_2\left(1+\frac{P_r}{P_N}\right) \tag{4-1}$$

where B_w is the bandwidth in Hz, P_r is the received power and P_N is total noise power at the receiver over the bandwidth B_w. Therefore, when a digital communication link is built upon near-field coupling mechanism, not only the transferred power, but also the bandwidth of the communication system is of importance to the capacity performance of such a link. The fractional bandwidth of a NFC system can be estimated from the loaded quality factors Q_1 and Q_2 of the transmitter and the receiver respectively through the following equation,

$$B_f = \frac{B_w}{f_o} = \begin{cases} \frac{1}{Q_1}, & if \quad Q_1 > Q_2 \\ \frac{1}{Q_2}, & if \quad Q_2 > Q_1 \end{cases} \tag{4-2}$$

where f_o is the center frequency. A termination based on critical coupling increases the signal to noise ratio by improving the received power, yet it may not offer the optimal system capacity as the signal bandwidth may be sacrificed. It suggests that the transferred power and the bandwidth of a NFC system must be traded-off for the optimal capacity.

The source of noises in the receiver can be either natural interference P_N^E dominated or thermal noise P_N^t dominated, and the total receiver noise P_{N} is the sum of natural interference and thermal noise. The capacity performance of such a system is further discussed as follows.

4.1 CAPACITY PERFORMANCE IN THERMAL NOISE LIMITED SCENARIO

According to Planck's blackbody radiation law, the thermal noise power P_N^t is approximately given by

$$P_N^t = KT_{system}B_w \tag{4-3}$$

where, K is the Boltzmann's constant having value 1.38×10^{-23} (J/K) and T_{sys} is the system noise temperature measured in Kelvin. By substituting (3-18), (4-2) and (4-3) into (4-1), the capacity of a NFC system in a situation where the thermal noise is the dominant source of noise is expressed entirely as a function of loaded quality factors of the transmitter and receiver.

$$C = \begin{cases} \dfrac{f_o}{Q_1}\log_2\left(1+\dfrac{4P_t k^2 {Q_1}^2 Q_2\left(1-\dfrac{Q_1}{Q_{1,\mathrm{int}}}\right)\left(1-\dfrac{Q_2}{Q_{2,\mathrm{int}}}\right)}{KT_{system}f_o}\right), & if\ Q_1 \geq Q_2 \\ \dfrac{f_o}{Q_2}\log_2\left(1+\dfrac{4P_t k^2 Q_1 {Q_2}^2\left(1-\dfrac{Q_1}{Q_{1,\mathrm{int}}}\right)\left(1-\dfrac{Q_2}{Q_{2,\mathrm{int}}}\right)}{KT_{system}f_o}\right), & if\ Q_2 \geq Q_1 \end{cases} \tag{4-4}$$

Hence, one needs to search through all the possible values of loaded quality factors Q_1 and Q_2 in both the transmitter and the receiver respectively for an optimum pair that maximizes the system capacity of a NFC link given by (4-4).

4.2 CAPACITY PERFORMANCE IN NATURAL INTERFERENCE LIMITED SCENARIO

In many situations, natural interference caused by lightning in the ionosphere may become the main source of the receiver noise. This is particularly the case when the system operates at low frequencies such as ELF/VLF bands [24]. The received interference power P_N^E from ELF/VLF noise over a bandwidth B_w is (See Appendix),

$$P_N^E = X r_2^3 B_w \frac{Q_2}{f_o}\left(1-\frac{Q_2}{Q_{2,\text{int}}}\right) \tag{4-5}$$

where $$X = \frac{2\pi^2 B_{\text{int}\,erference}^2 f^2}{\mu_o} = 1.6\times 10^{-17}$$

The capacity performance of such a system is thus given by,

$$C = B_w \log_2\left(1+\frac{4P_t r_1^3 Q_1\left(1-\frac{Q_1}{Q_{1,\text{int}}}\right)}{X\frac{B_w}{f_o}R^6}\right) \tag{4-6}$$

$$C = \begin{cases} \dfrac{f_o}{Q_1}\log_2\left(1+\dfrac{4P_t r_1^3 Q_1^2\left(1-\dfrac{Q_1}{Q_{1,\text{int}}}\right)}{XR^6}\right), & Q_1 \geq Q_2 \\ \dfrac{f_o}{Q_2}\log_2\left(1+\dfrac{4P_t r_1^3 Q_1 Q_2\left(1-\dfrac{Q_1}{Q_{1,\text{int}}}\right)}{XR^6}\right), & Q_2 \geq Q_1 \end{cases} \tag{4-7}$$

The first equation in (4-7) shows that in the case that the transmitter limits the system bandwidth, the capacity performance becomes independent of the size and the quality factor of the receiver antenna.

4.3 COMPARISON OF THERMAL AND NATURAL INTERFERENCE

The ratio of natural interference to thermal noise in the receiver is obtained by dividing the natural interference noise picked up by receiver in (4-5) by the thermal noise power in (4-3)

$$\frac{P_N^E}{P_N^t} = \frac{X}{KT} r_2^3 \frac{Q_2}{f_o}\left(1 - \frac{Q_2}{Q_{2,\text{int}}}\right) \tag{4-8}$$

The natural interference can be comparable to the thermal noise in power depending on the size of coil, loaded quality factor, termination efficiency and temperature at the receiver. The noise temperature of a receiver can vary between 100K and 400K. Termination efficiency factor ($1-Q_2/Q_{2,\text{int}}$) in general varies between 0.5 for high Q receiver when $R_L=R_{L2}$, and 1 for low Q receiver when $R_L>>R_{L2}$. In general, for receivers with low loaded Q_2, the thermal noise is comparable or higher than the received natural interference since large receiver bandwidth leads to more thermal noise, while for receivers with high loaded Q_2, the received natural interference can be dominant since high loaded Q_2 receiver intercepts greater amount of natural interference.

4.4 SIMULATION RESULTS FOR AIR-AIR LINK

An inductively coupled NFC air-air link operating at VLF frequencies is examined in this section to demonstrate the impact of quality factors to the capacity performance of a weakly coupled near-field communication system. The simulations are carried out in the following steps. First, the commercial software COMSOL Multiphysics is used to extract the equivalent *R*, *L* parameters and the coupling coefficient *k* of the coils by performing quasi-static electromagnetic simulations. One can calculate the quality factors from the extracted *R* and *L* parameters, which are then substituted into (3-18) to lead to the received power versus different distances. Finally,

equation (4-1) is used to compute the capacity performance of NFC link for various distances. Due to the axial symmetry of the coils, the simulation is performed in the two-dimensional space of the wire cross section. In all the simulation scenarios, two identical circular coils made of copper with loop radii $r_1=r_2=a$=0.5m, and wire radius b=1cm are chosen as the antennas at the transmitter and receiver. The coils consist of 50 wound turns and the spacing between two windings next to each other is s=2cm. Two identical circular coils centered on a single axis and separated by distance R in free space form a communication link in the air. The simulation is performed when the coils are operating at two resonant frequency points, $f = 1\ kHz$ and $f = 3\ kHz$, respectively. The obtained resistance of the two coils from simulations is $R_{L1}=R_{L2}=39.32m\Omega$ at *1 kHz* and $R_{L1}=R_{L2}=74.81m\Omega$ *at 3 kHz*. The self-inductance of the two coils from simulation is $L_1=L_2=1.0mH$ at both *1 kHz* and *3 kHz*. In contrast, the analytic value of the self-inductance, obtained from (3-1) is $L_1=L_2=2.5mH$ at both *1 kHz* and *3 kHz*. This is because that the uniformity assumption of the magnetic field made for inside the solenoids and the loops, leads to overestimations of self-inductance for loops than the simulated results. The intrinsic quality factor of the coils from the simulation is $Q_{1,int}=Q_{2,int}=159.8$ at *1 kHz* and $Q_{1,int}=Q_{2,int}$=252 at *3 kHz*.

Figure 4.1 shows the variations of the simulated mutual inductance M and coupling coefficient k versus the separation distance R between the transmitter and receiver in free space in the range of 1km to 10km, in comparison to analytical results obtained from equations (3-2) and (3-5). The solid blue curve represents the analytic value of mutual inductance and coupling coefficient and the asterisk and circle lines are the extracted results from the simulations. The analytic and simulation results of the mutual inductance show very good agreements between each other within the communication range from 1km to 10km, which verifies the applicability

of the assumption of the ignorable thickness of coil at the receiver and homogeneity of magnetic field in the area of the coil at the receiver. However, the extracted coupling coefficients k from simulations is around 2.5 times of the analytic values due to the discrepancy between the simulated self-inductance and those derived analytically. Furthermore, the simulation results show that the variation of coupling coefficient *k* between the two coils in free space is almost independent of their operating frequency and it does roll off at the rate of inverse cube of communication distance *R*. The coupling coefficient *k* drops from 3.1e-10 to 2.5e-13 when *R* increases from 1 km to 10 km.

To generate the capacity versus distance curves, it is assumed that the available transmitter power P_t is 60W and the noise temperature of the system is T_{sys}=400K. The received power is calculated using (3-18) and the noise power is the superposition of the thermal noise power (4-3) and natural interference power (4-5). Therefore, the capacity versus the transmitter/receiver loaded quality factor is computed for both *f*=1 kHz and *f*=3 kHz and plotted in Fig.4.2 (a) and (b) for several choices of distances. It shows that there exists an optimal quality factors for each distance that maximizes the link capacity as the transferred power and the bandwidth of the link must be traded off. It is observed that the optimal data rate of the system operating at *f* = 3 kHz is approximately 2.5 times that of the system operating at *f*=1 kHz. For example, at *R*=1.5km, the highest data rate at *f*=3 kHz is 1900 bps achieved at transmitter and receiver *Q* of 5, while, at *f*=1 kHz it is only 800 bps achieved at the transmitter and receiver *Q* of 4. Fig.4.3 shows the effect of available power from source on the capacity performance of the same link with a separation distance of *R*=3 km. The available transmitter power P_t varies from 125W to 375W. The maximum data rates for different available power level are 720bps at 375W, 600bps at 250W and 440bps at 125W. The corresponding transmitter and receiver Q are at 12, 14

and 16 respectively. A lower available power from the source leads to a lower optimal capacity of the system and a higher loaded transmitter Q requirement.

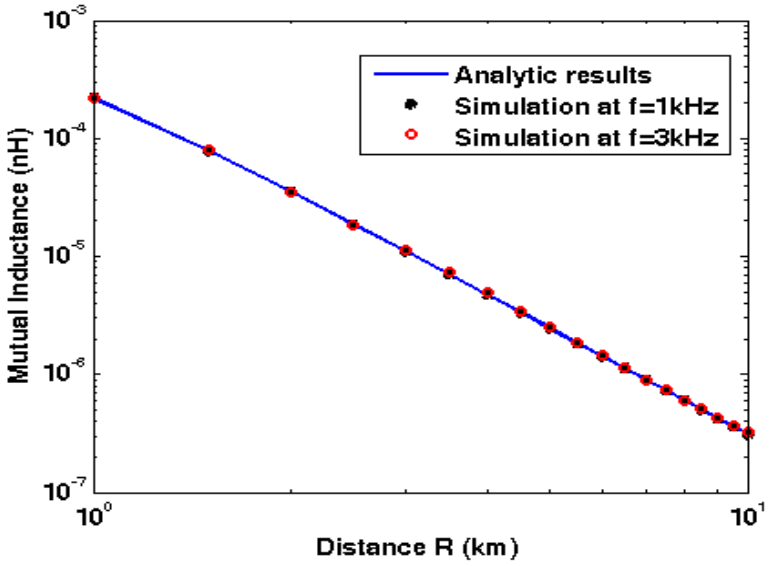

(a)

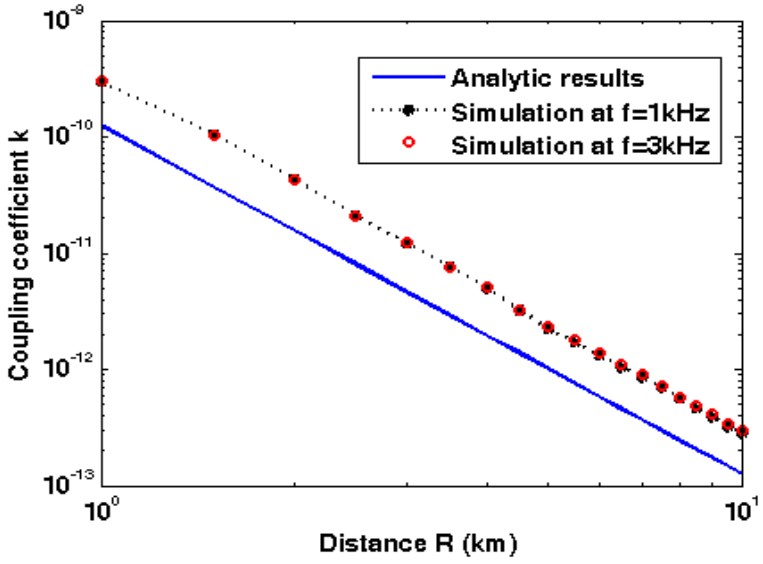

(b)

Fig. 4.1 Variation of (a) Mutual inductance 'M' and (b) coupling coefficient 'k' versus distance between coils

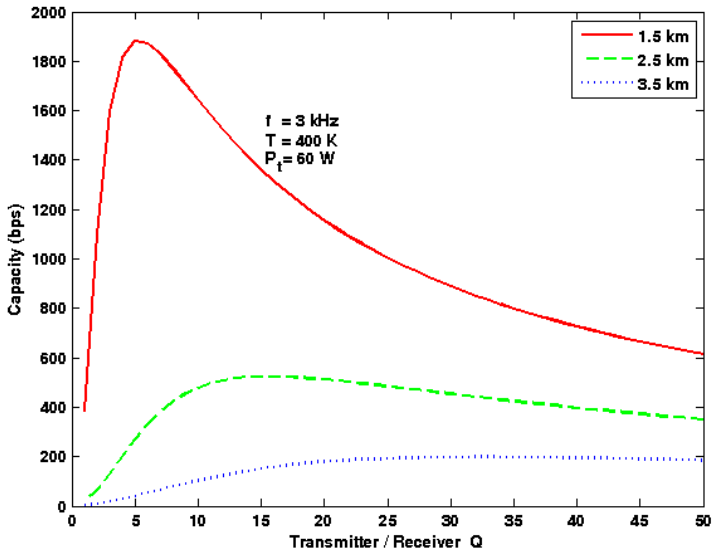

(a)

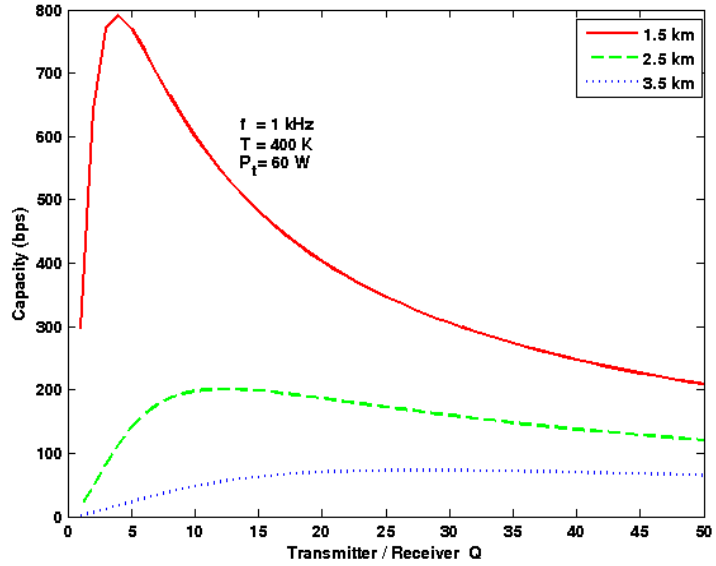

(b)

Fig. 4.2. Capacity versus transmitter/receiver Q of the near-field link for three difference distances (a) at *f*=3kHz (b) at *f*=1kHz

4.5 APPENDIX

The voltage '$v_{\text{interference}}$' received at the receiver due to ELF/VLF natural interference at an angular frequency ω can be found using Maxwell's equation,

$$v_{\text{int}erference} = \oint \vec{E}.\vec{dl} = -\frac{\partial}{\partial t}\oint \vec{B}.\vec{dS} = -j\omega B_{\text{int}ereference} N_2 A_2 \tag{A-1}$$

Where, $B_{interference}$ is the magnetic flux density due to ELF/VLF Noise floor. N_2 is the number of turns and A_2 is the cross-section area of the loop. The received power at a particular frequency f is,

$$P_N^E = \frac{1}{2}\frac{V_L^2}{R_L} == \frac{\left(\omega B_{\text{int}ereference} N_2 A_2\right)^2}{2R_L}.\left(\frac{R_L}{R_L + R_{L2}}\right)^2 = \frac{2\pi^2}{R_L} B_{\text{int}erference}^2 f^2 N_2^2 A_2^2 \left(1 - \frac{Q_2}{Q_{2,\text{int}}}\right)^2 \tag{A-2}$$

Total received power due to ELF/VLF interference is obtained by integrating the received power for all the frequencies within the bandwidth

$$P_N^E = \int_{B_w} \frac{2\pi^2}{R_L} B_{\text{int}erference}^2 f^2 N_2^2 A_2^2 \left(1 - \frac{Q_2}{Q_{2,\text{int}}}\right)^2 df \tag{A-3}$$

Vertical electric and horizontal magnetic flux density is given in dB in relative to $\sqrt{H_z}$ in [25]. In (A-3), B^2f^2 needs to be integrated over the bandwidth B_ω of the system. The value of B^2f^2 is approximately 10^{-24} for frequencies up to 0.1MHz. Hence the received natural noise power is given by

$$P_N^E \approx \frac{2\pi^2}{R_L} B_{\text{int}erference}^2 f^2 N_2^2 A_2^2 \left(1 - \frac{Q_2}{Q_{2,\text{int}}}\right)^2 B_w \tag{A-4}$$

Substituting the area $A_2 = \pi r_2^2$, and termination factor $1\text{-}Q_2/Q_{2,\text{int}} = R_L/(R_L + R_{L2})$ in (A-4), the received power takes the form

$$P_N^E \approx \left[\frac{2\pi^2}{\mu_o} B_{\text{int}erference}^2 f^2\right]\left[\frac{\mu_o N_2^2 \pi r_2}{2}\right]\frac{2\pi f_o}{f_o}.\frac{1}{R_L + R_{L2}} r_2^3 \left(1 - \frac{Q_2}{Q_{2,\text{int}}}\right) B_w \tag{A-5}$$

Using the definition of self inductance (3-1) and loaded quality factor at receiver (3-12), (A-5) takes the form

$$P_N^E \approx \left[\frac{2\pi^2}{\mu_o} B_{\text{int}\,erference}^2 f^2\right]\left[\frac{\mu_o N_2^2 \pi r_2}{2}\right]\frac{2\pi f_o}{f_o}\cdot\frac{1}{R_L + R_{L2}} r_2^3\left(1-\frac{Q_2}{Q_{2,\text{int}}}\right)B_w \qquad \text{(A-6)}$$

$$P_N^E = X r_2^3 B_w \frac{Q_2}{f_o}\left(1-\frac{Q_2}{Q_{2,\text{int}}}\right)e^{-2\alpha R} \qquad \text{(A-7)}$$

where

$$X = \frac{2\pi^2 B_{\text{int}\,erference}^2 f^2}{\mu_o} = 1.6\times 10^{-17}$$

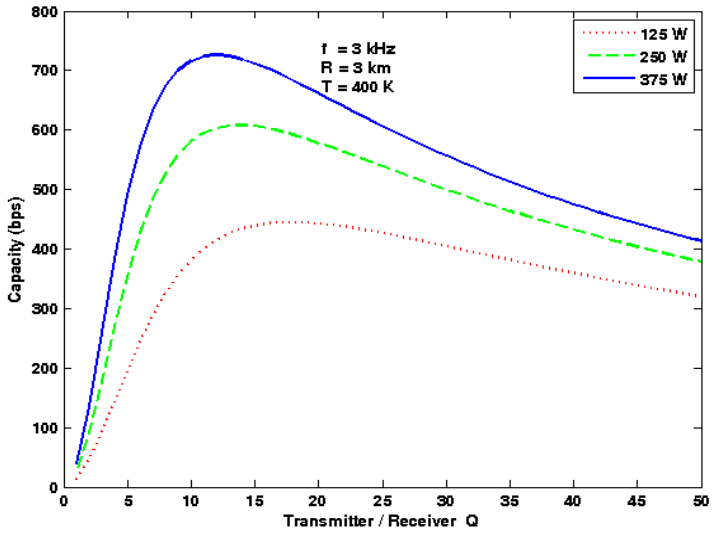

Fig. 4.3. Effect of the available power from transmitter on the capacity performance of the near-field link.

CHAPTER 5

Direct Antenna Modulation for Enhanced Capacity of Near-Field Communication System

5.1 NFC LINKS THROUGH COUPLED LOOPS

Shannon's capacity theorem (4-1) shows that the link capacity is determined by both the transferred power and the bandwidth of the communication system. As NFC is often used for the lower band of radio frequency spectrum such as ELF/VLF bands, natural interference (e.g., caused by lightning in the ionosphere) is often the main source of the receiver noise. The capacity of a NFC system in which received noise power from ELF/VLF interference noise is the main source of noise, is given by (4-6) [22]. It is evident from (4-6) that the link capacity depends on neither the quality factor nor the dimension of the receiver antenna as long as the ELF/VLF interference dominates the source of the noise in the receiver. On the other hand, the intrinsic quality factor of the transmitting loop determines the capacity performance and it is always beneficial if the transmitter coil can be made with its highest possible intrinsic quality factor. With a linear, time-invariant termination, the bandwidth of the NFC system B_w is limited by the loaded quality factor of the transmitter [22]

$$B_w \leq \frac{f_o}{Q_t} \tag{5-1}$$

The selection of Q_t can follow the aforementioned critical coupling condition to maximize the received power. However, critical coupling does not necessarily lead to the maximized capacity according to (4-1). It suggests that the transferred power and the bandwidth of a NFC system must be traded-off for the optimal capacity.

The primary purpose of introducing DAM here is to remove the constraint of the system bandwidth imposed by the quality factor of the transmitter as shown in (5-1). The capacity bound of NFC link can thus be improved in a way similar to how an ultra-wide band communication system can offer better capacity than a narrow-band communication system. The NFC link with DAM differs from the traditional setup by inserting a single pole double throw (SPDT) switch on the transmitter side, which connects the inductive loop antenna to either the source or the ground at the proper time of the modulation cycle. The equivalent circuit model of a NFC system utilizing DAM scheme is shown in Fig. 5.1.

Assuming a binary data sequence of ‘1’s and ‘0’s is sent with DAM. To transmit bit ‘1’, the SPDT switch connects the transmitter coil to the source via an external capacitor C_1. Under the weak coupling condition, the impact of the receiver on the impedance of the transmitter can be ignored. Thus resonance is formed in the transmitter loop in a way similar to any series LC resonator. At resonance, the reactive energy alternates between the forms of electric energy stored in capacitor and magnetic energy stored in the inductance of the loop antenna. The total amount of reactive energy remains approximately as a constant except the dissipation on the source and inductor resistance. To transmit bit ‘0’, the SPDT switch connects the loop antenna to the ground and disconnects from the source and external capacitor. The transmitter in this case is a first order circuit and no longer supports the resonance. The current through the loop antenna is re-directed to the ground and remains approximately as a constant. There is no path for current to

flow through the source and the capacitor so that the charge stored in the capacitor, if any, also remains as a constant.

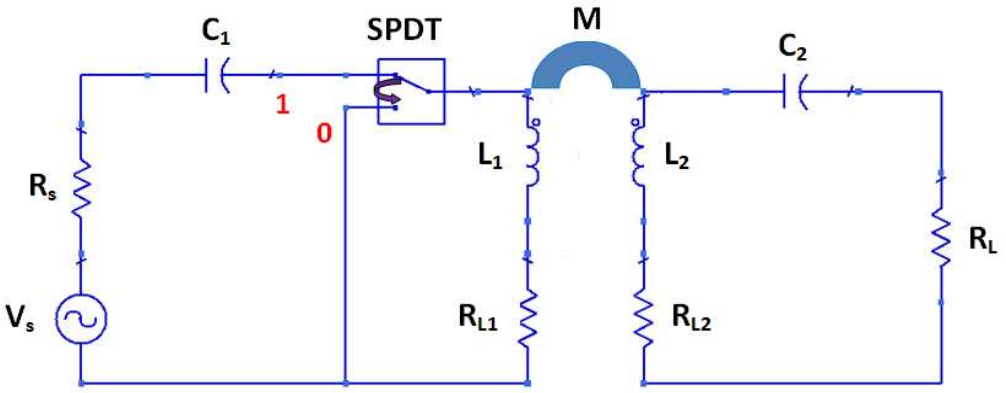

Fig. 5.1 Equivalent circuit model of a NFC link utilizing DAM scheme

The switching moment can be selected either as the moment when the voltage across the capacitor is zero and the current through the inductor is at its maximum or when the voltage across the capacitor is at its maximum and the current through the inductor is zero. To simplify the discussion, it is assumed in this chapter that the switching is incurred at the maximum inductor current. At this moment all the reactive energy of the system is stored in the inductor in the form of DC magnetic field and no energy dissipation is caused by the switching action alone. However, there will be a small amount of dissipation to the stored inductive energy due to losses on the coil resistance and the on-resistance of the switch, which is to be replenished during the next cycle of bit '1' transmission. When the transmission of the next bit '1' is initiated by SPDT, the LC resonator is already charged at the proximity of its maximum reactive energy state and does not require a completely new charging process starting from scratch. Therefore, data rate as high as 100% of the carrier frequency can be achieved even with a high-Q transmitter resonator. The conventional limit of the modulation bandwidth described by (5-1) is now modified to

$$B_w \leq f_o \tag{5-2}$$

which indicates that the modulation bandwidth in DAM assisted NFC link is regardless of the selection of the transmitter loaded quality factor. Critical coupling condition can thus be applied to the transmitter in this case for the optimal capacity.

5.2 TRANSIENT ANALYSIS OF LINK MODULATION BEHAVIOR

5.2.1 Current in the Transmitter Loop in Traditional Modulation

The traditional NFC link setup is shown in Fig. 3.1(b). The modulated signal source V_s drives the transmitter resonator with a constant source resistance during the transmission of both bit '0' and bit '1'. The transmitter current $i_{t1,TRAD}$ corresponding to transmission of bit '1' is given by (See Appendix A1)

$$i_{t1,TRAD} = \left[\frac{V_o}{\left(R_s + R_{L1}\right)} + \left(i_{initial} - \frac{V_o}{\left(R_s + R_{L1}\right)} \right) e^{-\frac{\omega_o t}{2Q_t}} \right] \cos\left(\omega_o t\right) \tag{5-3}$$

where $Q_t = \omega_o L_1/(R_s+R_{L1})$ is the loaded quality factor of transmitter, V_o is the amplitude of the sinusoidal voltage source over the bit "1". The time constant of the series LC second order resonant circuit is $\tau=2Q_t/\omega_o$. The initial and steady state currents during the transmission of bit '1' are respectively $i_{initial}cos(\omega_o t)$ and $V_o\, cos(\omega_o t)/(R_s+R_{L1})$.

Similarly, the transmitter current $i_{t0,TRAD}$ corresponding to the transmission of bit '0' is given by (See Appendix A2)

$$i_{t0,TRAD} = i_{initial} \cos(\omega_o t) e^{-\frac{\omega_o t}{2Q_t}} \tag{5-4}$$

Equation (5-4) shows that the transmitter current is sinusoidal during the transmission of bit '0' with an exponentially decaying envelope. The time constant of the transmitter is $\tau=2Q_t/\omega_o$. If a

high Q_t transmitter is used to improve the power transfer efficiency as suggested by (3-18), a great number of carrier cycles are required before the loop antenna is fully charged or discharged, which sets the limit to the modulation bandwidth of the link. The transmitter resonator current for traditional modulation scheme corresponding to data sequence 10101010 is simulated and plotted in Fig. 5.2. The sequence is modulated on the carrier at the rate of one bit per RF cycle, with the modulated signal shown in the dash line in Fig. 5.2. It is assumed that transmitter is with a Q_t of 25. It is evident from Fig. 5.2 that the transmitter loop current does not follow the source modulation well and the modulation information is mostly lost.

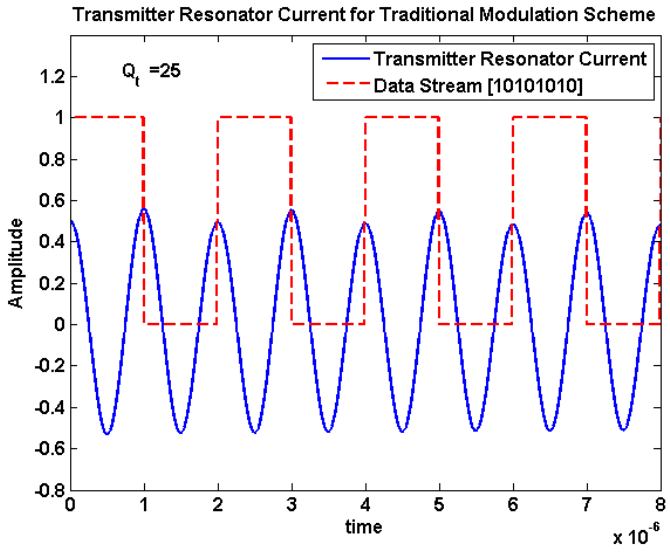

Fig. 5.2. Transmitter resonator current corresponding to the data stream 10101010 [Traditional modulation scheme]

5.2.2 Current in the Transmitter Loop in DAM

The transmitter loop current $i_{t1,DAM}$ for DAM scheme during the transmission of bit '1' is given by (See Appendix A1)

$$i_{t1,DAM} = \left[\frac{V_o}{(R_s + R_{L1})} + \left(i_{initial} - \frac{V_o}{(R_s + R_{L1})} \right) e^{-\frac{\omega_o t}{2Q_t}} \right] \cos(\omega_o t) \tag{5-5}$$

When bit '0' is transmitted, the current of the transmitter loop is (See Appendix A2)

$$i_{t0,DAM} = i_{initial} e^{-\frac{\omega_o t}{Q_{to}}} \quad (5\text{-}6)$$

where $Q_{to} = \omega_o L_1/(R_{switch}+R_{L1})$ is the quality factor of first order transmitter corresponding to transmission of bit '0'. Assuming that switching is incurred at the maximum inductor current, the current in the loop antenna decreases exponentially from its peak value. For high Q_{t0}, the time constant is far larger than the carrier cycle so that the current can be approximately considered as a constant within the time frame of a few carrier cycles.

A circuit simulation is carried out to illustrate the concept with the simulation results plotted in Fig. 5.3, where the solid curve shows the normalized source voltage while the dash line shows the switch control signal applied on the SPDT switch for transmission of data stream corresponding to 10101010. A high switch control signal corresponds to the transmission of bit ‘1’, while a low switch control signal corresponds to the transmission of bit ‘0’. From Fig. 5.3, it is observed that switching is incurred at the maximum inductor current, which is the same moment when the source voltage reaches its maximum.

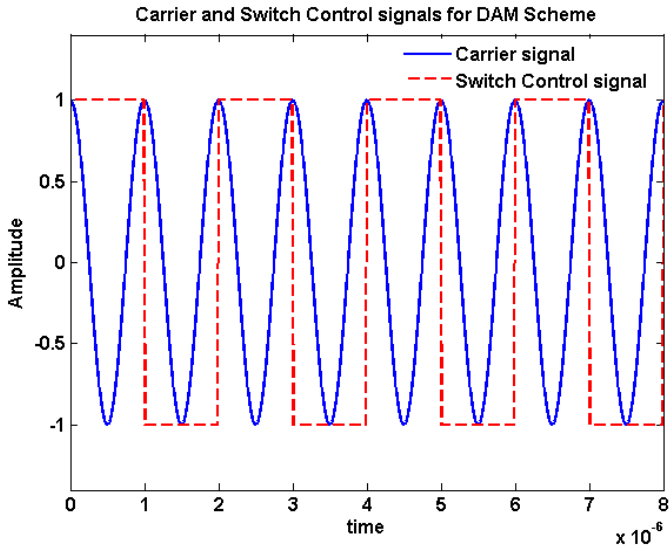

Fig. 5.3. Normalized source voltage and switch control signal corresponding to the data stream 10101010 [DAM scheme]

The corresponding transmitter resonator current is plotted for DAM in Fig. 5.4. It is assumed that the loaded quality factor of the transmitter Q_t is 25. It can be seen from Fig. 5.4 that the monocycle sinusoidal current flows through the transmitter corresponding to bit '1'. The current decays exponentially during the transmission of bit '0'. However, with a large time constant, very little change in value change of the current is observed over the period of one RF cycle.

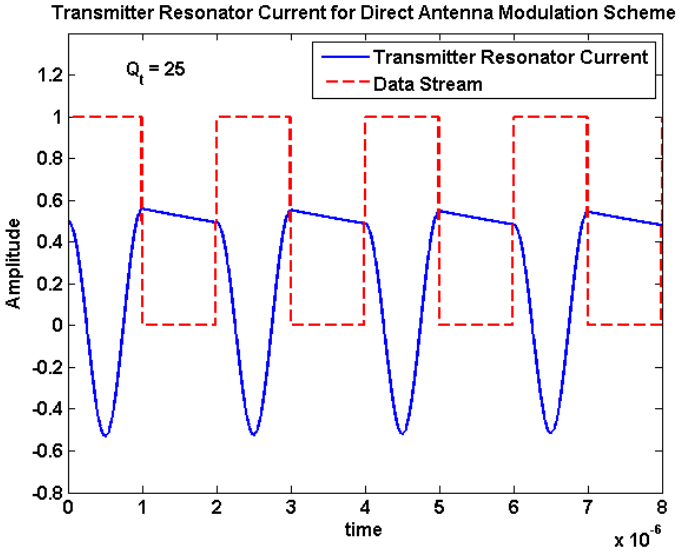

Fig.5.4. Current of the transmitter loop corresponding to the data stream 10101010 [DAM scheme]

5.2.3 Current in the Receiver Loop

The induced voltage on the receiver loop is proportional to the rate of current change in the transmitter i.e.,

$$v_{ind} = -M_{rt} \frac{di_t}{dt} \tag{5-7}$$

where M_{rt} is the mutual-inductance between the transmitter loop and the receiver loop. Assuming the receiver is terminated with a low loaded quality factor, the current in the receiver loop can thus be calculated approximately by dividing the induced voltage with the total resistance, e.g.

$$i_r = -\frac{M_{rt}}{R_L + R_{L2}} \frac{di_t}{dt} \tag{5-8}$$

For both traditional modulation and DAM, the receiver current for bit "1" is

$$i_{t1,TRAD} \approx \frac{\omega_o M_{rt}}{R_L + R_{L2}} \left[\frac{V_o}{(R_s + R_{L1})} + \left(i_{initial} - \frac{V_o}{(R_s + R_{L1})} \right) e^{-\frac{\omega_o t}{2Q_t}} \right] \sin(\omega_o t) \tag{5-9}$$

When the bit "0" is received, the receiver current can be derived in a similar way for both the traditional modulation scheme and DAM scheme, which are respectively,

$$\begin{cases} i_{r0,TRAD} \approx \dfrac{\omega_o M_{rt}}{R_L + R_{L2}} i_{initial} \sin(\omega t) e^{-\frac{\omega t}{Q_t}} \\ i_{r0,DAM} \approx \dfrac{1}{Q_{to}} \dfrac{\omega_o M_{rt}}{R_L + R_{L2}} i_{initial} e^{-\frac{\omega t}{Q_{to}}} \end{cases} \tag{5-10}$$

In the DAM scheme the receiver current for bit '0' is signficantly smaller than that during bit '1' if $Q_{t0}>>1$. On the other hand, when the transmitter loaded quality factor is high, there is almost no discernible difference in the traditional modulation scheme between the current at both states. This implies the transmission of the binary data through DAM is successful while in traditional modulation the high speed binary modulation information fails to pass.

5.3 EXPERIMENTAL SETUP AND MEASURED RESULTS

In order to validate the improvement in capacity performance offered by DAM over the traditional modulation scheme, two coils of 5cm radius and 24 tightly packed turns are built using a copper wire with radius of 1mm. The measured value of self-inductance and intrinsic quality factor of coils using the HP 4342A Q-meter are 74μH and 35 respectively. 4700pF Capacitor is attached to both the transmitter and receiver coil and the resonant frequency is observed to be 270 kHz. The transmitter coil is connected to a signal generator with 50Ω output

impedance and the receiver coil is connected to an oscilloscope with 50Ω input impedance, both with transformers. Using impedance transformer, transmitter is matched to source under critical coupling condition with the Q_t value of 17.5. The transforming ratio at the receiver is selected to obtain a low load Q_r value of 0.7. The data sequence to be transmitted is 10101010.

5.3.1 Measured Results for Traditional Modulation Scheme

In traditional modulation scheme, the modulated data is applied directly to the transmitter high Q_t resonator. The data rate is chosen to be the same as the carrier frequency. The modulation source in the transmitter and the corresponding receiver current are shown respectively in Fig. 5.5 (a) and (b). From (5-3) and (5-4), the transmitter resonator requires approximately 6 cycles to charge to 63% of its full energy or discharge to 37% of its full energy. Shown in Fig. 5.5, when the modulation is at the rate of 1-bit per RF cycle, the transmitter current does not follow the modulation voltage well due to the bandpass effect caused by the high transmitter Q. In the receiver, the current is sampled at a sampling frequency of 50MSPS. The spectrum of the received signal, computed through DFT, is displayed in Fig. 5.6 where the spectral lines at index +/-16 correspond to the carrier frequency. It is evident from Fig. 5.6 that while some carrier power is transferred through; the modulation tones are invisible which indicates the loss of the modulation information in the link.

5.3.2 Measured Results for DAM Scheme

The testing setup for DAM is shown in Fig 5.7. Tektronix arbitrary waveform generator AWG 520 generates the carrier signal, while Tektronix arbitrary function generator AFG 3021 generates the data sequence, which controls the SPDT in the transmitter. Commercially available SPDT ISL43L220 is used because of its low on resistance (0.22 Ohm). The frequency of

Tektronix AWG 520 and Tektronix AFG 3021 is locked. AFG 3021 contains a digital phase shifter, which is used to generate appropriate switching timing.

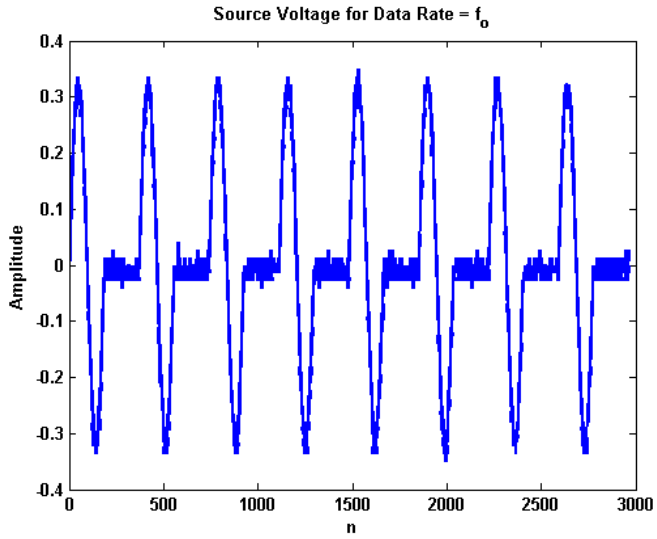

(a)

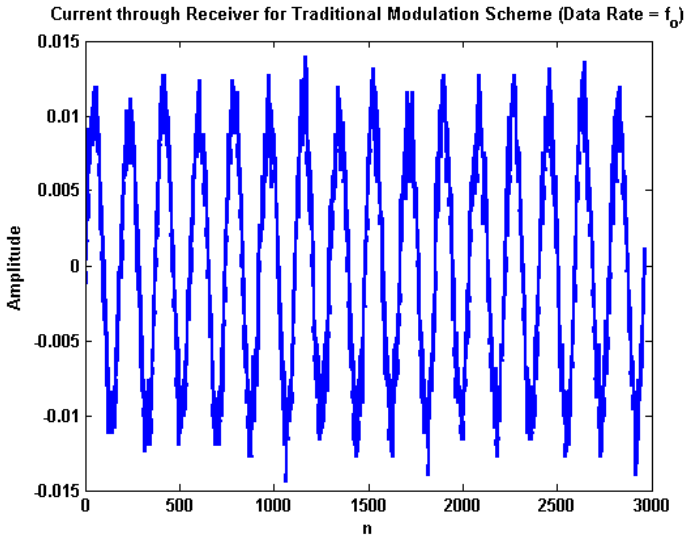

(b)

Fig. 5.5. (a) Modulated source voltage (b) The corresponding receiver current, for the data stream 10101010 in traditional modulation. [Data rate = carrier frequency]

The data sequence 10101010 is generated at the data rate equals to the carrier frequency and both the RF carrier and the switch control signal are captured on the oscilloscope shown in Fig. 5.8,

which indicates that the switching moments are at the maximum RF voltage or the maximum inductor current in the transmitter loop.

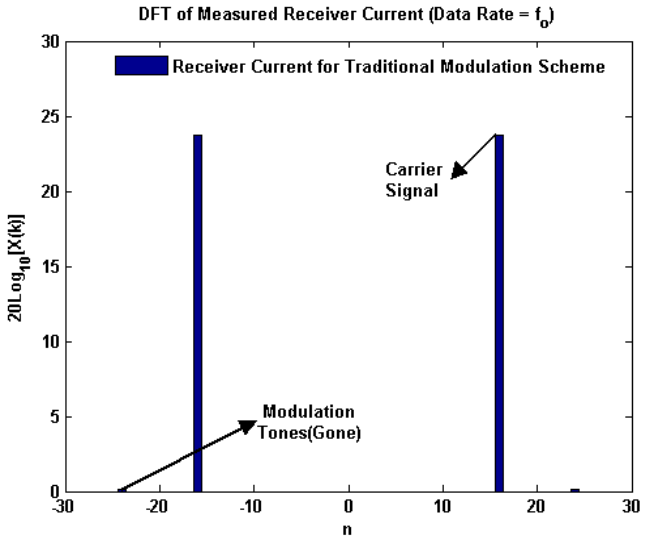

Fig. 5.6. Spectrum of receiver current corresponding to data stream 10101010 in traditional modulation

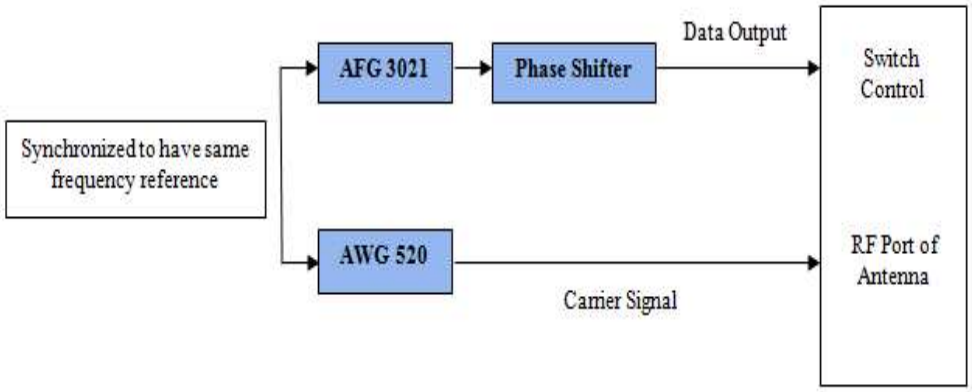

Fig. 5.7. Testing setup for the DAM scheme

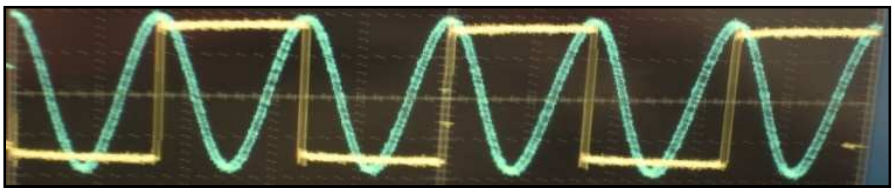

Fig. 5.8 The waveform of the RF carrier voltage and the switch control signal captured on screen when switching is at the maximum inductor current in DAM

The received current is captured and shown in the blue line in Fig. 5.9, with the theoretical prediction made from (5-9) and (5-10) overlaid in the same figure. The data pattern modulating

on the carrier can now be clearly identified. The theoretical results agree very well with the measured result.

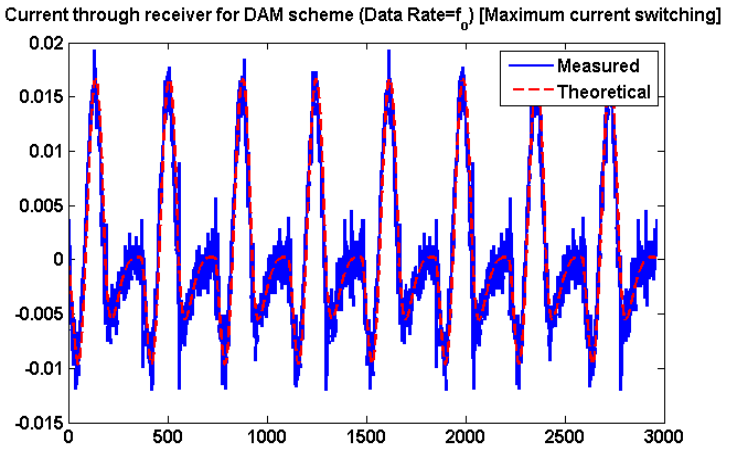

Fig.5.9. Measured and analytical receiver currents corresponding to the data stream 10101010 transmitted using DAM [Data rate= carrier frequency]

The spectrum of the receiver current through DFT is plotted in Fig. 5.10. The modulation tones on the two sides of the carrier tone are now clearly visible.

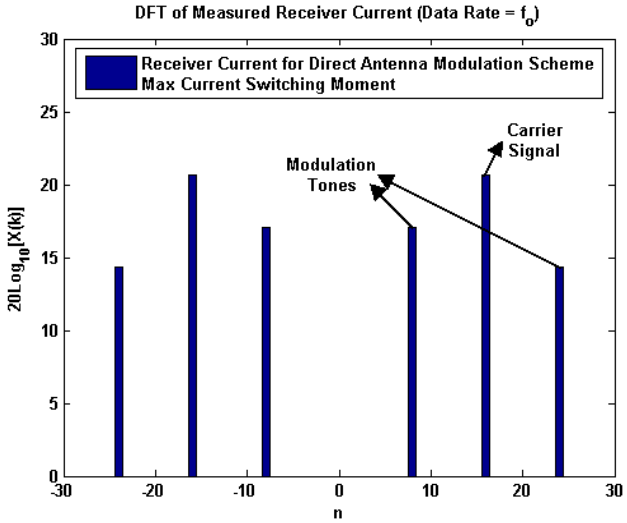

Fig. 5.10. Spectrum of the receiver current through DFT for DAM

The same experiment is carried out for different modulation data rates from $f_0/8$ to f_0 and the amplitudes of modulation tones in the received signal at those data rates are plotted in Fig. 5.11 for both the traditional and DAM schemes. For low data rates, both schemes show similar

performance. However, for higher data rates all the way to the carrier frequency, the link with DAM transmits the modulation information for up to 18dB stronger than the traditional scheme does, which indicates its potential for a better capacity performance.

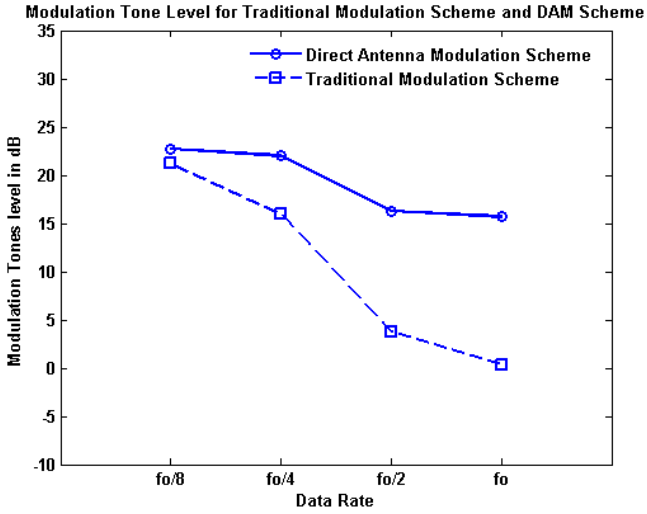

Fig. 5.11. Comparison of the modulation tone amplitudes versus different data rates for traditional modulation scheme and direct antenna modulation scheme

5.4 APPENDIX

5.4.1 Transmitter Current during Transmission of Bit '1'

As NFC link is typically established in weak coupling regime, the impact of receiver current on the transmitter impedance match is often neglected. The transmitter can thus be considered as a resonator in isolation and the current 'i_{t1}' through it can thus be calculated. The transmitter configuration during the transmission of bit '1' is the same for both traditional modulation and DAM. The equivalent circuit of the transmitter corresponding to the transmission of bit '1' is shown in Fig. A-1. Applying Kirchoff's voltage law in time-domain yields,

$$L_1 \frac{di_{t1}}{dt} + (R_s + R_{L1}) i_{t1} + \frac{1}{C_1} \int i_{t1}\, dt = 0 + V_s = 0 + V_o \cos(\omega_o t) \qquad \text{(A-1)}$$

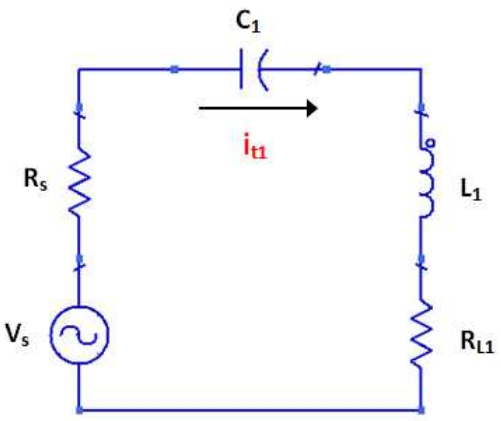

Fig.A-1 Equivalent circuit of transmitter during transmission of bit '1' for both DAM and Traditional modulation scheme

The solution of the differential equation (A-1) for 0 stimulus represents the natural response '$i_{t1,natural}$' of the system, while the solution to stimulus $V_o cos(\omega t)$ represents the forced response '$i_{t1,forced}$'. The total response is the superposition of both the natural and forced responses

$$i_{t1} = i_{t1,natural} + i_{t1,\,forced} \tag{A-2}$$

In Laplace transform domain, (A-1) for zero stimulus can be written as,

$$L_1 s^2 + (R_s + R_{L1})s + \frac{1}{C_1} = 0 \Rightarrow \left(\frac{s}{\omega_o}\right)^2 + \frac{s}{Q_t \omega_o} + 1 = 0 \tag{A-3}$$

where $\omega_o = 1/\sqrt{L_1 C_1} = 1/\sqrt{L_2 C_2}$ and $Q_t = \omega_o L_1/(R_s + R_{L1})$. The variables ω_o and Q_t are sufficient to capture the properties of a second order series LC resonant circuit. The roots of the quadratic equation (A-3) are

$$s = -\frac{\omega_o}{2Q_t} \pm j\omega_o \sqrt{1 - \frac{1}{(2Q_t)^2}} \approx -\frac{\omega_o}{2Q_t} \pm j\omega_o \;\; for\, Q_t >> 1 \tag{A-4}$$

The natural response of the system is thus

$$i_{t1,natural} = \left(A_1 e^{j\omega_o t} + A_2 e^{-j\omega_o t}\right) e^{-\frac{\omega_o t}{2Q_t}} \tag{A-5}$$

where A_1 and A_2 are the unknown coefficiencts determined by the intial conditions.

Equation (A-1) for the forced response can be written as,

$$L_1 \frac{d^2 i_{t1,\,forced}}{dt^2} + \left(R_s + R_{L1}\right)\frac{di_{t1,\,forced}}{dt} + \frac{1}{C_1} i_{t1,\,forced} = -\omega_o V_o \sin\left(\omega t\right) \tag{A-6}$$

Assuming $i_{t1,\,forced} = B_1 \cos\left(\omega_o t\right) + B_2 \sin\left(\omega_o t\right)$ and substituting the first and second derivatives of $i_{t1,forced}$ into (A-6) yields

$$B_1 = \frac{V_o}{\left(R_s + R_{L1}\right)}, B_2 = 0 \tag{A-7}$$

The forced response of the transmitter to a sinusoidal voltage during transmission of bit '1' is

$$i_{t1,\,forced} = \frac{V_o}{\left(R_s + R_{L1}\right)} \cos\left(\omega_o t\right) \tag{A-8}$$

The total response of the system is obtained by adding the natural response (A-5) and forced response (A-8),

$$i_{t1} = \left(A_1 e^{j\omega_o t} + A_2 e^{-j\omega_o t}\right) e^{-\frac{\omega_o t}{2Q_t}} + \frac{V_o}{\left(R_s + R_{L1}\right)} \cos\left(\omega_{\,o} t\right) \tag{A-9}$$

The corresponding voltage 'V_{Ct1}' across the capacitor 'C_1' during the transmission of bit 1, assuming $Q_t >> 1$, is

$$V_{C,t1} = \frac{1}{C_1}\left[\left(A_1 e^{j\omega_o t} - A_2 e^{-j\omega_o t}\right)\frac{1}{j\omega_o} e^{-\frac{\omega_o t}{2Q_t}} + \frac{V_o}{\omega_o\left(R_s + R_{L1}\right)} \sin\left(\omega_o t\right)\right] \tag{A-10}$$

The state variables here are the current through inductor i_{t1} and voltage across the capacitor V_{Ct1}. The initial circuit conditions of state variables are used to determine unknown coefficients A_1 and A_2.

Assume that switching is done at the maximum current instant. If '$i_{initial}$' is the current through the resonator at the switching moment for the next bit of information and the corresponding voltage 'V_{Ct1}' across the capacitor 'C_1' is zero, then the intial conditions of the transmitter resonator at the maximum current switching moment are

$$i_{t1}(0) = i_{initial} \quad , \quad V_{Ct1}(0) = 0 \tag{A-11}$$

The unknown coefficiencts A_1 and A_2 are determined by substituting initial conditions given by (A-11) into (A-9) and (A-10), yielding

$$A_1 = A_2 = \left(i_{initial} - \frac{V_o}{(R_s + R_{L1})} \right) / 2 \tag{A-12}$$

The current through the transmitter resonator corresponding to the data bit '1' is thus obtained by substituting coefficients A_1 and A_2 from (A-12) into (A-9)

$$i_{t1} = \left(i_{initial} - \frac{V_o}{(R_s + R_{L1})} \right) \cos(\omega_o t) e^{-\frac{\omega_o t}{2Q_t}} + \frac{V_o}{(R_s + R_{L1})} \cos(\omega_o t) \tag{A-13}$$

The first term and second term in (A-13) represent the natural response and forced response respectively.

5.4.2 Transmitter Current during Transmission of Bit '0'

5.4.2.1 Traditional Modulation Scheme

In the traditional modulation scheme, transmitter configuration remains same during the transmission of bit '1' and '0'. However, zero voltage source is a generalized short circuit, which leads to equivalent circuit of the transmitter shown in Fig. A-2 for the transmission of bit '0'. The transmitter current $i_{t0,TRAD}$ for bit '0' is thus described by the differential equation,

$$L_1 \frac{di_{t0,TRAD}}{dt} + (R_s + R_{L1}) i_{t0,TRAD} + \frac{1}{C_1} \int i_{t0,TRAD} \, dt = 0 \tag{A-14}$$

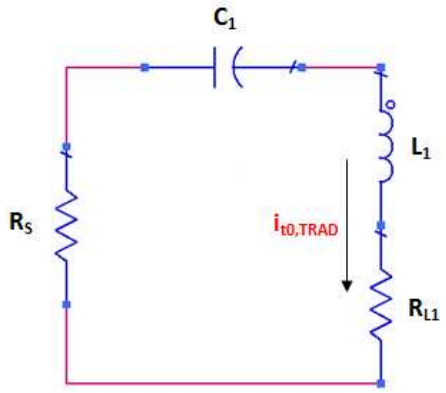

Fig.A-2 Equivalent circuit of transmitter during the transmission of bit '0' for traditional modulation scheme

The solution for the current contains only the natural response of the second order LC resonant circuit in (A-5),

$$i_{t0,TRAD} = \left(E_1 e^{j\omega_o t} + E_2 e^{-j\omega_o t}\right) e^{-\frac{\omega_o t}{2Q_t}} \tag{A-15}$$

The corresponding voltage $V_{Cto,TRAD}$ across the capacitor C_1 during transmission of bit '0', assuming $Q_t >> 1$, is

$$V_{Ct0,TRAD} = \frac{1}{C_1}\left[\left(E_1 e^{j\omega_o t} - E_2 e^{-j\omega_o t}\right)\frac{1}{j\omega_o} e^{-\frac{\omega_o t}{2Q_t}}\right] \tag{A-16}$$

Assuming that the switching action is performed at the maximum inductor current and zero capacitor voltage, the initial conditions at the switching instant are

$$i_{t0,TRAD}(0) = i_{initial} \quad , \quad V_{Ct0,TRAD}(0) = 0 \tag{A-17}$$

The initial conditions at the switching instant given by (A-17) are now substituted into (A-15) and (A-16) to determine the unknown coefficients 'E_1' and 'E_2', which leads to

$$i_{t0,TRAD} = i_{initial} \cos(\omega_o t) e^{-\frac{\omega_o t}{2Q_t}} \tag{A-18}$$

5.4.2.2 DAM Scheme

In DAM, during the transmission of bit '0', the inductor is short circuited, while the capacitor is disconnected from the circuit such that there is no closed loop path for the capacitor to discharge. Assuming that the switching is incurred at the maximum current moment, the inductor stores all the energy at the switching moment while the stored energy in the capacitor is zero. The equivalent circuit of DAM transmitter during the transmission of bit '0' is shown in Fig.A-3.

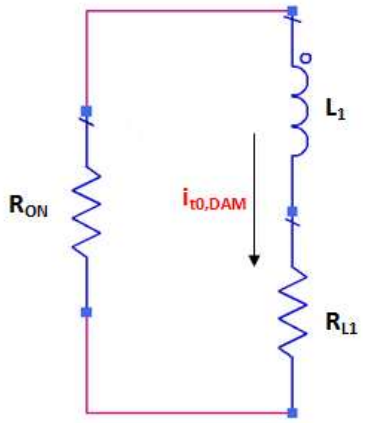

Fig.A-3 Equivalent circuit of transmitter during transmission of bit '0' for DAM Scheme

R_{ON} is the switch ON resistance. Ideally R_{ON} will be of very small value. The energy stored in the inductor will decrease exponentially during the transmission of bit '0' due to losses on coil and switch resistances. The transmitter current can be described by the differential equation

$$L_1 \frac{di_{t0,DAM}}{dt} + \left(R_{ON} + R_{L1}\right) i_{t0,DAM} = 0 \tag{A-19}$$

In Laplace domain (A-19) can be written as,

$$L_1 s + \left(R_s + R_{ON}\right) = 0 \tag{A-20}$$

which leads to the time-domain solution of the transmitter current for DAM,

$$i_{t0,DAM} = i_{initial} e^{-\frac{\omega_o t}{Q_{to}}} \tag{A-21}$$

where $i_{initial}$ is the current through the inductor at the switching instant, Q_{t0} is the quality factor of transmitter during the transmission of bit ‘0’, defined by $Q_{t0}=\omega_0 L_1/(R_{L1}+R_{ON})$.

CHAPTER 6

Resonant Coupling Efficiency Limit for Single and Multiple Receivers in a Wireless Power Transfer System

6.1 RCE LIMIT FOR SINGLE TRANSMITTER AND SINGLE RECEIVER BASED ON COUPLED MODE THEORY

The expression for the efficiency,η, based on the coupled mode theory [1-2] is

$$\eta = \frac{\frac{\Gamma_W K^2}{\Gamma_2 \Gamma_1 \Gamma_2}}{\left[\left(1+\frac{\Gamma_W}{\Gamma_2}\right)\frac{K^2}{\Gamma_1\Gamma_2}\right]+\left[\left(1+\frac{\Gamma_W}{\Gamma_2}\right)^2\right]} \tag{6-1}$$

where, $\Gamma_{2'} = overall\ decay\ rate\ at\ Load = \frac{\omega_o}{2Q_2} = \Gamma_2 + \Gamma_W$;

$$\Gamma_1 = Source\ Coil\ decay\ rate = \frac{\omega_o}{2Q_{1,int}}\ ;$$

$$\Gamma_2 = Load\ Coil\ decay\ rate = \frac{\omega_o}{2Q_{2,int}}\ ;$$

$$K = Coupling\ Factor = \frac{\omega_o}{2}\frac{M}{\sqrt{L_1 L_2}} = \frac{\omega_o}{2}\mathrm{k}$$

$Q_{1,int}$, and $Q_{2,int}$ are the intrinsic quality factors of source coil and load coil respectively, Q_2 is the loaded quality factors of load coil, ω_o is the operating frequency in radians, L_1 and L_2 are the self-inductances of source and load coils, M is the mutual inductance, and k is the coupling coefficient.

Assuming perfect matching at the source side, the load resistance which yields upper bound efficiency was given as

$$\frac{\Gamma_w}{\Gamma_2} = \sqrt{1 + \frac{K^2}{\Gamma_1 \Gamma_2}} \; i.e, \frac{R_L}{R_{L2}} = \sqrt{1 + k^2 Q_{1,int} Q_{2,int}} = \sqrt{1 + \frac{(\omega_o M)^2}{R_{L1} R_{L2}}} \qquad (6\text{-}2)$$

Here, R_L, R_{L1}, and R_{L2} are the load, source coil and load coil resistances respectively. Impedance matching was achieved by varying the coupling coefficients K_S and K_D at source and load respectively, using the 4-coil configuration shown in Fig. 6.1.

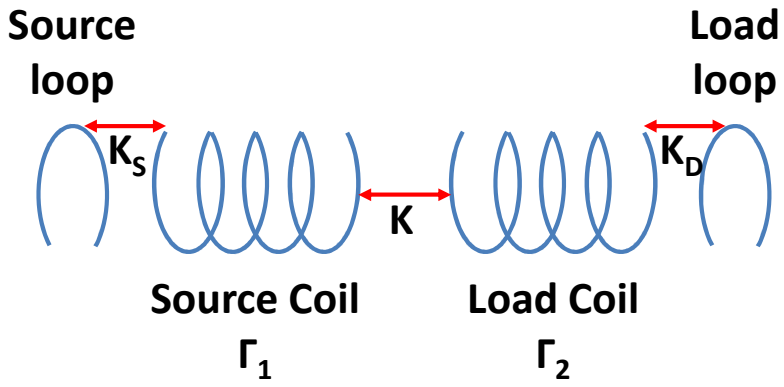

Fig. 6.1. An inductively coupled WPT system consisting of loop-coil at both source and load side (4-coil configuration)

6.2 RCE Limit for Single Transmitter and Single Receiver based on Equivalent Circuit Model

6.2.1 Resonant Coupling Efficiency (RCE)

Resonant coupling efficiency (RCE) for a single transmitter and receiver is obtained by dividing received power expression (3-11) by transmitter power.

$$\eta = \frac{P_r}{P_t} = \frac{4(\omega_o M)^2 R_S R_L}{[(R_S + R_{L1})(R_L + R_{L2}) + (\omega_o M)^2]^2} \qquad (6\text{-}3)$$

6.2.2 Input and Output Impedances

Using (3-9), current i_2 in the receiver resonator is expressed as a function of current i_1 flowing in the transmitter resonator,

$$i_2 = \frac{j\omega_o M i_1}{(R_L+R_{L2})} \tag{6-4}$$

Input Impedance seen by the source R_{source} is calculated by substituting i_2 from (6-4) into (3-9) and calculating V_s/i_1

$$-V_s + i_1(R_s + R_{L1}) + \frac{(\omega_o M)^2 i_1}{(R_L+R_{L2})} = 0 \tag{6-5}$$

$$R_{source} = \frac{V_s}{i_1} - R_s = R_{L1} + \frac{(\omega_o M)^2}{R_L+R_{L2}} \tag{6-6}$$

Similarly, it can be proved that output impedance seen by the load R_{Rx} is

$$R_{Rx} = R_{L2} + \frac{(\omega_o M)^2}{R_s+R_{L1}} \tag{6-7}$$

6.2.3 Optimal RCE and Conditions to Achieve Optimal RCE

The efficiency expression (6-3) is differentiated with respect to source and load resistance R_S and R_L and the derivatives are set to zero to obtain source and load resistance values that yield maximum efficiency.

$$\frac{\partial \eta}{\partial R_s} = \frac{[(R_s + R_{L1})(R_L + R_{L2}) + (\omega_o M)^2]^2 4(\omega_o M)^2 R_L}{[(R_s + R_{L1})(R_L + R_{L2}) + (\omega_o M)^2]^4} -$$
$$\frac{4(\omega_o M)^2 R_S R_L 2\left[(R_S+R_{L1})(R_L+R_{L2})+(\omega_o M)^2\right](R_L+R_{L2})}{[(R_S+R_{L1})(R_L+R_{L2})+(\omega_o M)^2]^4} \tag{6-8}$$

Setting the derivative to zero yields,

$$\frac{\left[(R_S+R_{L1})(R_L+R_{L2})+(\omega_o M)^2\right]4(\omega_o M)^2 R_L - 8(\omega_o M)^2 R_S R_L (R_L+R_{L2})}{[(R_S+R_{L1})(R_L+R_{L2})+(\omega_o M)^2]^3} = 0 \tag{6-9}$$

The source resistance which gives optimal efficiency is

$$R_s = R_{L1} + \frac{(\omega_o M)^2}{(R_L + R_{L2})} \tag{6-10}$$

Similarly, it can be shown that load resistance which leads to optimal efficiency is

$$R_L = R_{L2} + \frac{(\omega_o M)^2}{(R_s + R_{L1})} \tag{6-11}$$

Equation (6-10) and (6-11) show that source and load resistances which yield optimal efficiency are same as the input and output impedance seen by source and load respectively.

Source and load resistances can be written as a function of mutual inductance *M* and coil resistances R_{L1} and R_{L2} only, by simultaneously solving (6-10) and (6-11). Using (6-10),

$$R_L + R_{L2} = \frac{(\omega_o M)^2}{(R_s - R_{L1})} \tag{6-12}$$

Substituting load resistance for optimal efficiency given by (6-11) into (6-12) yields

$$2R_{L2} = \frac{(\omega_o M)^2}{(R_s - R_{L1})} - \frac{(\omega_o M)^2}{(R_s + R_{L1})} \tag{6-13}$$

$$R_S = R_{L1}\sqrt{1 + \frac{(\omega_o M)^2}{R_{L1} R_{L2}}} \tag{6-14}$$

Similarly, it can be shown that

$$R_L = R_{L2}\sqrt{1 + \frac{(\omega_o M)^2}{R_{L1} R_{L2}}} \tag{6-15}$$

For coils having different coil resistances the ratio of source and load resistances R_S/R_L should be same as the ratio of respective coil resistances R_{L1}/R_{L2},

$$\frac{R_S}{R_L} = \frac{R_{L1}}{R_{L2}} \tag{6-16}$$

Furthermore, the ratio of source to source coil resistance (R_S/R_{L1}), load to load coil resistances (R_L/R_{L2}) should be same and equal to the value specified in (6-17) to provide optimal efficiency for a wireless power transfer system consisting of single transmitter and receiver,

$$\frac{R_S}{R_{L1}} = \frac{R_L}{R_{L2}} = \sqrt{1 + \frac{(\omega_o M)^2}{R_{L1}R_{L2}}} = \sqrt{1 + k^2 Q_{1int} Q_{2int}} \tag{6-17}$$

The load impedance which results in optimal efficiency performance given by (6-17) is equal to the load impedance derived based on coupled mode theory in (6-2).

The corresponding optimum efficiency under simultaneous impedance match at source and load is then

$$\eta_{opt} = \frac{1}{\left[\sqrt{\left(1+\frac{1}{k^2 Q_{1int} Q_{2int}}\right)}+\frac{1}{k\sqrt{Q_{1int} Q_{2int}}}\right]^2} \tag{6-18}$$

6.2.4 Comparison of Optimal RCE derived based on Coupled Mode Theory and Equivalent Circuit Model

The optimal efficiency expression based on equivalent circuit model (6-18) is compared against the efficiency derived based on coupled mode theory given by (6-1), when load impedance satisfies (6-2), in Fig. 6.2. It is observed that upper bound on efficiency derived based on coupled mode theory is same as that derived using equivalent circuit model. For a certain coupling between coils with a given quality factor, this curve sets the limit on maximum achievable efficiency.

Optimal efficiency is plotted versus $k\sqrt{Q_{1int}Q_{2int}}$, which is equal to $\omega_o M/\sqrt{R_{L1}R_{L2}}$ in Fig. 6.2. As seen, the higher the value of $\omega_o M/\sqrt{R_{L1}R_{L2}}$, the higher is efficiency. This is why coils used in wireless power transfer are preferred to have very small loss resistance. Therefore, the equivalent series resistance (ESR) of the capacitors used to resonate the system, or any additional resistances introduced due to interconnecting wires and solder will lower the system efficiency. Efficiency is degraded more when the system is operating at lower $\omega_o M/\sqrt{R_{L1}R_{L2}}$

values. As an example, assume that coils are designed such that $\omega_o M/\sqrt{R_{L1}R_{L2}}$= 4; then looking at Fig. 6.2 the maximum efficiency is expected to be 60%. However, if ESR of capacitor, possible interconnects, and soldering on both transmitter and receiver add resistance equal to the coil resistance, then the value of $\omega_o M/\sqrt{R_{L1}R_{L2}}$ drops from 4 to 2, and the corresponding efficiency drops from 60% to 40%.

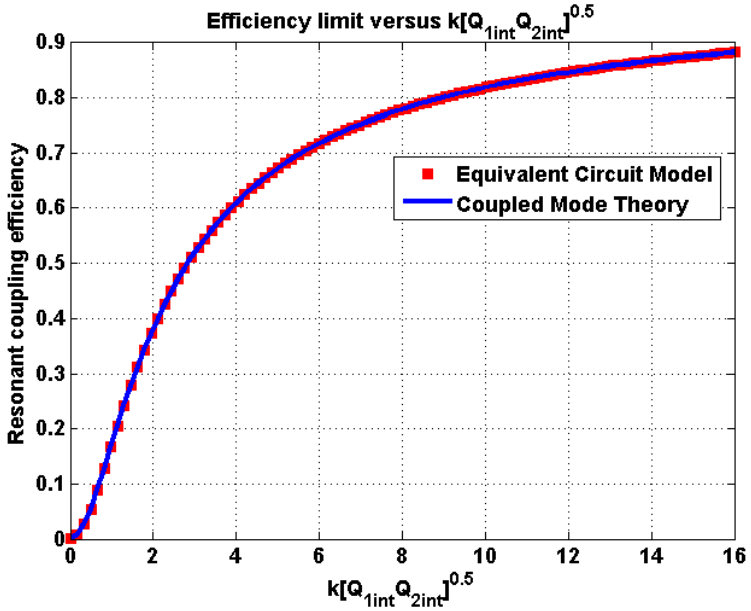

Fig. 6.2. Comparison of efficiency limit for a wireless power transfer system consisting of single transmitter and receiver derived using coupled mode theory and equivalent circuit model.

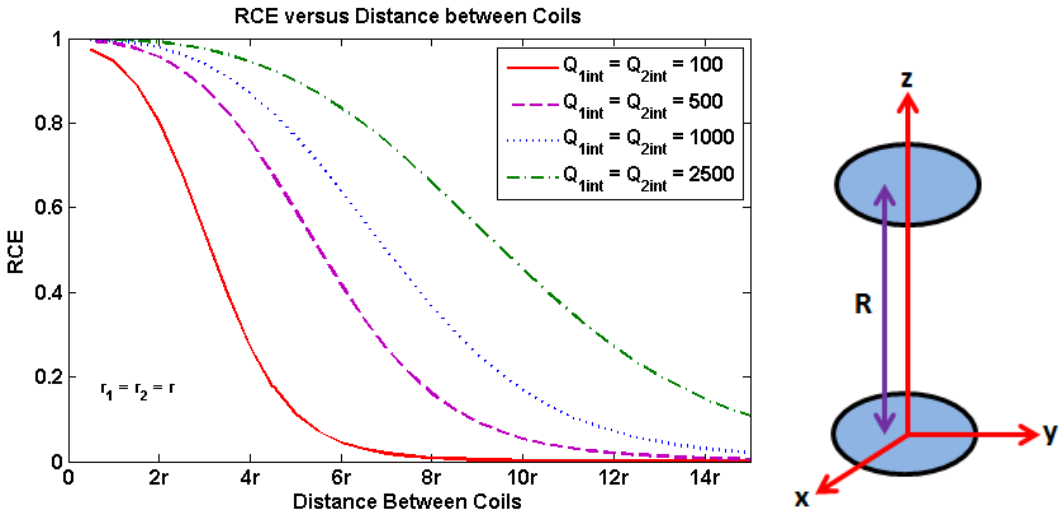

Fig.6.3 Optimal RCE versus distance for perfectly aligned coils

The coupling coefficient between the co-axially aligned coils is given by (3-6). Using (3-6) and (6-18), optimal RCE, under the condition of simultaneous impedance match at source and load, is plotted for two co-axially aligned coils of equal radii versus the spacing *R* between the coils, for realistic values of intrinsic quality factor of coils in Fig. 6.3.

6.3 TUNING MECHANISM FOR OPTIMAL RCE PERFORMANCE IN 2-COIL AND 4-COIL CONFIGURATIONS

The mutual inductance between source and load coil changes as the distance between the two coils changes. Effectively, impedances seen by the source (6-6) and the load (6-7) change. A dynamic impedance matching network is required to match the source and load resistance, R_S and R_L, to varying input impedances R_{source} and R_{Rx} respectively.

6.3.1 Impedance Matching Technique for 2-Coil Configuration

In a 2-coil configuration, a transformer with variable turn ratio can be inserted between source and source coil, load and load coil respectively as shown in Fig. 6.4 to provide dynamic impedance matching capability.

6.3.2 Impedance Matching Technique for 4-Coil Configuration

A 4-coil configuration is analyzed based on equivalent circuit model, shown in Fig. 6.5, in [18]. The ratio of load voltage V_{Load} to source voltage V_{Source} for the same source and load resistances, and the same coil and loop parameters at both source and load side is

$$\left|\frac{V_{Load}}{V_{Source}}\right| = \frac{\omega^3 k_{lc}^2 k_{cc} L_{coil}^2 L_{loop} R_{load}}{\left[\begin{array}{c} k_{lc}^4 L_{coil}^2 L_{loop}^2 \omega^4 + Z_{coil}^2 Z_{loop}^2 + \\ \omega^2\left(2k_{lc}^2 L_{loop} L_{coil} Z_{loop} Z_{loop} + k_{cc}^2 L_{coil}^2 Z_{loop}^2\right) \end{array}\right]} \quad (6\text{-}19)$$

Fig. 6.4 Impedance matching scheme for 2-coil configuration: Impedance transformers with variable turn ratios

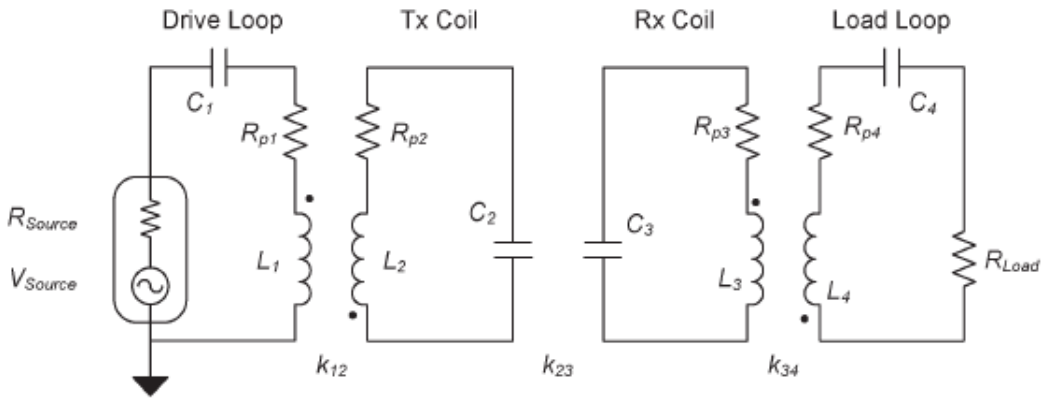

Fig. 6.5 Equivalent circuit model of 4-coil WPT system (Each antenna is modeled as series resonator)

where,

$$Z_{loop} = R_{source}(or\ R_{Load}) + R_{loop} + j\omega L_{loop} - \frac{j}{\omega C_{loop}}$$

$$Z_{coil} = R_{coil} + j\omega L_{coil} - \frac{j}{\omega C_{coil}}$$

$$k_{12} = k_{34} = k_{lc}\ \ and\ k_{23} = k_{cc}$$

6.3.2.1 Frequency Tuning

If the coupling between loop and coil k_{lc} is stronger than the critical coupling value $k_{critical}$, then the system is said to be over-coupled and frequency tuning can be done to achieve optimal performance.

$$k_{critical} = \frac{1}{Q_{coil}} + k_{lc}^2 Q_{loop} \qquad (6\text{-}20)$$

and the corresponding optimal RCE at the critical coupling point is

$$\eta_{FrequencyTuning} = \left(\frac{1}{1+\frac{1}{k_{lc}^2 Q_{loop} Q_{coil}}} \right)^2 \quad (6\text{-}21)$$

6.3.2.2 Coupling Tuning

However, frequency tuning might not be a very practical option if the wireless power transfer frequency band is narrow. Alternatively in 4-coil configuration, optimal RCE can also be achieved by varying the coupling between the loop and the coil in order to provide an impedance match. If the applied frequency is same as the resonant frequency of the circuit and $R_{load} >> R_{loop}$, then the ratio of load to source voltage is

$$\left| \frac{V_{Load}}{V_{Source}} \right|_{\omega=\omega_0} = \frac{k_{lc}^2 k_{cc} Q_{coil}^2 Q_{loop}}{\left[k_{cc}^2 Q_{coil}^2 + (1+k_{lc}^2 Q_{loop} Q_{coil})^2 \right]} \quad (6\text{-}22)$$

The optimum coil-loop coupling coefficient that yields optimal RCE is obtained by differentiating (6-22) with respect to k_{lc} and setting the derivative to zero

$$\left[k_{cc}^2 Q_{coil}^2 + (1 + k_{lc}^2 Q_{loop} Q_{coil})^2 \right] 2 k_{lc} k_{cc} Q_{coil}^2 Q_{loop} - k_{lc}^2 k_{cc} Q_{coil}^2 Q_{loop} \left(4\, k_{lc} Q_{coil} Q_{loop} \right) \left(1 + k_{lc}^2 Q_{loop} Q_{coil} \right) = 0 \quad (6\text{-}23)$$

$$2 k_{lc} {k_{cc}}^3 Q_{coil}^4 Q_{loop} + (1 + k_{lc}^2 Q_{loop} Q_{coil}) \left(2 k_{lc} k_{cc} Q_{coil}^2 Q_{loop} - 2 k_{lc}^3 k_{cc} Q_{coil}^3 Q_{loop}^2 \right) = 0 \quad (6\text{-}24)$$

$$2 k_{lc} {k_{cc}}^3 Q_{coil}^4 Q_{loop} + 2 k_{lc} k_{cc} Q_{coil}^2 Q_{loop} \left(1 - \left[k_{lc}^2 Q_{loop} Q_{coil} \right]^2 \right) = 0 \quad (6\text{-}25)$$

$${k_{cc}}^2 Q_{coil}^2 + (1 - {k_{lc}}^4 Q_{coil}^2 Q_{loop}^2) = 0 \quad (6\text{-}26)$$

$$\frac{1}{Q_{loop}} \sqrt{{k_{cc}}^2 + \frac{1}{Q_{coil}^2}} = {k_{lc,optimum}}^2 \quad (6\text{-}27)$$

The corresponding optimal RCE achieved by varying the coupling between loop and coil in a 4-coil configuration is expressed by substituting the optimum loop-coil coupling factor $k_{lc,optimum}$ given by (6-27) into (6-22),

$$\eta_{(k_{lc}tuning)} = \frac{1}{\left[\frac{1}{k_{cc}Q_{coil}} + \sqrt{1+\frac{1}{k_{cc}{}^2 Q_{coil}^2}}\right]^2} \tag{6-28}$$

The optimal RCE (6-28) derived for 4-coil configuration, assuming same source and load coils and loops parameters, is exactly same as RCE limit provided for 2-coil configuration in (6-18). Hence, in 4-coil configuration, optimal RCE performance can be achieved by varying the loop-coil coupling which has the same effect as varying the turn ratio of impedance matching transformer in 2-coil configuration. However, variable loop-coil coupling tuning in 4-coil configuration requires a mechanism to mechanically displace coils to vary coupling between them.

6.3.2.3 Comparison of frequency tuning and coupling tuning

In order to compare performance of a 4-coil WPT system which has frequency retuning capability to a system which has loop-coil coupling coefficient tuning capability, the parameters assumed for source and load are given in table 6.1.

Component	Value	Component	Value
$\mathbf{L_{loop}}$	0.965 uH	$\mathbf{L_{coil}}$	39.1 uH
$\mathbf{C_{loop}}$	449.8 pF	$\mathbf{C_{coil}}$	11.04 pF
$\mathbf{R_{loop}}$	0.622 Ohms	$\mathbf{R_{coil}}$	6.19 Ohms
$\mathbf{R_{source}}$	50 Ohms	$\mathbf{R_{load}}$	50 Ohms
$\mathbf{Q_{loop}}$	0.91	$\mathbf{Q_{coil}}$	304.3
$\mathbf{f_o}$	7.65 MHz	$\mathbf{f_o}$	7.65 MHz

Table 6.1. Loop and coil parameters for comparing loop-coil coupling tuning and frequency tuning

The performance of frequency tuning for different loop-coil coupling values is compared against the loop-coil coupling tuning for 4-coil configuration in Fig. 6.6.

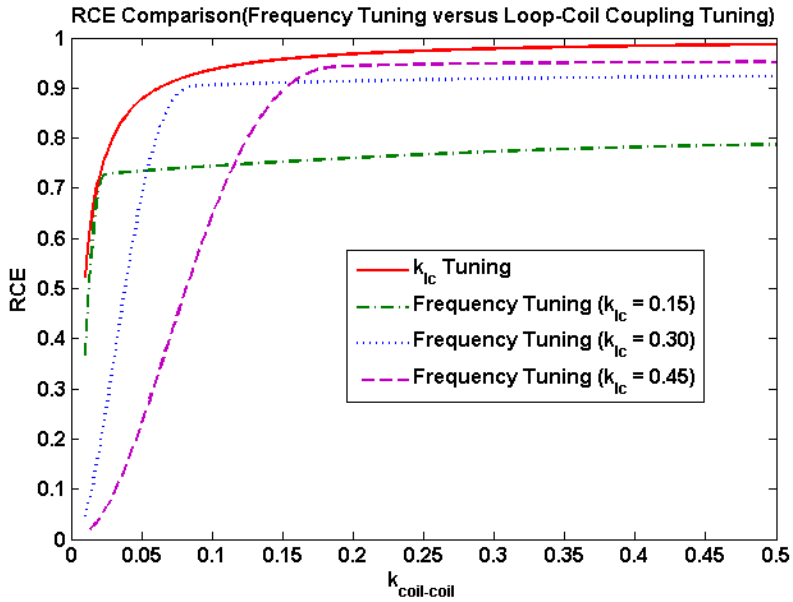

Fig. 6.6. Optimal RCE comparison for frequency tuning and Loop-Coil coupling coefficient tuning

6.4 RCE LIMIT FOR SINGLE TRANSMITTER AND TWO RECEIVERS

The RCE limit is now evaluated for a WPT system consisting of two receivers. Both the receivers are coupled to the transmitter; however for simplicity, coupling between receivers is assumed to be negligibly small. This is the case when there is a large transmitter and small receivers or small receivers on opposite side of the transmitter, as shown in Fig. 6.7

6.4.1 Impedance seen by Source and Loads

A wireless power transfer system consisting of a single transmitter and two non-coupled receivers can be represented in the matrix form given below,

$$\begin{bmatrix} R_s + R_{L1} & j\omega M_{12} & j\omega M_{13} \\ j\omega M_{12} & R_2 + R_{L2} & 0 \\ j\omega M_{13} & 0 & R_3 + R_{L3} \end{bmatrix} \begin{bmatrix} i_1 \\ i_2 \\ i_3 \end{bmatrix} = \begin{bmatrix} v_s \\ 0 \\ 0 \end{bmatrix} \quad (6\text{-}29)$$

where, R_s, R_2, R_3 are source and load's resistances, R_{L1}, R_{L2}, R_{L3} are source and load coil resistances, M_{12} and M_{13} are mutual inductances between source coil and first receiver coil, and second receiver coil respectively. The current through the transmitter and two receivers is i_1, i_2 and i_3 respectively. The input impedance seen by transmitter and receivers is

$$R_{source} = (R_{L1}) + \frac{(\omega M_{12})^2}{(R_{L2}+R_2)} + \frac{(\omega M_{13})^2}{(R_{L3}+R_3)} \tag{6-30}$$

$$R_{Rx2} = (R_{L2}) + \frac{(\omega M_{12})^2}{(R_{L1}+R_s)+\frac{(\omega M_{13})^2}{(R_{L3}+R_3)}} \tag{6-31}$$

$$R_{Rx3} = (R_{L3}) + \frac{(\omega M_{13})^2}{(R_{L1}+R_s)+\frac{(\omega M_{12})^2}{(R_{L2}+R_2)}} \tag{6-32}$$

We report that it is not possible to simultaneously match the transmitter and both receivers. Under low loss assumption i.e., $R_s >> R_{L1}$, $R_2 >> R_{L2}$ and $R_3 >> R_{L3}$, and matching the impedance seen by the receivers to their respective loads i.e., $R_{Rx2} = R_2$ and $R_{Rx3} = R_3$ in (6-31) and (6-32)

$$R_2 = \frac{(\omega M_{12})^2}{R_s+\frac{(\omega M_{13})^2}{R_3}} \xrightarrow{yields} (\omega M_{12})^2 = R_2\left(R_s + \frac{(\omega M_{13})^2}{R_3}\right) \tag{6-33}$$

$$R_3 = \frac{(\omega M_{13})^2}{R_s+\frac{(\omega M_{12})^2}{R_2}} \xrightarrow{yields} (\omega M_{13})^2 = R_3\left(R_s + \frac{(\omega M_{12})^2}{R_2}\right) \tag{6-34}$$

Now, substituting the conditions (6-32) and (6-33) for impedance matching at receivers into (6-30)

$$R_{source} = 2R_s + \frac{(\omega M_{12})^2}{R_2} + \frac{(\omega M_{13})^2}{R_3} \neq R_s \tag{6-35}$$

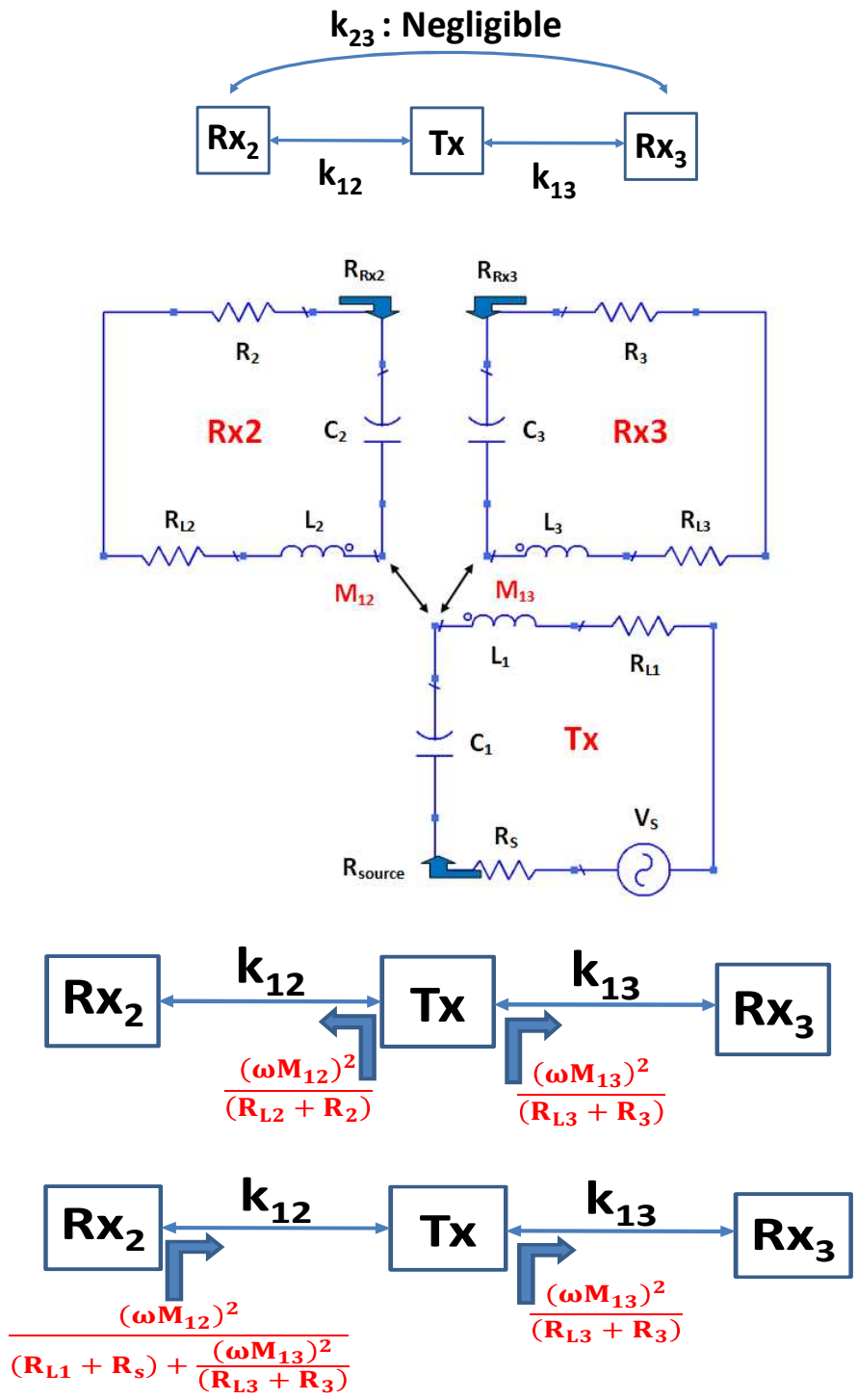

Fig.6.7. Single transmitter and two receivers with negligible mutual coupling, Equivalent circuit model, Impedance seen by the source, and Impedance seen by receiver R_{x2}

This clearly shows that if the loads are matched then the source cannot be matched simultaneously. Either source will be matched or two receivers will be matched. For practical

reasons and because the power levels at the transmitter are multiple times those at the receiver, any mismatch at the source side will lead to excessive heat generation. On the other hand a mismatched receiver will not receive power. Therefore, to maximize efficiency we assumed that source is matched to the input impedance (6-30) and found the load impedances which lead to optimal efficiency.

6.4.2 Efficiency expression for each receiver and total efficiency

The efficiency for receivers Rx2 and Rx3 using matrix model in (6-29) are

$$\eta_{21} = \frac{4(\omega M_{12})^2 R_s R_2}{\left[(R_s+R_{L1})(R_2+R_{L2})+(\omega M_{12})^2+\frac{(R_2+R_{L2})(\omega M_{13})^2}{(R_3+R_{L3})}\right]^2} \tag{6-36}$$

$$\eta_{31} = \frac{4(\omega M_{13})^2 R_s R_3}{\left[(R_s+R_{L1})(R_3+R_{L3})+(\omega M_{13})^2+\frac{(R_3+R_{L3})(\omega M_{12})^2}{(R_2+R_{L2})}\right]^2} \tag{6-37}$$

Matching the source resistance R_S to the input impedance seen at the source port R_{source}, efficiency expressions given by (6-36) and (6-37) can be written as

$$\eta_{21} = \frac{\alpha}{\alpha+1}\left(\frac{1}{1+\frac{\alpha+1}{{k_{12}}^2 Q_{1int}Q_{2int}}+\left(\frac{\alpha+1}{\beta+1}\right)\left(\frac{{k_{13}}^2 Q_{1int}Q_{3int}}{{k_{12}}^2 Q_{1int}Q_{2int}}\right)}\right) \tag{6-38}$$

$$\eta_{31} = \frac{\beta}{\beta+1}\left(\frac{1}{1+\frac{\beta+1}{{k_{13}}^2 Q_{1int}Q_{3int}}+\left(\frac{\beta+1}{\alpha+1}\right)\left(\frac{{k_{12}}^2 Q_{1int}Q_{2int}}{{k_{13}}^2 Q_{1int}Q_{3int}}\right)}\right) \tag{6-39}$$

$$where\ \alpha = \frac{R_2}{R_{L2}}, \beta = \frac{R_3}{R_{L3}}$$

$$Q_{1int} = \frac{\omega L_1}{R_{L1}}, Q_{2int} = \frac{\omega L_2}{R_{L2}}, Q_{3int} = \frac{\omega L_3}{R_{L3}}$$

The total efficiency is obtained by adding the efficiencies at Rx2 and Rx3,

$$\eta_{total} = \eta_{21} + \eta_{31} \tag{6-40}$$

6.4.3 Optimal RCE for Single Transmitter and Two Receivers

Total efficiency expression given by (6-40) is differentiated w.r.t α and β and derivative is set to zero. Two equations are simultaneously solved and values of α and β which yield optimal efficiency performance are

$$\alpha_{best} = \beta_{best} = \sqrt{1 + {k_{12}}^2 Q_{1int} Q_{2int} + {k_{13}}^2 Q_{1int} Q_{3int}} \tag{6-41}$$

Substituting α and β for optimal efficiency performance into (6-30),

$$\frac{R_S}{R_{L1}} = \frac{R_2}{R_{L2}} = \frac{R_3}{R_{L3}} = \sqrt{1 + {k_{12}}^2 Q_{1int} Q_{2int} + {k_{13}}^2 Q_{1int} Q_{3int}} \tag{6-42}$$

Hence optimal efficiency is obtained when the ratio of source resistance to source coil resistance, and ratio of load resistances to their respective coil resistances are same and equal to the value specified in (6-42) which is consistent with the observation for a wireless power transfer system consisting of a single transmitter and receiver. The corresponding efficiencies at two receivers are

$$\eta_{21} = \frac{\sqrt{1 + {k_{12}}^2 Q_{1int} Q_{2int} + {k_{13}}^2 Q_{1int} Q_{3int}}}{\sqrt{1 + {k_{12}}^2 Q_{1int} Q_{2int} + {k_{13}}^2 Q_{1int} Q_{3int}} + 1} \times \frac{1}{1 + \frac{\sqrt{1 + {k_{12}}^2 Q_{1int} Q_{2int} + {k_{13}}^2 Q_{1int} Q_{3int}} + 1}{{k_{12}}^2 Q_{1int} Q_{2int}} + \left(\frac{{k_{13}}^2 Q_{1int} Q_{3int}}{{k_{12}}^2 Q_{1int} Q_{2int}}\right)} \tag{6-43}$$

$$\eta_{31} = \frac{\sqrt{1 + {k_{12}}^2 Q_{1int} Q_{2int} + {k_{13}}^2 Q_{1int} Q_{3int}}}{\sqrt{1 + {k_{12}}^2 Q_{1int} Q_{2int} + {k_{13}}^2 Q_{1int} Q_{3int}} + 1} \times$$

$$\frac{1}{1 + \frac{\sqrt{1 + {k_{12}}^2 Q_{1int} Q_{2int} + {k_{13}}^2 Q_{1int} Q_{3int}} + 1}{{k_{13}}^2 Q_{1int} Q_{3int}} + \left(\frac{{k_{12}}^2 Q_{1int} Q_{2int}}{{k_{13}}^2 Q_{1int} Q_{3int}}\right)} \quad (6\text{-}44)$$

6.4.4 Validation of Optimal RCE Expression using ADS

In order to validate the results, efficiency at Rx_2 and Rx_3, and total efficiency given by (6-43), (6-44) and (6-40) respectively are plotted under optimal source and load conditions given by (6-42), for a fixed coupling between transmitter and Rx_3 in Fig. 6.8(b). Coupling between transmitter and Rx_2 is varied as shown in Fig. 6.8(a). The efficiencies are also calculated from equivalent circuit model in ADS software and the theoretical and simulated (ADS) results exactly correspond to each other. It is observed that if one of the receivers is coupled much strongly to the transmitter compared to the other receiver, then almost all the power goes to the strongly coupled receiver. When both the receives are equally coupled to the transmitter, then they share the received power equally.

6.4.5 Optimal RCE Contours

Efficiency contours are plotted for efficiency at Rx2, Rx3 and total efficiency in Fig. 6.9(a), (b) and (c) respectively. The vertical and horizontal axis represent the varying coupling between transmitter and Rx2, and transmitter and Rx3 respectively. It is observed that if Rx2 is strongly coupled to Tx compared to Rx3, then most of the transmitter power is coupled to Rx2. Conversely, if Rx3 is strongly coupled to Tx compared to Rx2, then most of the transmitter

power is coupled to Rx3. The total power coupled, which is sum of power coupled to receivers, increases if both the receivers are strongly coupled to the transmitter.

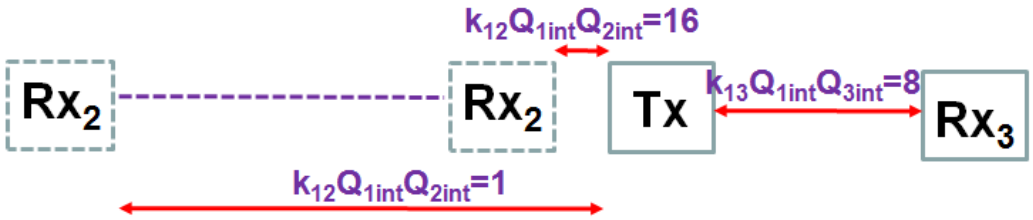

(a)

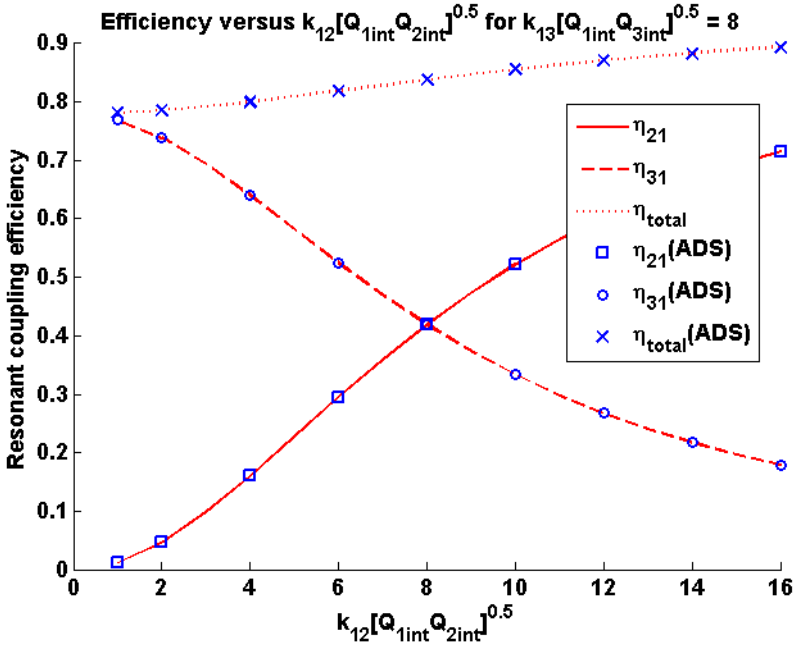

(b)

Fig.6.8. Efficiency for single transmitter and two receivers using ADS and equations.

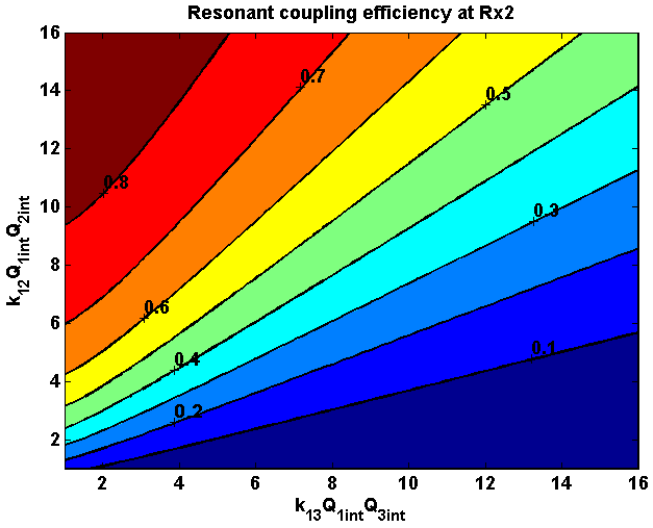

(a)

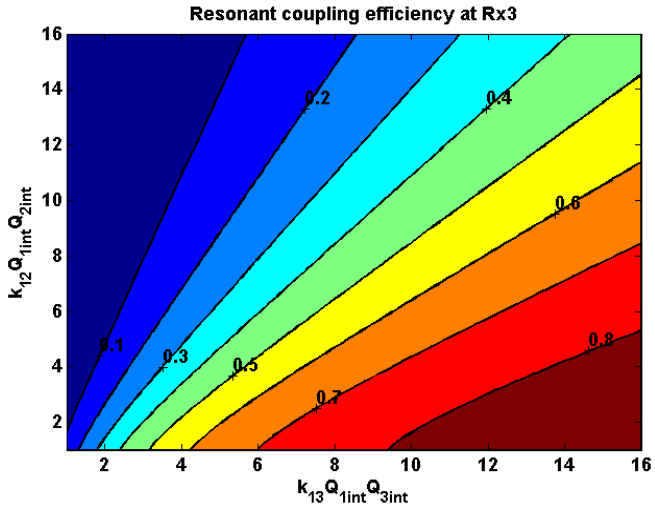

(b)

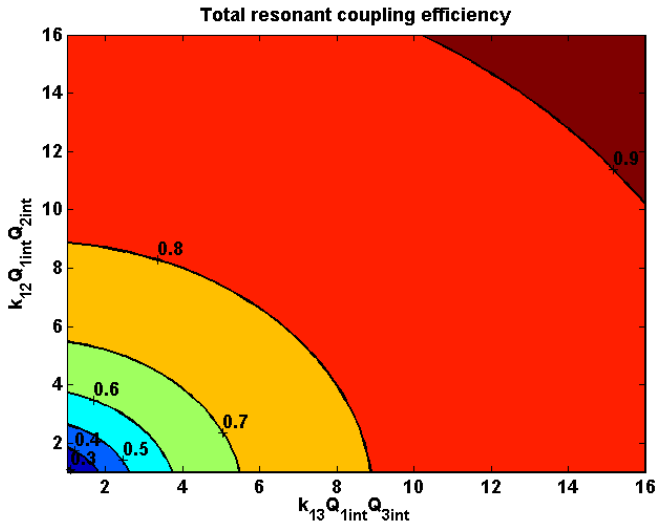

(c)

Fig.6.9. Efficiency at (a)Rx2 (b) Rx3 (c) Total efficiency.

6.5 RCE LIMIT FOR SINGLE TRANSMITTER AND MULTIPLE RECEIVERS

The efficiency analysis can be extended to multiple receivers, which are coupled directly to the transmitter and their mutual couplings are ignored. Such a wireless power transfer system consisting of single transmitter and (n-1) non-coupled receivers is shown in Fig. 6.10.

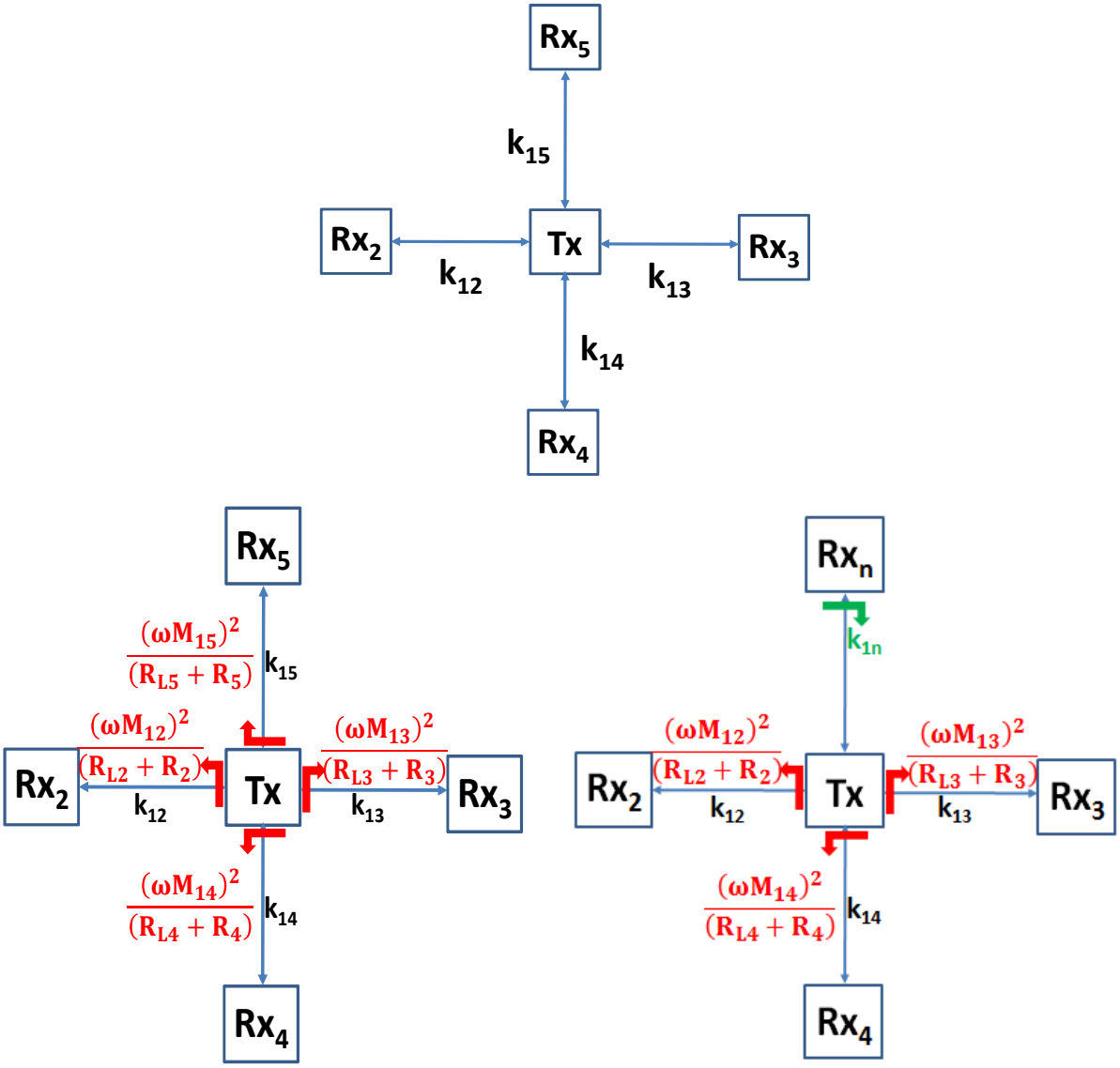

Fig 6.10. Wireless power transfer system consisting of single transmitter and multiple non-coupled receivers and impedance seen by source and loads

6.5.1 Impedance seen by Source and Loads

The input impedance seen by transmitter and receivers is

$$R_{source} = R_{L1} + \frac{(\omega M_{12})^2}{(R_{L2}+R_2)} + \frac{(\omega M_{13})^2}{(R_{L3}+R_3)} + \cdots + \frac{(\omega M_{1n})^2}{(R_{L3}+R_n)} \tag{6-45}$$

$$R_{Rx2} = R_{L2} + \frac{(\omega M_{12})^2}{(R_{L1}+R_s)+\frac{(\omega M_{13})^2}{(R_{L3}+R_3)}+\frac{(\omega M_{14})^2}{(R_{L4}+R_4)}+\cdots+\frac{(\omega M_{1n})^2}{(R_{Ln}+R_n)}} \tag{6-46}$$

$$R_{Rx3} = R_{L3} + \frac{(\omega M_{13})^2}{(R_{L1}+R_S)+\frac{(\omega M_{12})^2}{(R_{L2}+R_2)}+\frac{(\omega M_{14})^2}{(R_{L4}+R_4)}+\cdots+\frac{(\omega M_{1n})^2}{(R_{Ln}+R_n)}} \tag{6-47}$$

$$\vdots$$

$$R_{Rxn} = R_{Ln} + \frac{(\omega M_{1n})^2}{(R_{L1}+R_S)+\frac{(\omega M_{12})^2}{(R_{L2}+R_2)}+\frac{(\omega M_{13})^2}{(R_{L3}+R_3)}+\cdots+\frac{\left(\omega M_{1(n-1)}\right)^2}{\left(R_{L(n-1)}+R_{(n-1)}\right)}} \tag{6-48}$$

6.5.2 Optimal RCE for Single Transmitter and Multiple Receivers

The optimal efficiency is obtained when the transmitter and load resistances follow the following criteria,

$$\frac{R_s}{R_{L1}} = \frac{R_2}{R_{L2}} = \frac{R_3}{R_{L3}} = \cdots = \frac{R_n}{R_{Ln}} = \gamma = \sqrt{1 + {k_{12}}^2 Q_{1int} Q_{2int} + {k_{13}}^2 Q_{1int} Q_{3int} + \cdots + {k_{1n}}^2 Q_{1int} Q_{nint}} \tag{6-49}$$

The ratio of source resistance to source coil resistance should be equal to the ratio of load resistances to corresponding load coil resistances. The efficiency expressions for each receiver under optimal efficiency conditions at source and loads are

$$\eta_{21} = \frac{\gamma}{\gamma+1}\left(\frac{1}{\frac{\gamma+1}{{k_{12}}^2 Q_{1int} Q_{2int}}+\left(\frac{{k_{12}}^2 Q_{1int} Q_{2int}}{{k_{12}}^2 Q_{1int} Q_{2int}}\right)+\cdots+\left(\frac{{k_{1n}}^2 Q_{1int} Q_{nint}}{{k_{12}}^2 Q_{1int} Q_{2int}}\right)}\right) \tag{6-50}$$

$$\eta_{31} = \frac{\gamma}{\gamma+1}\left(\frac{1}{\frac{\gamma+1}{{k_{13}}^2 Q_{1int} Q_{3int}}+\left(\frac{{k_{12}}^2 Q_{1int} Q_{3int}}{{k_{13}}^2 Q_{1int} Q_{3int}}\right)+\cdots+\left(\frac{{k_{1n}}^2 Q_{1int} Q_{nint}}{{k_{13}}^2 Q_{1int} Q_{3int}}\right)}\right) \tag{6-51}$$

$$\vdots$$

$$\eta_{n1} = \frac{\gamma}{\gamma+1}\left(\frac{1}{\frac{\gamma+1}{{k_{1n}}^2 Q_{1int}Q_{nint}}+\left(\frac{{k_{12}}^2 Q_{1int}Q_{3int}}{{k_{1n}}^2 Q_{1int}Q_{nint}}\right)+\cdots+\left(\frac{{k_{1n}}^2 Q_{1int}Q_{nint}}{{k_{1n}}^2 Q_{1int}Q_{nint}}\right)}\right) \quad (6\text{-}52)$$

6.5.3 Efficiency Limit for Multiple Receivers Equally Coupled to Transmitter

As the number of receivers increases, it is observed from (6-49) that ratio of source and load resistances to their respective coil resistances increases, effectively reducing the losses across the coil resistances in wireless power transfer system. Therefore, overall efficiency improves as the number of receivers increases as shown in Fig. 6.11.

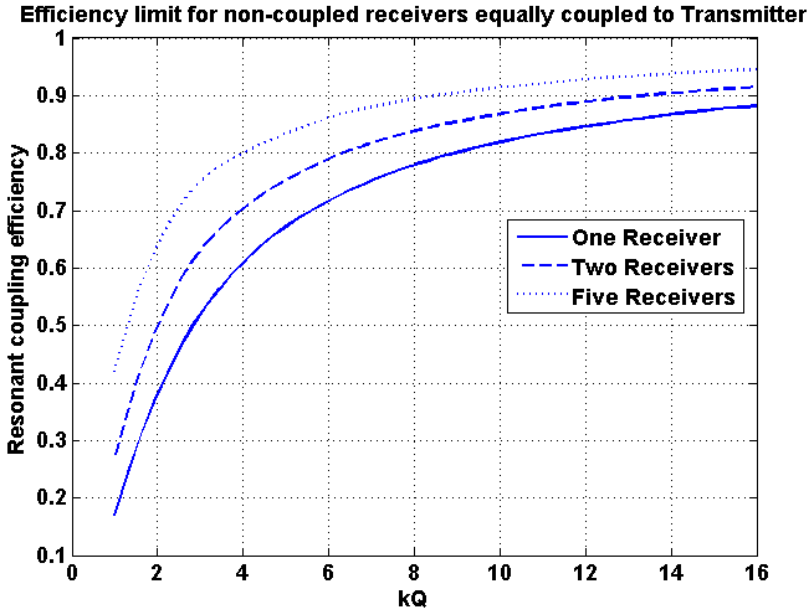

Fig.6.11 Efficiency limit for mutually non-coupled receivers equally coupled to the transmitter.

6.6 Impact of Mutual Coupling Between Receivers on RCE

So far, we based our analysis on non-coupled receivers. This is the simplest case, because the input impedance at the transmitter and receivers is real at the resonance frequency. However, if the coupling between the receivers is not zero as shown in Fig. 6.12(a), then the impedance

seen by the transmitter and receiver is complex. As such, the capacitor used to cancel out the inductance of each coil and create resonance is not enough, and a more complex matching circuit is needed. The mathematical derivation of that case is tedious and explicit solutions could not be found at this point, regarding the maximum efficiency and optimal load conditions. The input and output complex impedances are

$$Z_{source} = (Z_S) + \frac{(\omega M_{12})^2 Z_{L3}}{(\omega M_{23})^2 + Z_{L2} Z_{L3}} + \frac{(\omega M_{13})^2 Z_{L2}}{(\omega M_{23})^2 + Z_{L2} Z_{L3}} - j \frac{2(\omega M_{12})(\omega M_{13})(\omega M_{23})}{(\omega M_{23})^2 + Z_{L2} Z_{L3}} \quad (6\text{-}53)$$

$$Z_{Rx2} = (Z_2) + \frac{(\omega M_{12})^2 Z_{L3}}{(\omega M_{13})^2 + Z_S Z_{L3}} + \frac{(\omega M_{23})^2 Z_S}{(\omega M_{13})^2 + Z_S Z_{L3}} - j \frac{2(\omega M_{12})(\omega M_{13})(\omega M_{23})}{(\omega M_{13})^2 + Z_S Z_{L3}} \quad (6\text{-}54)$$

$$Z_{Rx3} = (Z_3) + \frac{(\omega M_{13})^2 Z_{L2}}{(\omega M_{12})^2 + Z_S Z_{L2}} + \frac{(\omega M_{23})^2 Z_S}{(\omega M_{12})^2 + Z_S Z_{L2}} - j \frac{2(\omega M_{12})(\omega M_{13})(\omega M_{23})}{(\omega M_{12})^2 + Z_S Z_{L2}} \quad (6\text{-}55)$$

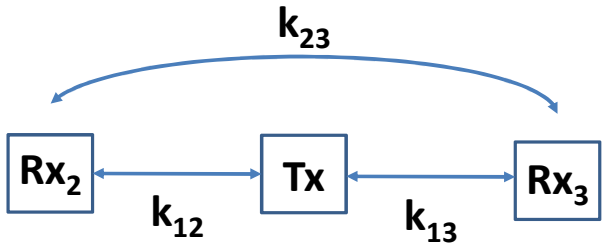

(a)

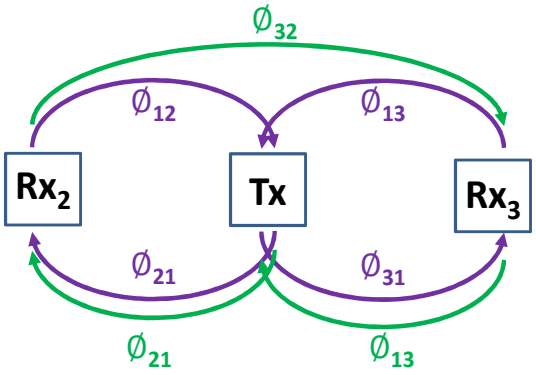

(b)

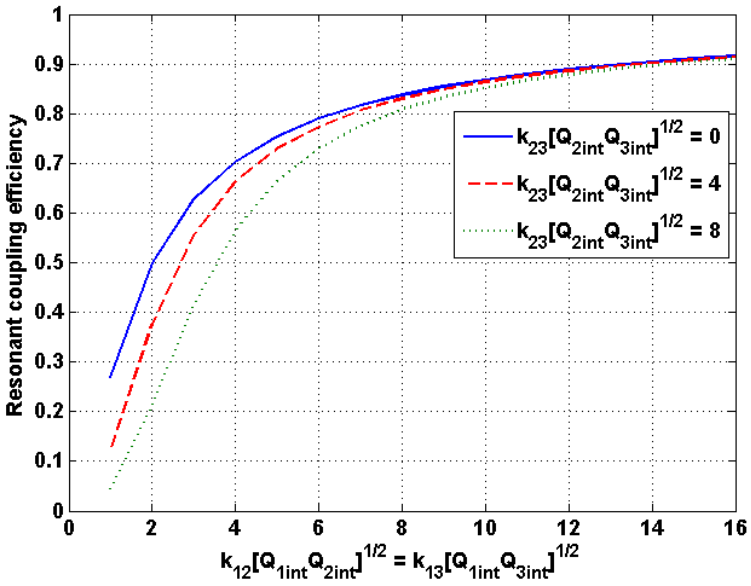

(c)

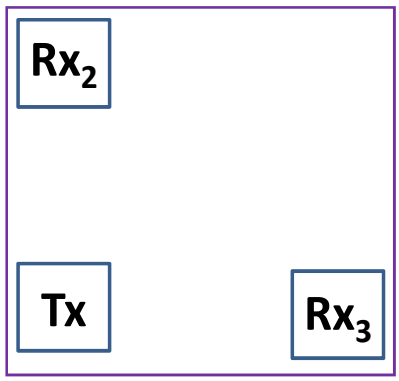

(d)

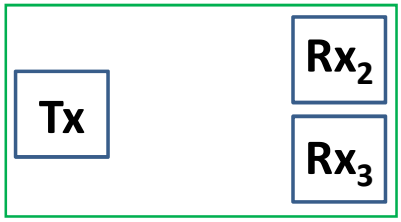

(e)

Fig.6.12 (a) Coupled receivers (b) Input impedance for coupled receivers (c) Efficiency limit for mutually coupled receivers equally coupled to the transmitter (d) Relatively weak inter-receiver mutual coupling (e) Strong inter-receiver mutual coupling

However, it is interesting to assess the effect of mutual coupling between the receivers, in a system tuned for maximum efficiency under the non-coupled receiver assumption. Let us

assume a system of a single transmitter and two coupled receivers. If the load impedance of each receiver is chosen based on the non-coupled receivers assumption, and an impedance match is done at the transmitter, then the efficiency (maximum only when coupling between receivers is zero) obtained in such a case for different values of coupling between receivers is plotted in Fig. 6.12(c). It is observed that for strong coupling between transmitter and receiver compared to the inter-receiver coupling as depicted in Fig. 6.12(d), efficiency is close to the optimal efficiency. However for stronger inter-receiver coupling compared to the coupling between transmitter and receivers as depicted in Fig. 6.12(e), the efficiency drops below the optimal efficiency value derived for non-coupled receivers.

CHAPTER 7

RCE Limit for Single and Multiple Repeaters between a Transmitter and a Receiver in a NFC System

7.1 SINGLE REPEATER BETWEEN TRANSMITTER AND RECEIVER

Repeaters have been used between transmitter and receiver to enhance the power transfer efficiency and the transmission distance from single transmitter to single receiver [45]. A single repeater is introduced between the transmitter and the receiver as shown in Fig. 7.1. It is observed that repeater should only be a resonant coil at the resonance frequency of transmitter and receiver with no external resistance attached to it, since any additional resistance increases the power loss at repeater. The direct coupling between transmitter and receiver is neglected. Such a wireless power transfer system can be represented by the following matrix

$$\begin{bmatrix} R_s + R_{L1} & j\omega M_{12} & 0 \\ j\omega M_{12} & R_{L2} & j\omega M_{23} \\ 0 & j\omega M_{23} & R_3 + R_{L3} \end{bmatrix} \begin{bmatrix} i_1 \\ i_2 \\ i_3 \end{bmatrix} = \begin{bmatrix} v_s \\ 0 \\ 0 \end{bmatrix} \tag{7-1}$$

The source is matched to the input impedance so that no power fed to the coil is reflected back to the transmitter.

$$R_S = R_{input} = R_{L1} + \frac{(\omega M_{12})^2}{R_{L2} + \frac{(\omega M_{23})^2}{(R_{L3} + R_L)}} \tag{7-2}$$

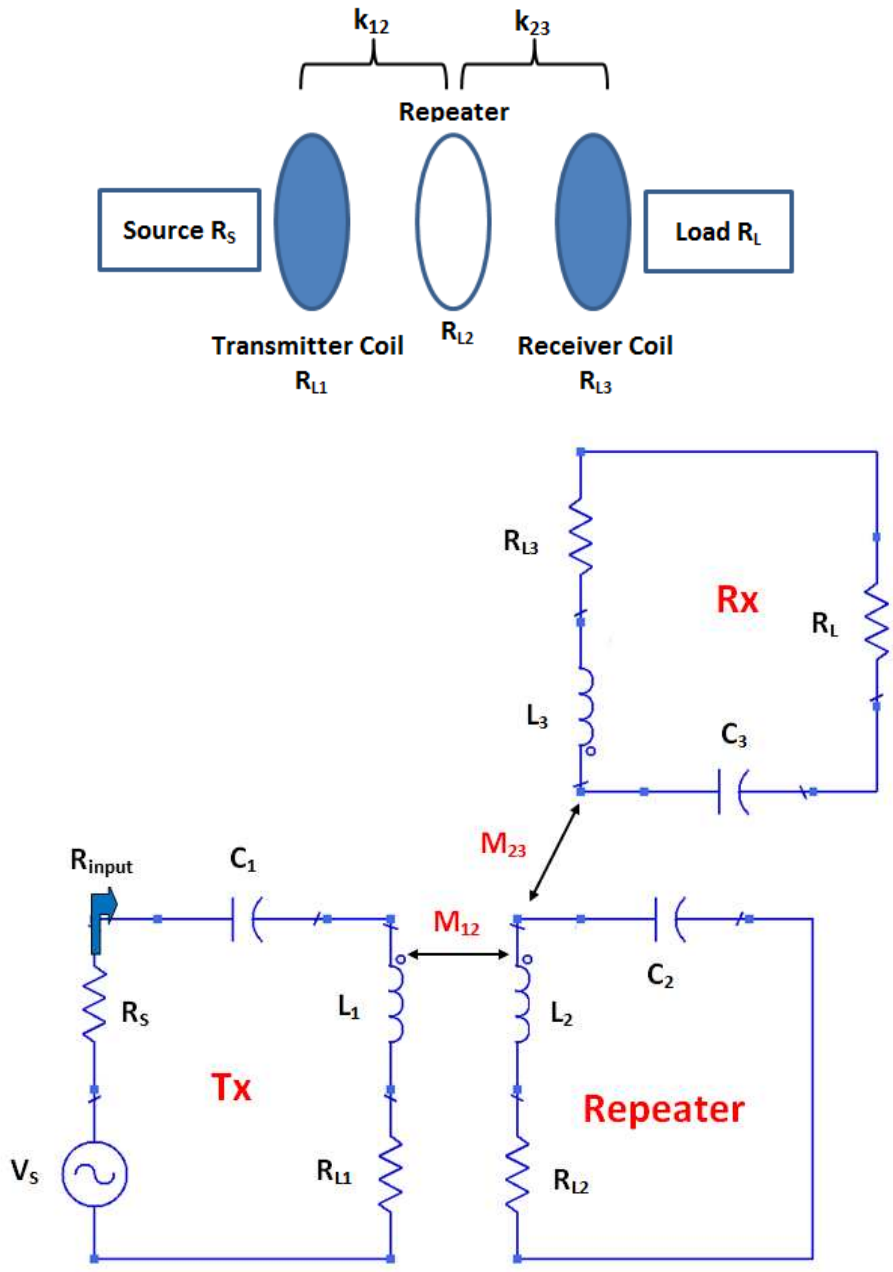

Fig. 7.1 WPT system consisting of a single repeater between transmitter and receiver

The receiver coupling efficiency under the condition of impedance match at source is

$$\eta = \frac{\beta\left(k_{12}{}^2 Q_{1int} Q_{2int}\right)\left(k_{23}{}^2 Q_{2int} Q_{3int}\right)}{(\beta+1)^2\left[1+\frac{k_{12}{}^2 Q_{1int} Q_{2int}}{1+\frac{k_{23}{}^2 Q_{2int} Q_{3int}}{(\beta+1)}}\right]\left[1+\frac{k_{23}{}^2 Q_{2int} Q_{3int}}{(\beta+1)}\right]^2} \tag{7-3}$$

where, β is the ratio of load to loss resistance of the coil at receiver i.e., R_L/R_{L3}. In order to find optimum load which leads to the highest resonant coupling efficiency, above expression is differentiated w.r.t β and the derivative is set to zero.

$$\beta = \sqrt{\frac{\left(1+{k_{23}}^2 Q_{2int}Q_{3int}\right)\left(1+{k_{12}}^2 Q_{1int}Q_{2int}+{k_{23}}^2 Q_{2int}Q_{3int}\right)}{\left(1+{k_{12}}^2 Q_{1int}Q_{2int}\right)}} \tag{7-4}$$

Efficiency contours for a wireless power transfer system consisting of a single repeater between transmitter and receiver are plotted in Fig. 7.2, which give the efficiency for a given pair of coupling between transmitter-repeater and repeater-receiver. It is worthwhile to note here that the repeater does not need to be placed exactly between transmitter and receiver.

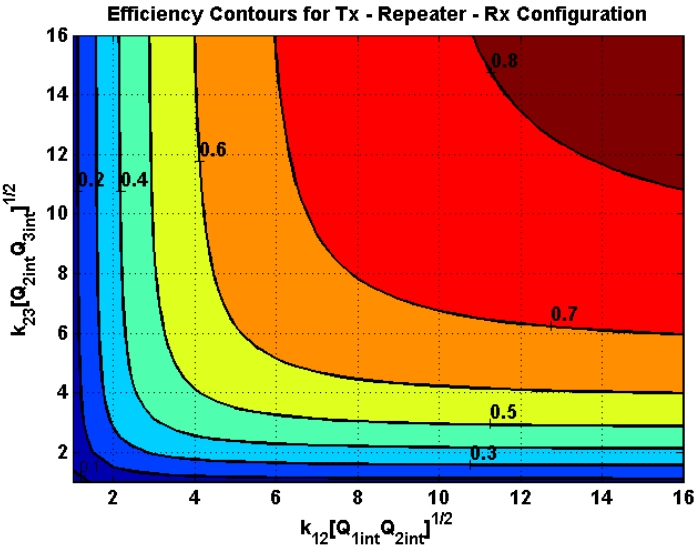

Fig. 7.2 RCE for WPT configuration consisting of a repeater between transmitter and receiver.

Another interesting comparison is to compare the performance of a WPT system consisting of a repeater placed halfway between transmitter and a receiver, with the case of single transmitter and receiver without a repeater. The coupling between transmitter and receiver decreases with $1/R^3$ for distances much larger than the individual radii of coils. For distances comparable to the radius of the loops, the coupling coefficient decreases approximately with $1/R^2$.

The improvement in efficiency provided by the repeater over the case without repeater is shown in Fig. 7.3.

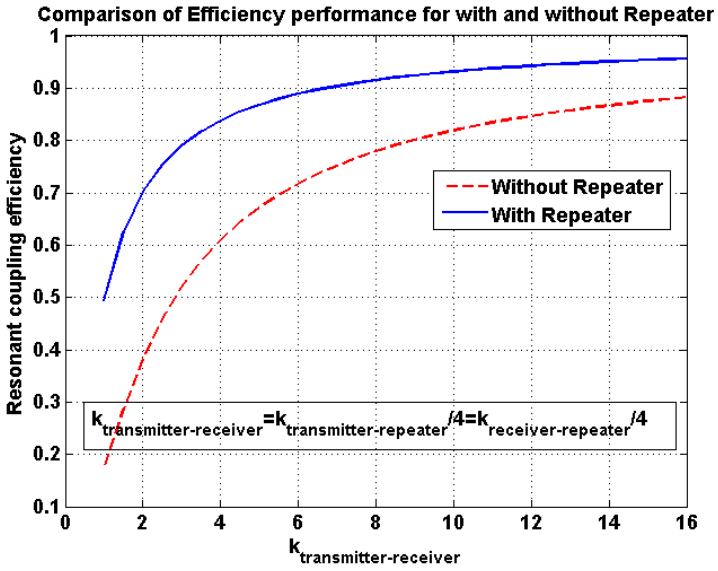

Fig. 7.3 Comparison of efficiency for single transmitter and receiver with and without repeater.

7.2 TWO REPEATERS BETWEEN TRANSMITTER AND RECEIVER

For the scenario involving two repeaters between transmitter and receiver, as shown in Fig. 7.4, the input impedance, RCE and optimal β are

$$R_S = R_{input} = R_{L1} + \frac{(\omega M_{12})^2}{R_{L2} + \frac{(\omega M_{23})^2}{R_{L3} + \frac{(\omega M_{34})^2}{R_{L4} + R_L}}} \tag{7-5}$$

$$\eta = \frac{\beta\left(k_{12}{}^2 Q_{1int} Q_{2int}\right)\left(k_{23}{}^2 Q_{2int} Q_{3int}\right)\left(k_{34}{}^2 Q_{3int} Q_{4int}\right)}{(\beta+1)^2\left[1+\frac{k_{12}{}^2 Q_{1int} Q_{2int}}{1+\frac{k_{23}{}^2 Q_{2int} Q_{3int}}{1+\frac{k_{34}{}^2 Q_{3int} Q_{4int}}{(\beta+1)}}}\right]\left[1+\frac{k_{23}{}^2 Q_{2int} Q_{3int}}{1+\frac{k_{34}{}^2 Q_{3int} Q_{4int}}{(\beta+1)}}\right]^2\left[1+\frac{k_{34}{}^2 Q_{3int} Q_{4int}}{(\beta+1)}\right]^2} \tag{7-6}$$

$$\beta = \sqrt{\frac{\left(1+{k_{12}}^2 Q_{1int}Q_{2int}+{k_{23}}^2 Q_{2int}Q_{3int}+{k_{34}}^2 Q_{3int}Q_{4int}+{k_{12}}^2 Q_{1int}Q_{2int}{k_{34}}^2 Q_{3int}Q_{4int}\right)}{\left(1+{k_{23}}^2 Q_{2int}Q_{3int}+{k_{34}}^2 Q_{3int}Q_{4int}\right)}}{\left(1+{k_{23}}^2 Q_{2int}Q_{3int}\right)\left(1+{k_{12}}^2 Q_{1int}Q_{2int}+{k_{23}}^2 Q_{2int}Q_{3int}\right)}$$

(7-7)

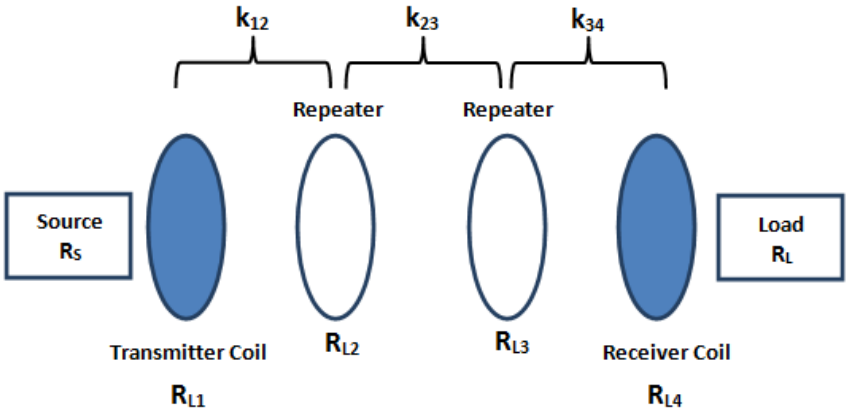

Fig. 7.4 WPT system consisting of two repeaters between transmitter and receiver

7.3 THREE REPEATERS BETWEEN TRANSMITTER AND RECEIVER

For the scenario involving three repeaters between transmitter and receiver, as shown in Fig. 7.5, the input impedance, RCE and optimal β are

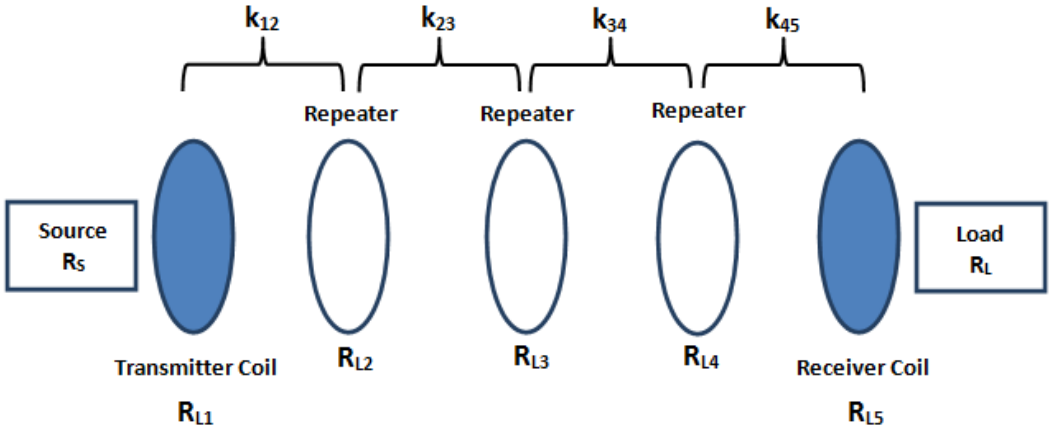

Fig. 7.5 WPT system consisting of three repeaters between transmitter and receiver

$$R_S = R_{input} = R_{L1} + \frac{(\omega M_{12})^2}{R_{L2} + \frac{(\omega M_{23})^2}{R_{L3} + \frac{(\omega M_{34})^2}{R_{L4} + \frac{(\omega M_{45})^2}{R_{L5} + R_L}}}} \tag{7-8}$$

$$\eta = \frac{\beta\left(k_{12}{}^2 Q_{1int} Q_{2int}\right)\left(k_{23}{}^2 Q_{2int} Q_{3int}\right)\left(k_{34}{}^2 Q_{3int} Q_{4int}\right)\left(k_{45}{}^2 Q_{4int} Q_{5int}\right)}{(\beta+1)^2 \left[1 + \frac{k_{12}{}^2 Q_{1int} Q_{2int}}{1 + \frac{k_{23}{}^2 Q_{2int} Q_{3int}}{1 + \frac{k_{34}{}^2 Q_{3int} Q_{4int}}{1 + \frac{k_{45}{}^2 Q_{4int} Q_{5int}}{(\beta+1)}}}}\right]\left[1 + \frac{k_{23}{}^2 Q_{2int} Q_{3int}}{1 + \frac{k_{34}{}^2 Q_{3int} Q_{4int}}{1 + \frac{k_{45}{}^2 Q_{4int} Q_{5int}}{(\beta+1)}}}\right]^2 \left[1 + \frac{k_{34}{}^2 Q_{3int} Q_{4int}}{1 + \frac{k_{45}{}^2 Q_{4int} Q_{5int}}{(\beta+1)}}\right]^2 \left[1 + \frac{k_{45}{}^2 Q_{4int} Q_{5int}}{(\beta+1)}\right]^2} \tag{7-9}$$

$$\beta = \sqrt{\frac{\begin{pmatrix} 1 + k_{12}{}^2 Q_{1int} Q_{2int} + k_{23}{}^2 Q_{2int} Q_{3int} + k_{34}{}^2 Q_{3int} Q_{4int} + k_{45}{}^2 Q_{4int} Q_{5int} + \\ k_{12}{}^2 Q_{1int} Q_{2int} k_{34}{}^2 Q_{3int} Q_{4int} + k_{12}{}^2 Q_{1int} Q_{2int} k_{45}{}^2 Q_{4int} Q_{5int} + k_{23}{}^2 Q_{2int} Q_{3int} k_{45}{}^2 Q_{4int} Q_{5int} \end{pmatrix}}{\begin{pmatrix} 1 + k_{23}{}^2 Q_{2int} Q_{3int} + k_{34}{}^2 Q_{3int} Q_{4int} + k_{45}{}^2 Q_{4int} Q_{5int} + \\ k_{23}{}^2 Q_{2int} Q_{3int} k_{45}{}^2 Q_{4int} Q_{5int} \end{pmatrix}}}{\frac{\left(1 + k_{12}{}^2 Q_{1int} Q_{2int} + k_{23}{}^2 Q_{2int} Q_{3int} + k_{34}{}^2 Q_{3int} Q_{4int} + k_{12}{}^2 Q_{1int} Q_{2int} k_{34}{}^2 Q_{3int} Q_{4int}\right)}{\left(1 + k_{23}{}^2 Q_{2int} Q_{3int} + k_{34}{}^2 Q_{3int} Q_{4int}\right)}}} \tag{7-10}$$

7.4 GENERALIZED CASE OF (N-2) REPEATERS BETWEEN TRANSMITTER AND RECEIVER

The above analysis can be extended to multiple repeaters inserted between transmitter and receiver as shown in Fig. 7.6. Assuming there are *n* resonators. Resonator 1 is connected to the source and resonator *n* is connected to the load. Resonators 2…*n-1* are the repeaters. Repeaters consist of coils resonant at the resonance frequency of transmitter and receiver. Coil resistance is the only source of loss at the repeaters. Such a wireless power transfer system can be represented by the following matrix

$$\begin{bmatrix} R_s + R_{L1} & j\omega M_{12} & 0 & & 0 \\ j\omega M_{12} & R_{L2} & j\omega M_{23} & \cdots & 0 \\ 0 & j\omega M_{23} & R_{L3} & & 0 \\ & \vdots & & \ddots & \vdots \\ 0 & 0 & 0 & \cdots & R_L + R_{Ln} \end{bmatrix} \begin{bmatrix} i_1 \\ i_2 \\ i_3 \\ \vdots \\ i_n \end{bmatrix} = \begin{bmatrix} v_s \\ 0 \\ 0 \\ \vdots \\ 0 \end{bmatrix} \tag{7-11}$$

The source is matched to the input impedance so that no power fed to the source coil is reflected back to the transmitter.

$$R_S = R_{input} = R_{L1} + \cfrac{(\omega M_{12})^2}{R_{L2} + \cfrac{(\omega M_{23})^2}{R_{L3} + \cfrac{(\omega M_{34})^2}{R_{L4} + \cfrac{(\omega M_{45})^2}{R_{L5} + \ddots \\ \vdots \\ R_{L(n-1)} + \cfrac{\left(\omega M_{(n-1)n}\right)^2}{R_{Ln} + R_L}}}}} \tag{7-12}$$

The receiver coupling efficiency under the condition of impedance match at source is

$$\eta = \cfrac{\beta\left(l_{12}{}^2\right)\left(l_{23}{}^2\right)\left(l_{34}{}^2\right)\ldots.\left(l_{(n-1)n}{}^2\right)}{1 + \cfrac{l_{12}{}^2}{1 + \cfrac{l_{23}{}^2}{1 + \cfrac{l_{34}{}^2}{1 + \cfrac{l_{45}{}^2}{1 + \ddots \\ \vdots \\ 1 + \frac{l_{(n-1)n}{}^2}{(\beta+1)}}}}}} \times \frac{1}{\left(1 + \cfrac{l_{23}{}^2}{1 + \cfrac{l_{34}{}^2}{1 + \cfrac{l_{45}{}^2}{1 + \ddots \\ \vdots \\ 1 + \frac{l_{(n-1)n}{}^2}{(\beta+1)}}}}\right)^2} \times \frac{1}{\left(1 + \cfrac{l_{34}{}^2}{1 + \cfrac{l_{45}{}^2}{1 + \ddots \\ \vdots \\ 1 + \frac{l_{(n-1)n}{}^2}{(\beta+1)}}}\right)^2}$$

$$\times \frac{1}{\left(1 + \cfrac{l_{45}{}^2}{1 + \ddots \\ \vdots \\ 1 + \frac{l_{(n-1)n}{}^2}{(\beta+1)}}\right)^2} \times \ldots \times \frac{1}{\left(1 + \frac{l_{(n-1)n}{}^2}{(\beta+1)}\right)^2} \times (\beta+1)^2 \tag{7-13}$$

where $l_{(n-1)n}{}^2 = k_{(n-1)n}{}^2 Q_{(n-1)} Q_{(n)}$

The value of β that maximizes the efficiency for a general case of 'n-2' repeaters is

$$\beta = \sqrt{\frac{(num1)(num2)}{(den1)(den2)}} \tag{7-14}$$

where

$$num1 = 1 + \sum_{i=1}^{n-1} l_{i,i+1}^2 + \sum_{n>j>i+1>1} l_{i,i+1}^2 l_{j,j+1}^2 + \sum_{n>k>j+1>j>i+1>1} l_{i,i+1}^2 l_{j,j+1}^2 l_{k,k+1}^2 + \cdots$$

$$num2 = 1 + \sum_{i=2}^{n-1} l_{i,i+1}^2 + \sum_{n>j>i+1>2} l_{i,i+1}^2 l_{j,j+1}^2 + \sum_{n>k>j+1>j>i+1>2} l_{i,i+1}^2 l_{j,j+1}^2 l_{k,k+1}^2 + \cdots$$

$$den1 = 1 + \sum_{i=2}^{n-2} l_{i,i+1}^2 + \sum_{n-1>j>i+1>2} l_{i,i+1}^2 l_{j,j+1}^2 + \sum_{n-1>k>j+1>j>i+1>2} l_{i,i+1}^2 l_{j,j+1}^2 l_{k,k+1}^2 + \cdots$$

$$den2 = 1 + \sum_{i=1}^{n-2} l_{i,i+1}^2 + \sum_{n-1>j>i+1>1} l_{i,i+1}^2 l_{j,j+1}^2 + \sum_{n-1>k>j+1>j>i+1>1} l_{i,i+1}^2 l_{j,j+1}^2 l_{k,k+1}^2 + \cdots$$

$$l_{i,i+1}{}^2 = k_{i,i+1}{}^2 Q_{(i)} Q_{(i+1)}$$

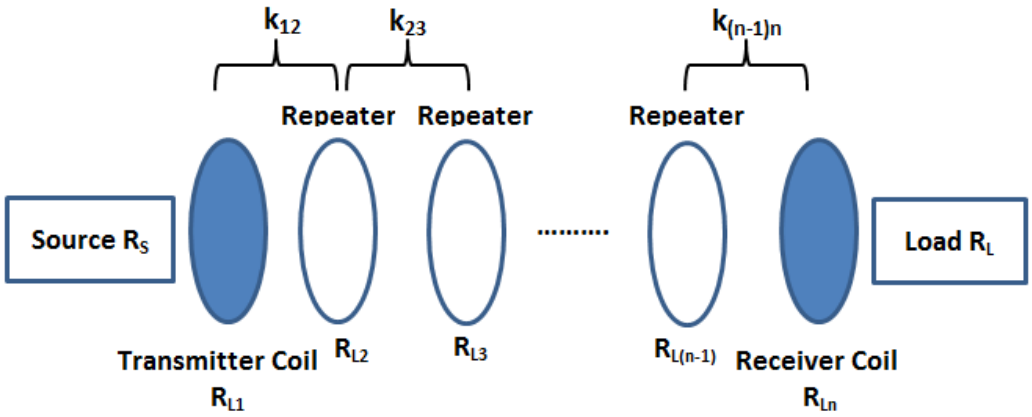

Fig. 7.6 WPT system consisting of multiple (n-2) repeaters between transmitter and receiver.

CHAPTER 8

Impact of PEC Platform and Receiver Coil Misalignment on RCE

8.1 Impact of PEC on Quality Factor of Electrically Small Loop Antenna

A single-turn loop of dimensions 4.4cm x 6.8cm and copper thickness of 1.5mm is simulated for three scenarios in HFSS, as shown in Fig. 8.1.

1. A free Standing Loop.

2. A loop placed on top of a PEC. The dimensions of the PEC are 6cm x 12cm.

3. Ferrite placed between the loop and the PEC. The ferrite sheet is of 0.6mm thickness and its magnetic loss tangent is 0.00884. A ferrite sheet with hole in the center is used in an attempt to reduce the weight of the device.

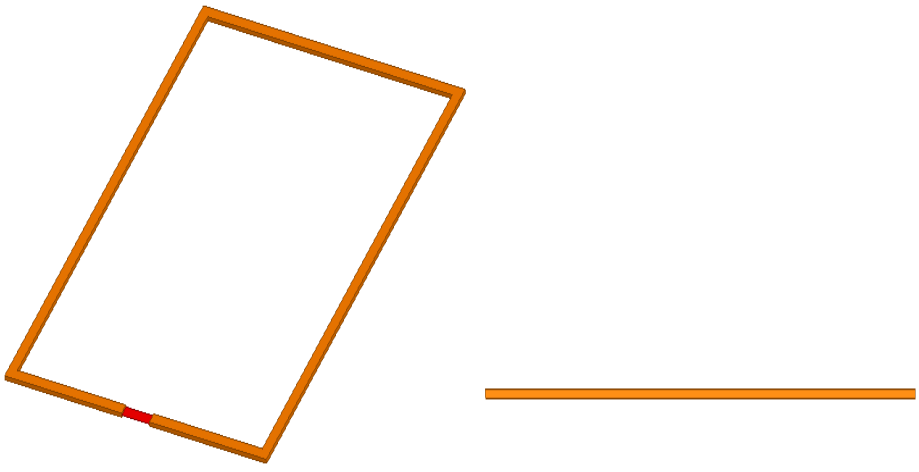

(a)

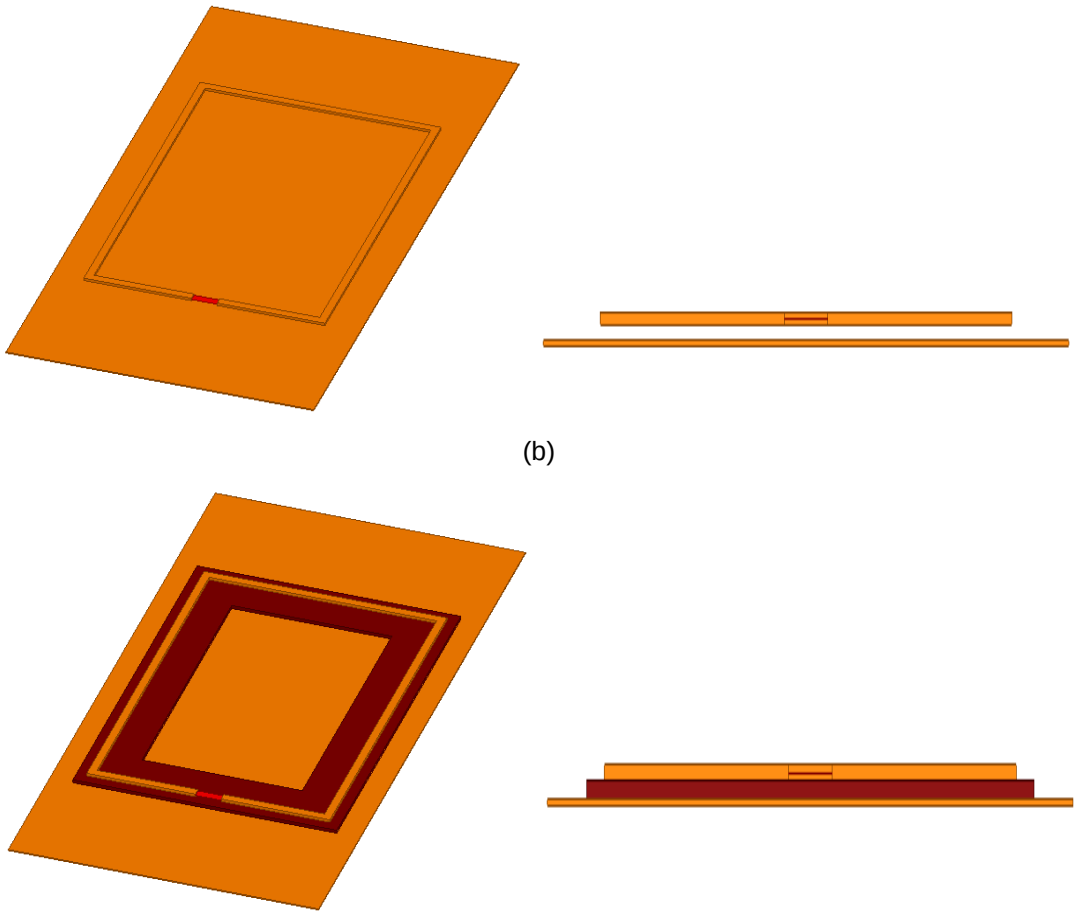

(b)

(c)

Fig. 8.1. Pictures of (a) A free standing loop (b) A loop placed over a PEC (c) Ferrite inserted between the loop and the PEC

The inductance, resistance and quality factor for three scenarios are plotted in Fig. 8.2.

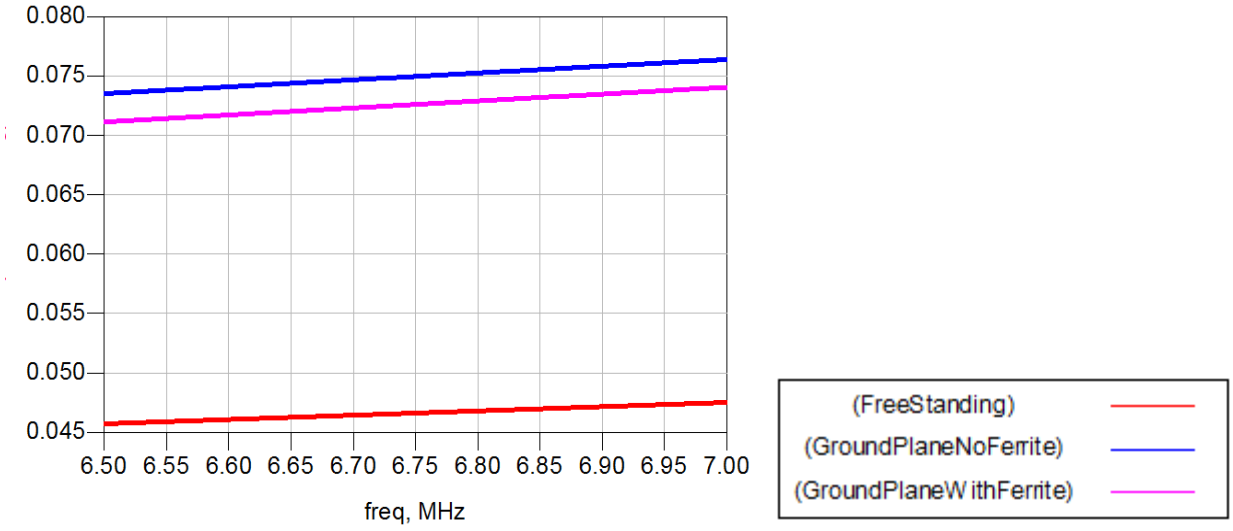

(a) Resistance

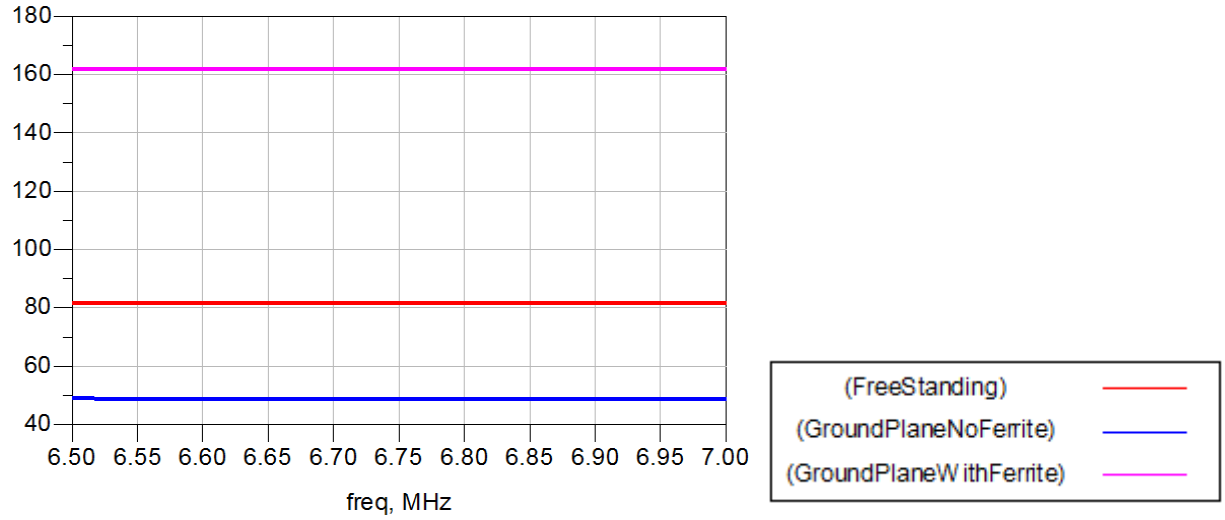

(b) Inductance (nH)

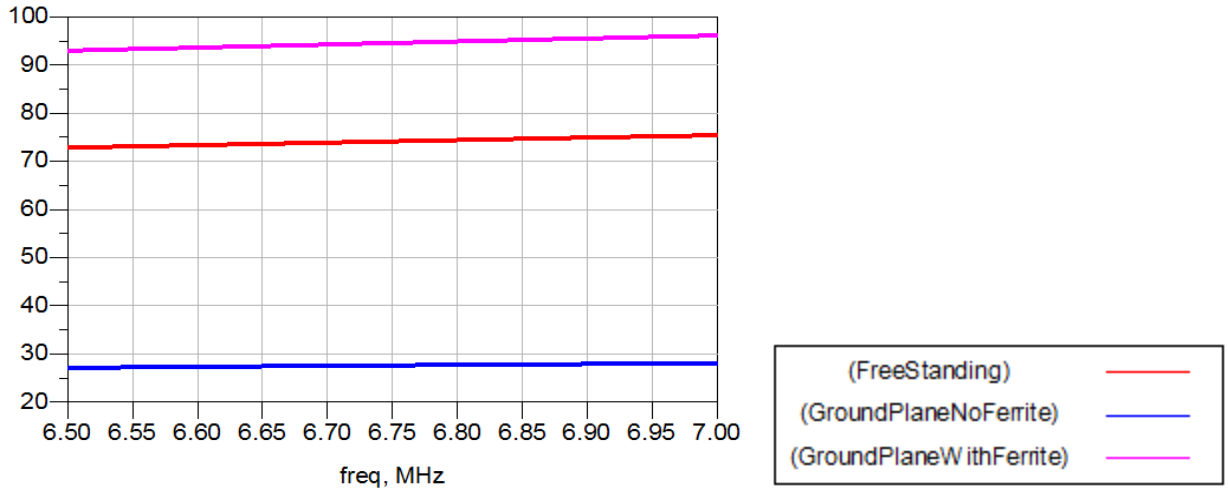

(c) Quality Factor

Fig. 8.2. The resistance, inductance and quality factor of a free-standing loop, a loop placed over a PEC, and a loop placed over a PEC with ferrite inserted between the loop and the PEC

It is observed that when the loop is placed above a PEC, the current induced in PEC is such as to oppose the magnetic field generated by the loop itself and this lowers the inductance of the loop. Also due to losses on the PEC, the resistance of the loop also increases, hence lowering the Q value. The eddy current phenomenon is depicted in Fig. 8.3. When a ferrite sheet is inserted between the loop and the PEC, it isolates the PEC from the magnetic field of the loop, and hence restores the Q value of the loop.

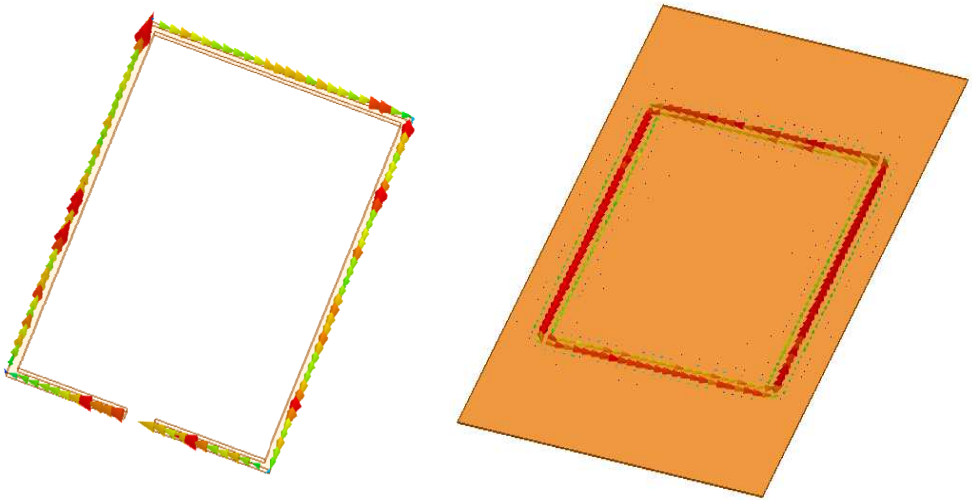

Fig. 8.3. For clockwise current on loop, the current induced on PEC is anticlockwise

8.2 IMPACT OF MISALIGNMENT ON COUPLING COEFFICIENT

8.2.1 Near-Field Magnetic Flux Density of an Electrically Small Loop Antenna

Magnetic field due to a small loop antenna (of radius r_1 and N_1 turns) in *xy* plane carrying current I_1, at point *P* (position vector of point makes an angles θ_1 with z-axis) at a distance $R << \lambda$ from the loop, as shown in Fig. 8.4(a) is [59]

$$B_r = j\frac{\mu_o N_1 \beta {r_1}^2 I_1 \cos\theta_1}{2r^2}\left[1+\frac{1}{j\beta r}\right] \tag{8-1}$$

$$B_\theta = -\frac{\mu_o N_1 (\beta r_1)^2 I_1 \sin\theta_1}{4r}\left[1+\frac{1}{j\beta r}-\frac{1}{(\beta r)^2}\right] \tag{8-2}$$

where $\beta=2\pi/\lambda$ is the wave number. For distances much smaller than the wavelength $\beta r<<1$, the magnetic flux density expressions can be simplified as

$$B_r = \frac{\mu_o N_1 {r_1}^2 I_1 \cos\theta_1}{2r^3} \tag{8-3}$$

$$B_\theta = \frac{\mu_o N_1 {r_1}^2 I_1 \sin\theta_1}{4r^3} \tag{8-4}$$

8.2.2 General Case of Laterally and Angularly Misaligned Coils

A general scenario involving a misaligned receiver coil is shown in Fig. 8.4(b). Receiver coil is displaced laterally by distance *d* and vertically by distance *R*, where

$$d = \sqrt{{x_1}^2 + {y_1}^2} \tag{8-5}$$

The position vector and the area vector of the receiver coil are described by angles (Φ_1, θ_1) and (Φ_o, θ_o) respectively.

The calculation of mutual inductance between the transmitter and the receiver coil requires evaluation of magnetic flux through the receiver coil due to magnetic field generated by the transmitter coil. The magnetic field due to the transmitter coil is expressed in spherical co-ordinates in (8-3) and (8-4). The rectangular components of area vector A_2 can be written as

$$A_{2x} = A_2 \sin\theta_o \cos\Phi_o \quad , \quad A_y = A_2 \sin\theta_o \sin\Phi_o \quad , \quad A_z = A_2 \cos\theta_o \tag{8-6}$$

The area vector A_2 is expressed in spherical co-ordinates by rectangular-to-spherical vector transformation

$$\begin{bmatrix} A_r \\ A_\theta \\ A_\Phi \end{bmatrix} = \begin{bmatrix} \sin\theta_1 \cos\Phi_1 & \sin\theta_1 \sin\Phi_1 & \cos\theta_1 \\ \cos\theta_1 \cos\Phi_1 & \cos\theta_1 \sin\Phi_1 & -\sin\theta_1 \\ -\sin\Phi_1 & \cos\Phi_1 & 0 \end{bmatrix} \begin{bmatrix} A_2 \sin\theta_o \cos\Phi_o \\ A_2 \sin\theta_o \sin\Phi_o \\ A_2 \cos\theta_o \end{bmatrix} \tag{8-7}$$

Therefore A_r and A_θ are

$$A_r = A_2[\sin\theta_o \sin\theta_1 \cos(\Phi_o - \Phi_1) + \cos\theta_o \cos\theta_1] \tag{8-8}$$

$$A_\theta = A_2[\sin\theta_o \cos\theta_1 \cos(\Phi_o - \Phi_1) - \cos\theta_o \sin\theta_1] \tag{8-9}$$

The flux through the receiver coil is

$$\emptyset_{21} = A_2[\sin\theta_o \sin\theta_1 \cos(\Phi_o - \Phi_1) + \cos\theta_o \cos\theta_1] \frac{\mu_o N_1 N_2 \pi r_2^2 {r_1}^2 I_1 \cos\theta_1}{2r^3} + A_2[\sin\theta_o \cos\theta_1 \cos(\Phi_o - \Phi_1) - \cos\theta_o \sin\theta_1] \frac{\mu_o N_1 N_2 \pi r_2^2 {r_1}^2 I_1 \sin\theta_1}{4r^3} \tag{8-10}$$

$$\emptyset_{21} = [\sin\theta_o \sin\theta_1 \cos\theta_1 \cos(\Phi_o - \Phi_1) + \cos\theta_o \cos\theta_1 \cos\theta_1] \frac{\mu_o N_1 N_2 \pi r_2^2 {r_1}^2 I_1}{2r^3} + [\sin\theta_o \cos\theta_1 \sin\theta_1 \cos(\Phi_o - \Phi_1) - \cos\theta_o \sin\theta_1 \sin\theta_1] \frac{\mu_o N_1 N_2 \pi r_2^2 I_1}{4r^3} \tag{8-11}$$

$$\emptyset_{21} = [\sin\theta_o \sin\theta_1 \cos\theta_1 \cos(\Phi_o - \Phi_1) + \cos\theta_o \cos\theta_1 \cos\theta_1] \frac{\mu_o N_1 N_2 \pi r_2^2 {r_1}^2 I_1}{2r^3} + \left[\frac{\sin\theta_o \cos\theta_1 \sin\theta_1 \cos(\Phi_o - \Phi_1)}{2} - \frac{\cos\theta_o \sin\theta_1 \sin\theta_1}{2}\right] \frac{\mu_o N_1 N_2 \pi r_2^2 {r_1}^2 I_1}{2r^3} \tag{8-12}$$

where N_2 is the number of turns of the receiver coil.

The mutual inductance between the coils is obtained using [Ch3 Eq (A-5)]

$$M = \frac{\mu_o N_1 N_2 \pi {r_1}^2 {r_2}^2}{2r^3}\left(\frac{3}{2}\sin\theta_o \sin\theta_1 \cos\theta_1 \cos(\Phi_o - \Phi_1) + \cos\theta_o \left\{\cos^2\theta_1 - \frac{1}{2}\sin^2\theta_1\right\}\right) \tag{8-13}$$

The coupling coefficient is obtained by substituting the mutual inductance between the transmitter and the misaligned receiver coil (8-13) and the self-inductance of the transmitter and the receiver coil (3-1) into the formula for coupling coefficient (3-5)

$$k = \left(\frac{\sqrt{r_1 r_2}}{r}\right)^3 \left(\frac{3}{2}\sin\theta_o \sin\theta_1 \cos\theta_1 \cos(\Phi_o - \Phi_1) + \cos\theta_o \left\{\cos^2\theta_1 - \frac{1}{2}\sin^2\theta_1\right\}\right) \tag{8-14}$$

where

$$r = \begin{cases} \sqrt{R^2 + d^2 + {r_1}^2 - 2d\sqrt{R^2 + {r_1}^2}\cos\left(90 + tan^{-1}\left(\frac{r_1}{R}\right)\right)}, r_1 \geq r_2 \\ \sqrt{R^2 + d^2 + {r_2}^2 - 2d\sqrt{R^2 + {r_2}^2}\cos\left(90 + tan^{-1}\left(\frac{r_1}{R}\right)\right)}, r_2 \geq r_1 \end{cases} \tag{8-15}$$

The coupling coefficient expression for the misaligned receiver and the transmitter coil is analyzed for special cases of misalignment to gain an insight into the impact of misalignment on the coupling.

8.2.3 Perfectly Aligned Coils (Co-Axially Placed Coils)

Perfectly aligned coils are shown in Fig. 8.4(c). This is a special case when $\theta_o = 0^o, \theta_1 = 0^o, and\ d = 0$. Equation (8-14) and (8-15) simplify to give,

$$k = \begin{cases} \left(\frac{\sqrt{r_1 r_2}}{\sqrt{R^2 + {r_1}^2}}\right)^3, r_1 \geq r_2 \\ \left(\frac{\sqrt{r_1 r_2}}{\sqrt{R^2 + {r_2}^2}}\right)^3, r_2 \geq r_1 \end{cases} \tag{8-16}$$

$$k = \left(\frac{\sqrt{r_1 r_2}}{R}\right)^3, R >> r_1, r_2 \tag{8-17}$$

Equation (8-17), same as Eq. (3-6), shows that the coupling coefficient between two perfectly aligned conductor coils in free space is frequency independent and varies with inverse cube of distance $1/R^3$ when the distance between the transmitter coil and the receiver coil is much larger than their radii i.e., $R >> r_1, r_2$. This coincides with the near field of an infinitesimal loop, which is in the order of $1/R^3$.

8.2.4 Axially Placed Angularly Misaligned Coils

Axially placed angularly misaligned coils are shown in Fig. 8.4(d). This is the special case when $\theta_o = \alpha, \theta_1 = 0^o, and\ d = 0$. Simplifying (8-14) and (8-15) results in,

$$k = \begin{cases} \left(\frac{\sqrt{r_1 r_2}}{\sqrt{R^2 + {r_1}^2}}\right)^3 \cos\alpha\,, r_1 \geq r_2 \\ \left(\frac{\sqrt{r_1 r_2}}{\sqrt{R^2 + {r_2}^2}}\right)^3 \cos\alpha\,, r_2 \geq r_1 \end{cases} \tag{8-18}$$

For α=0, (8-18) reduces to (8-16) i.e., the coils are perfectly aligned. When α=90°, the coupling coefficient reduces to zero and the coils are completely misaligned. Therefore, for co-axially placed coils, as the misalignment angle α increases from 0 to 90 degrees, the coupling coefficient value decreases from that of perfectly aligned co-axially placed coils to zero coupling.

8.2.5 Laterally Displaced Coils

Laterally displaced coils are shown in Fig. 8.4(e). This is the special case when $\theta_0 = 0^o$. The coupling coefficient for this case is

$$k = \left(\frac{\sqrt{r_1 r_2}}{r}\right)^3 (cos^2\theta_1 - 0.5\ sin^2\theta_1) \tag{8-19}$$

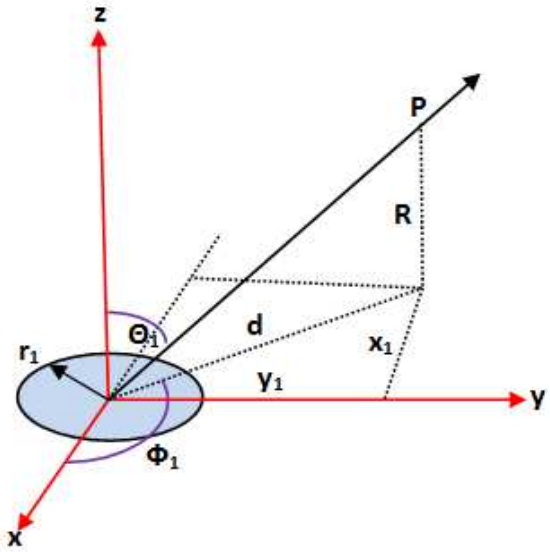
z
P
R
d
Θ_1
r_1
x_1
y_1
y
Φ_1
x

(a)

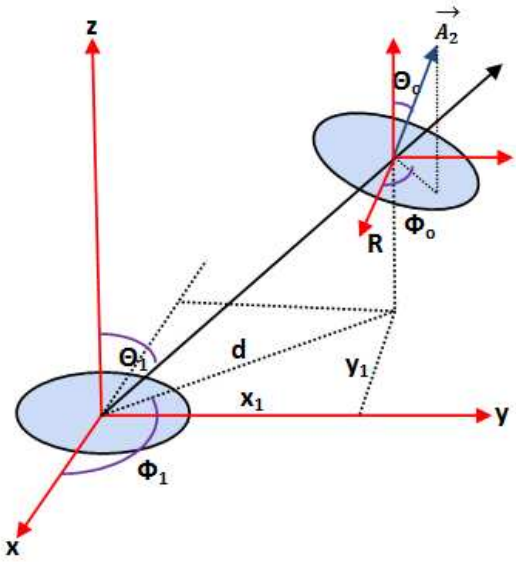
z
$\vec{A_2}$
Θ_o
R
Φ_o
Θ_1
d
y_1
x_1
y
Φ_1
x

(b)

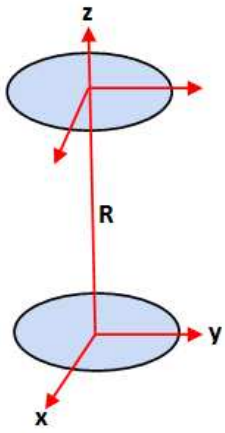
z
R
y
x

(c)

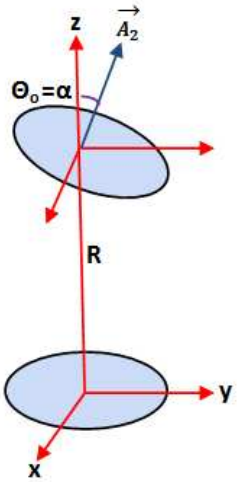
z
$\vec{A_2}$
$\Theta_o=\alpha$
R
y
x

(d)

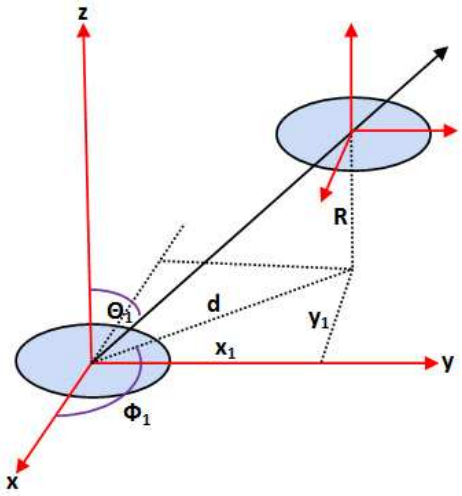
z
R
Θ_1
d
y_1
x_1
y
Φ_1
x

(e)

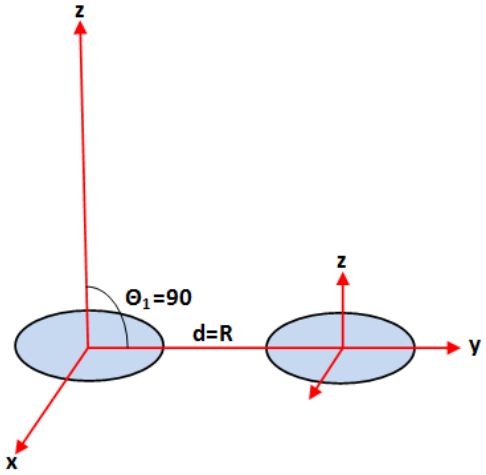
z
$\Theta_1=90$
d=R
z
y
x

(f)

Fig. 8.4 (a) Magnetic field at point *P* due to small loop antenna (b) A misaligned receiver coil (c) Perfectly aligned coils (d) Axially placed angularly misaligned coils (e) Laterally displaced coils (f) Co-planar laterally displaced coils

8.2.6 Co-planar Coils

Co-planar coils is a special case of the laterally displaced coils such that $\theta_1 = 90^o$, $and\ R = 0$ i.e., the coils are placed in the same plane and are laterally displaced as shown in Fig. 8.4(f). Then the coupling coefficient is

$$|k| = \begin{cases} \frac{1}{2}\left(\frac{\sqrt{r_1 r_2}}{\sqrt{R^2 + {r_1}^2}}\right)^3, r_1 \geq r_2 \\ \frac{1}{2}\left(\frac{\sqrt{r_1 r_2}}{\sqrt{R^2 + {r_1}^2}}\right)^3, r_2 \geq r_1 \end{cases} \tag{8-20}$$

$$|k| = \frac{1}{2}\left(\frac{\sqrt{r_1 r_2}}{R}\right)^3, R >> r_1, r_2 \tag{8-21}$$

Equation (8-21) shows that for the laterally displaced coils, the coupling coefficient (8-21) is half that of the coupling coefficient for perfectly aligned coils (8-17) separated by the same distance. Therefore, the power received by laterally displaced receiver coil will be one-fourth of the power received by a perfectly aligned receiver coil separated by the same distance.

8.3 COUPLING BETWEEN ORTHOGONAL TRANSMITTER COILS AND A RECEIVER COIL

8.3.1 Coupling Coefficient between a Transmitter Coil in xy Plane and a Misaligned Receiver Coil

The magnetic field components of an electrically small loop in *xy plane*, as shown in Fig. 8.5(a), in its near-field are expressed in spherical co-ordinate system by (8-3) and (8-4). The

magnetic field can be represented in cartesian co-ordinate system by using the vector transformation from spherical to cartesian co-ordinate system

$$\begin{bmatrix} B_{x,xy} \\ B_{y,xy} \\ B_{z,xy} \end{bmatrix} = \begin{bmatrix} \sin\theta\cos\Phi & \cos\theta\cos\Phi & -\sin\Phi \\ \sin\theta\sin\Phi & \cos\theta\sin\Phi & \cos\Phi \\ \cos\theta & -\sin\theta & 0 \end{bmatrix} \begin{bmatrix} B_r \\ B_\theta \\ B_\Phi \end{bmatrix} \tag{8-22}$$

where $B_{x,xy}$, $B_{y,xy}$ and $B_{z,xy}$ are the *x, y, and z components* of the magnetic field due to an electrically small loop in *xy plane*.

$$B_{x,xy} = \frac{3\mu_o N_1 {r_1}^2 I_1}{4r^3} \sin\left[\tan^{-1}\left(\frac{\sqrt{x^2+y^2}}{z}\right)\right] \cos\left[\tan^{-1}\left(\frac{\sqrt{x^2+y^2}}{z}\right)\right] \cos\left[\tan^{-1}\left(\frac{y}{x}\right)\right] \tag{8-23}$$

$$B_{y,xy} = \frac{3\mu_o N_1 {r_1}^2 I_1}{4r^3} \sin\left[\tan^{-1}\left(\frac{\sqrt{x^2+y^2}}{z}\right)\right] \cos\left[\tan^{-1}\left(\frac{\sqrt{x^2+y^2}}{z}\right)\right] \sin\left[\tan^{-1}\left(\frac{y}{x}\right)\right] \tag{8-24}$$

$$B_{z,xy} = \frac{\mu_o N_1 {r_1}^2 I_1}{2r^3} \left[\cos^2\left[\tan^{-1}\left(\frac{\sqrt{x^2+y^2}}{z}\right)\right] - \frac{1}{2}\sin^2\left[\tan^{-1}\left(\frac{\sqrt{x^2+y^2}}{z}\right)\right]\right] \tag{8-25}$$

The position vector and the area vector of the receiver coil are represented by angles (Φ, θ) and (Φ_o, θ_o). The area vector of the receiver coil can be expressed in terms of its cartesian co-ordinate components.

$$A_x = A\sin\theta_o\cos\Phi_o \quad , \quad A_y = A\sin\theta_o\sin\Phi_o \quad , \quad A_z = A\cos\theta_o \tag{8-26}$$

Mutual inductance and coupling coefficient is calculated using Eq(A-5) [Ch 3], and (3-5),

$$k_{xy} = \left(\frac{\sqrt{r_1 r_2}}{r}\right)^3 \left[\frac{3}{2}\sin\left[\tan^{-1}\left(\frac{\sqrt{x^2+y^2}}{z}\right)\right] \cos\left[\tan^{-1}\left(\frac{\sqrt{x^2+y^2}}{z}\right)\right] \sin\theta_o \cos\left[\Phi_o - \tan^{-1}\left(\frac{y}{x}\right)\right] + \cos\theta_o \left[\cos^2\left[\tan^{-1}\left(\frac{\sqrt{x^2+y^2}}{z}\right)\right] - \frac{1}{2}\sin^2\left[\tan^{-1}\left(\frac{\sqrt{x^2+y^2}}{z}\right)\right]\right]\right] \tag{8-27}$$

8.3.2 Coupling Coefficient between a Transmitter Coil in xz Plane and a Misaligned Receiver Coil

In order to calculate the coupling coefficient due to a coil in *xz plane*, the coil and the observation point are kept fixed while the co-ordinate axes are rotated as shown in Fig. 8.5(b). $B_{x,xz}$, $B_{y,xz}$ and $B_{z,xz}$ are the *x, y, and z components* of the magnetic field due to an electrically small loop in xz plane

$$B_{x,xz} = B_{y,xy} \quad , \quad B_{y,xz} = B_{z,xy} \quad , B_{z,xz} = B_{x,xy} \tag{8-28}$$

Furthermore in (8-23), (8-24) and (8-25),

$$x \text{ is replaced by } z \quad , \quad y \text{ is replaced by } x, \quad z \text{ is replaced by } y \tag{8-29}$$

Therefore, the magnetic field expressions for the loop in *xz plane* are given by,

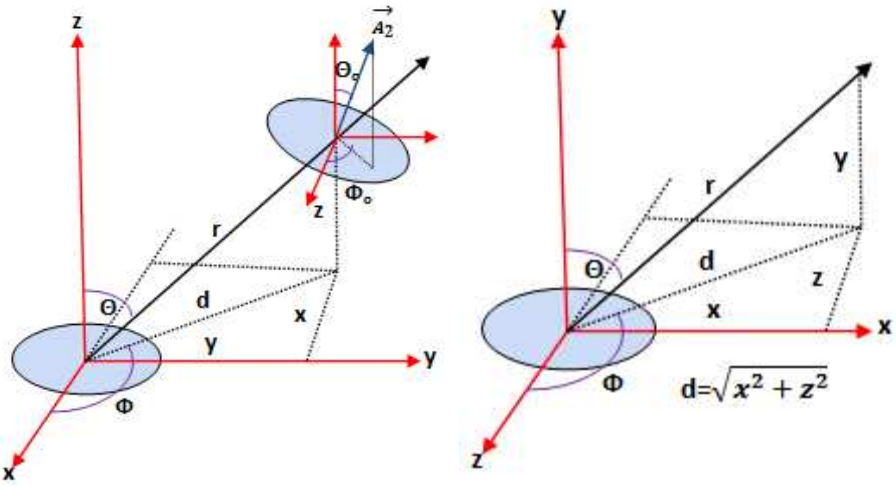

(a) (b)

Fig. 8.5. (a) Transmitter coil in xy plane (b) Transmitter coil in xz plane

$$B_{x,xz} = \frac{3\mu_o N_1 {r_1}^2 I_1}{4r^3} \sin\left[\tan^{-1}\frac{\sqrt{z^2+x^2}}{y}\right] \cos\left[\tan^{-1}\frac{\sqrt{z^2+x^2}}{y}\right] \sin\left[\tan^{-1}\frac{x}{z}\right] \tag{8-30}$$

$$B_{y,xz} = \frac{\mu_o N_1 {r_1}^2 I_1}{2r^3}\left[\cos^2\left[\tan^{-1}\left(\frac{\sqrt{z^2+x^2}}{y}\right)\right] - \frac{1}{2}\sin^2\left[\tan^{-1}\left(\frac{\sqrt{z^2+x^2}}{y}\right)\right]\right] \tag{8-31}$$

$$B_{z,xz} = \frac{3\mu_o N_1 {r_1}^2 I_1}{4r^3} \sin\left[\tan^{-1}\frac{\sqrt{z^2+x^2}}{y}\right] \cos\left[\tan^{-1}\frac{\sqrt{z^2+x^2}}{y}\right] \cos\left[\tan^{-1}\frac{x}{z}\right] \tag{8-32}$$

The mutual inductance is calculated using Eq(A-5) [Ch 3], and coupling coefficient is evaluated using Eq (3-5)

$$k_{xz} = \left(\frac{\sqrt{r_1 r_2}}{r}\right)^3 \left[\frac{3}{2}\sin\left[\tan^{-1}\left(\frac{\sqrt{z^2+x^2}}{y}\right)\right]\cos\left[\tan^{-1}\left(\frac{\sqrt{z^2+x^2}}{y}\right)\right]\left[\sin\left[\tan^{-1}\frac{x}{z}\right]\sin\theta_o\cos\Phi_o + \cos\left[\tan^{-1}\frac{x}{z}\right]\cos\theta_o\right] + \sin\theta_o\sin\Phi_o\left[\cos^2\left[\tan^{-1}\left(\frac{\sqrt{z^2+x^2}}{y}\right)\right] - \frac{1}{2}\sin^2\left[\tan^{-1}\left(\frac{\sqrt{z^2+x^2}}{y}\right)\right]\right]\right] \quad (8\text{-}33)$$

8.3.3 Coupling Coefficient between a Transmitter Coil in yz Plane and a Misaligned Receiver Coil

Similarly, the coupling coefficient between a transmitter coil in *yz plane* and a misaligned receiver coil is given by,

$$k_{yz} = \left(\frac{\sqrt{r_1 r_2}}{r}\right)^3 \left[\frac{3}{2}\sin\left[\tan^{-1}\left(\frac{\sqrt{y^2+z^2}}{x}\right)\right]\cos\left[\tan^{-1}\left(\frac{\sqrt{y^2+z^2}}{x}\right)\right]\left[\cos\left[\tan^{-1}\frac{z}{y}\right]\sin\theta_o\sin\Phi_o + \sin\left[\tan^{-1}\frac{z}{y}\right]\cos\theta_o\right] + \sin\theta_o\cos\Phi_o\left[\cos^2\left[\tan^{-1}\left(\frac{\sqrt{y^2+z^2}}{x}\right)\right] - \frac{1}{2}\sin^2\left[\tan^{-1}\left(\frac{\sqrt{y^2+z^2}}{x}\right)\right]\right]\right] \quad (8\text{-}34)$$

8.3.4 Simulation Results

The simulations are carried out for transmitter and receiver coils of radii 2cm each. The receiver coil is centered on z-axis and located at a distance of 10 cm from the transmitter. The simulations are carried out for three different cases as shown in Fig. 8.6.

It is observed that as the receiver coil rotates, the coupling between a single transmitter coil and the receiver coil may drop from maximum coupling to zero coupling. The advantage of using multiple transmitter coils is that one of the transmitter coils will always be coupled to the receiver coil and all power can be fed to that transmitter coil. For example in Fig. 8.6 (a) as the coil rotates, the coupling coefficient between the receiver and the transmitter coil in *xy plane*

decreases, while the coupling between the receiver coil and the transmitter coil in *yz plane* increases. Initially all the transmitter power is fed to the transmitter coil in *xy plane*. Beyond the tilt angle of 65 degrees, the transmitter coil in *yz plane* is more strongly coupled to the receiver coil and all the power is fed to it.

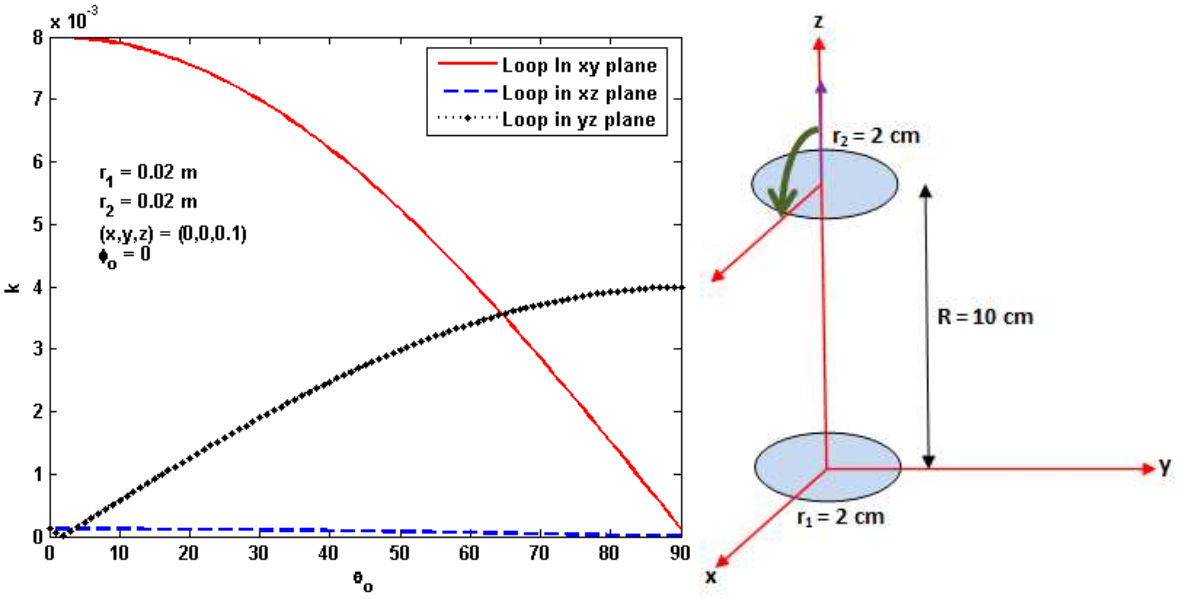

(a)

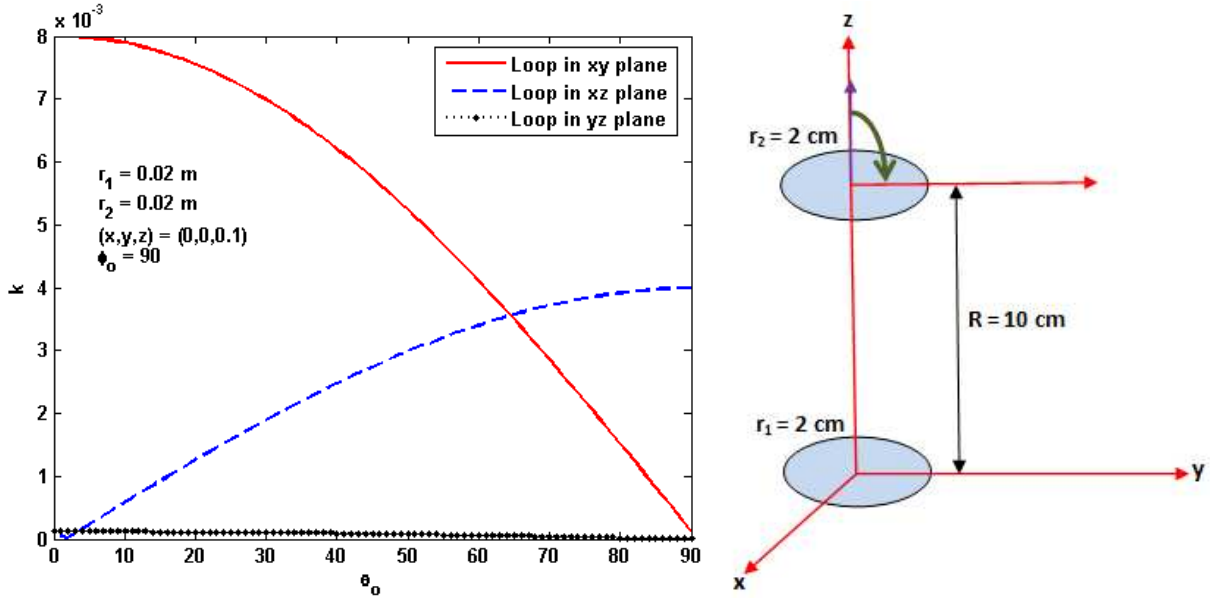

(b)

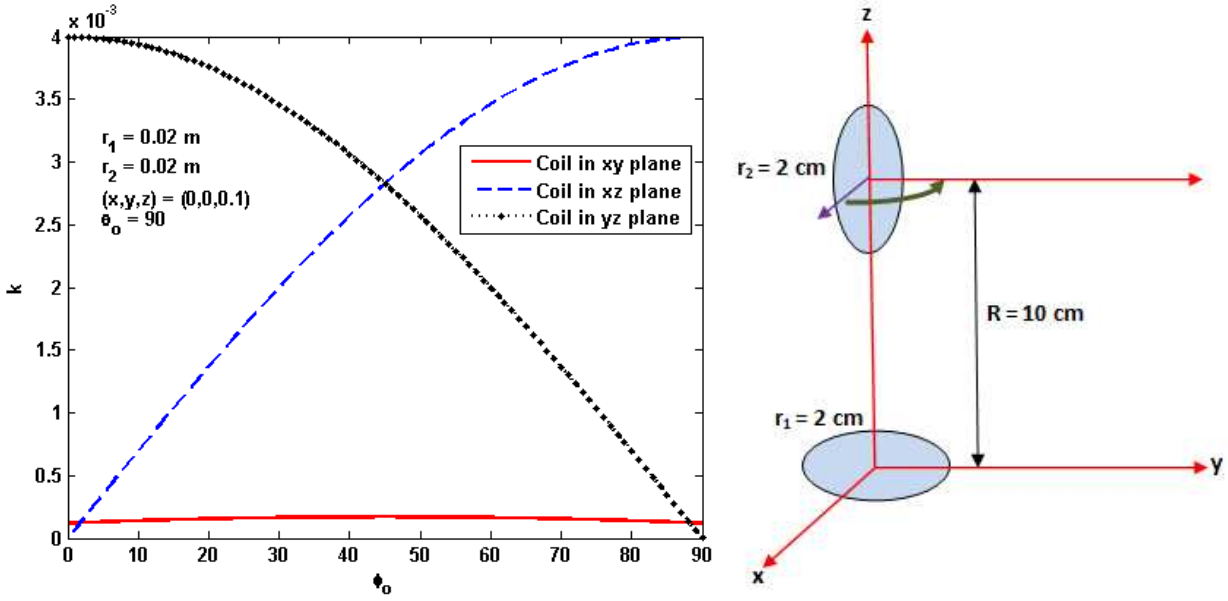

(c)

Fig. 8.6 kxy, kxz and kyz as the orientation of the receiver coil changes

8.4 TRANSMITTER COIL CONFIGURATION TO IMPROVE RCE OF A WPT SYSTEM CONSISTING OF A MISALIGNED RECEIVER COIL

A simple scenario involving two orthogonal transmitter coils in *xy and xz planes* respectively is considered. To setup the inductively coupled resonant loops, one must use capacitors to resonate with the self-inductance of both the coils in the transmitter and the coil at the receiver at the same resonant frequency $\omega_o = \frac{1}{\sqrt{L_1C_1}} = \frac{1}{\sqrt{L_2C_2}} = \frac{1}{\sqrt{L_3C_3}}$, as shown in Fig. 8.7 (a). The equivalent circuit model is shown in Fig. 8.7 (b). The transmitter coils are orthogonal and the mutual coupling between them is zero. Both the transmitter coils are coupled to the receiver coil. where, R_{S1}, R_{S2}, R_L are source and load resistances, R_{L1}, R_{L2}, R_{L3} are source and load coil resistances, M_{13} and M_{23} are mutual inductances between the first transmitter coil and the receiver coil, and the second transmitter coil and the receiver coil, respectively. The currents through the two transmitter coils and the receiver are i_1, i_2 and i_3 respectively.

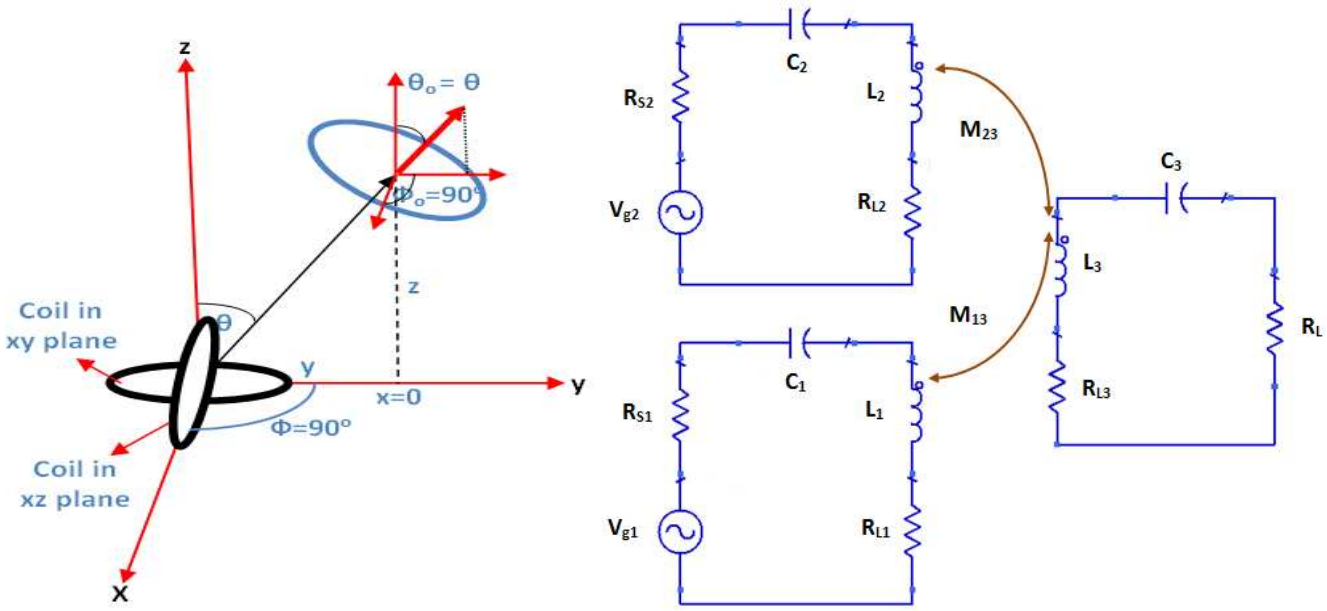

(a) (b)

Fig. 8.7 A transmitter consisting of orthogonal coils and its equivalent circuit model

Applying KVL to the three resonators,

$$\begin{cases} -v_{g1}+i_1R_{S1}+i_1R_{L1}-j\omega M_{13}i_3=0 \\ -v_{g2}+i_2R_{S2}+i_2R_{L2}-j\omega M_{23}i_3=0 \\ -j\omega M_{13}i_1-j\omega M_{23}i_2+i_3R_L+i_3R_{L3}=0 \end{cases} \Rightarrow \begin{bmatrix} R_{S1}+R_{L1} & 0 & -j\omega M_{13} \\ 0 & R_{S2}+R_{L2} & -j\omega M_{23} \\ -j\omega M_{13} & -j\omega M_{23} & R_L+R_{L3} \end{bmatrix} \begin{bmatrix} i_1 \\ i_2 \\ i_3 \end{bmatrix} = \begin{bmatrix} v_{g1} \\ v_{g2} \\ 0 \end{bmatrix} \quad (8\text{-}35)$$

If both the transmitter coils have the same parameters and the sources connected to the transmitter coils have the same source resistance i.e., $R_{L1} = R_{L2} = R_{Lt}$, $L_1 = L_2 = L_t$ and $R_{S1} = R_{S2} = R_S$, the received power can thus be written as a function of the quality factors,

$$\begin{aligned} P_r(\omega) = \frac{1}{2}\left|i_3^2\right| R_L = {} & P_{t1}\left[\frac{2\omega M_{13}}{(R_S+R_{Lt})(R_L+R_{L3})+\omega^2 M_{13}{}^2+\omega^2 M_{23}{}^2}\right]^2 R_{St}R_L + \\ & P_{t2}\left[\frac{2\omega M_{23}}{(R_S+R_{Lt})(R_L+R_{L3})+\omega^2 M_{13}{}^2+\omega^2 M_{23}{}^2}\right]^2 R_{St}R_L + \\ & \sqrt{P_{t1}P_{t2}}\left[\frac{2\sqrt{2}\omega}{(R_S+R_{Lt})(R_L+R_{L3})+\omega^2 M_{13}{}^2+\omega^2 M_{23}{}^2}\right]^2 M_{13}M_{23}R_{St}R_L + \end{aligned} \quad (8\text{-}36)$$

Applying the definition of quality factors to both the transmitting and receiving resonators, the received power eq (8-36) can be written as

$$P_r = P_{t1}\left(\frac{2}{1+k_{13}^2 Q_t Q_r + k_{23}^2 Q_t Q_r}\right)^2 k_{13}^2 Q_t Q_r \left(1-\frac{Q_t}{Q_{t,\text{int}}}\right)\left(1-\frac{Q_r}{Q_{r,\text{int}}}\right) +$$
$$P_{t2}\left(\frac{2}{1+k_{13}^2 Q_t Q_r + k_{23}^2 Q_t Q_r}\right)^2 k_{23}^2 Q_t Q_r \left(1-\frac{Q_t}{Q_{t,\text{int}}}\right)\left(1-\frac{Q_r}{Q_{r,\text{int}}}\right) +$$
$$2\sqrt{P_{t1}P_{t2}}\left(\frac{2}{1+k_{13}^2 Q_t Q_r + k_{23}^2 Q_t Q_r}\right)^2 k_{tr}^2 Q_t Q_r \left(1-\frac{Q_t}{Q_{t,\text{int}}}\right)\left(1-\frac{Q_r}{Q_{r,\text{int}}}\right)$$

where $Q_t = \frac{\omega_o L_t}{R_S + R_{Lt}}$, $Q_r = \frac{\omega_o L_r}{R_L + R_{Lr}}$, $Q_{t,\text{int}} = \frac{\omega_o L_t}{R_{Lt}}$, $Q_{r,\text{int}} = \frac{\omega_o L_r}{R_{Lr}}$ (8-37)

Q_t and Q_r are the loaded quality factors of the transmitter and the receiver; $Q_{t,\text{int}}$ and $Q_{r,\text{int}}$ are the intrinsic quality factors of the transmitting and the receiving antennas.

As show in Fig. 8.13, area vector of the receiver coil is in *yz plane* and is in same direction as its position vector. The power P_{t1} and P_{t2} fed to the transmitter $coil_1$ and $coil_2$ respectively are related to the total transmitter power P_t by

$$P_{t1} = \cos^2\alpha P_t \, , P_{t2} = \sin^2\alpha P_t \tag{8-38}$$

Substituting Eq (8-38) into (8-37),

$$P_r(\omega) = \left(\frac{2}{1+k_{13}{}^2 Q_1 Q_3 + k_{23}{}^2 Q_2 Q_3}\right)^2 Q_t Q_r \left(1-\frac{Q_t}{Q_{t,\text{int}}}\right)\left(1-\frac{Q_r}{Q_{r,\text{int}}}\right) P_t \left[k_{13}{}^2\cos^2\alpha + \sin^2\alpha k_{23}{}^2 + 2\cos\alpha\sin\alpha k_{13}k_{23}\right] \tag{8-39}$$

Consider the special case of the receiver coil in *yz plane* i.e., $x = 0, \phi_o = 90^o$, which is perfectly aligned with the position vector i.e., $\theta = \theta_o$, (8-27) and (8-33) simplify to

$$k_{xy} = \left(\frac{\sqrt{r_1 r_2}}{r}\right)^3 \cos\theta \tag{8-40}$$

$$k_{xz} = \left(\frac{\sqrt{r_1 r_2}}{r}\right)^3 \sin\theta \tag{8-41}$$

Substituting (8-40) and (8-41) into (8-39) and setting the first derivative of the received power with respect to α to zero, the maximum power transfer condition is given by,

$$\alpha = \theta \tag{8-42}$$

Hence instead of mechanically steering the transmitter coil to be aligned to receiver coil, the power ratio can be adjusted in the orthogonal transmitter coils which is equivalent to rotating a single transmitter coil to be in perfect alignment with the receiver coil.

CHAPTER 9

Conclusions

The near-field power transfer equation for inductively coupled resonant loops is derived and validated by experimental results. It has been demonstrated in the strong coupling case, for each distance there is an optimum impedance matching condition that maximizes the power transfer efficiency over this distance. In the weak coupling case the received power in the near-field system goes down inversely with the sixth power of distance and improves with increasing loaded Q at transmitter and receiver, i.e., improving matching at the source and the load side.

This work also presents the theoretical analysis of the capacity performance of an inductively coupled near-field communication system based on the derived near-field power transfer equation and the information theory. It is concluded that the capacity is limited respectively by thermal noise for low-Q receiver and natural interference for high-Q receiver. The capacity performance of an inductively coupled NFC link operating at VLF is evaluated. It is observed that higher operating frequency provides greater optimal capacity than that at a lower frequency in the air, but requires higher transmitter and receiver Q.

The theory of DAM for NFC link is presented, which shows its potential to break the dilemma of power and bandwidth trade-off in NFC systems with high-Q transmitters. Successful transmission of broadband binary modulation sequence is experimentally demonstrated on a DAM assisted NFC link, which implies an enhanced capacity performance of the NFC link over the traditional scheme.

The RCE limit is evaluated for a single transmitter and receiver. It is observed that

maximum efficiency is achieved under simultaneous matching at both the transmitter and the receiver. Further, the ratio of source resistance to source coil resistance is same as ratio of load to load coil resistance in order to transfer power most efficiently. Efficiency limit is then evaluated for two receivers and condition other than simultaneous match at source and loads leads to optimal efficiency. In particular, ratio of source resistance to source coil resistance should be same as ratio of load resistances to corresponding load coil resistances. Remarkably, it is also observed that efficiency limit improves as the number of receivers increases. Then, we considered the case of single and multiple repeaters between transmitter and receiver. We report that a repeater between transmitter and receiver improves the efficiency and can be used to extend the range of wireless power transfer.

Resonant coupling efficiency is limited by the product of quality factor and coupling coefficient. It is observed that a PEC platform reduces the Q value of coil, however a ferrite sheet can be inserted between the coil and platform to recover the same Q value as is in free space. Coupling coefficient decreases with inverse cube of distance between the coils for perfectly aligned coils, decreases from maximum coupling to no coupling as the angular misalignment of perfectly aligned coils increases, and for laterally displaced coplanar coils, the coupling coefficient is half that for perfectly aligned case separated by the same distance. In practical NFC systems, the transmitter and receiver coils can be angularly or laterally misaligned, thereby reducing the coupling between the coils and hence RCE. In this work, we propose a transmitter having three orthogonal coils. Depending upon the orientation of the receiver coil, power can be fed only to the transmitter coil which is best coupled to the receiver coil. Alternatively the ratio of power fed to three coils can be adjusted to rotate the magnetic field such that the coupling between transmitter and misaligned receiver is maximized.

Bibliography

[1] Andre Kurs, Aristeidis Karalis, Robert Moffatt, J. D. Joannopoulos, Peter Fisher and Marin Soljacic, "Wireless power transfer via strongly coupled magnetic resonances", *Science Express*, vol.317, no.5834, pp.83-86, July 2007.

[2] Aristeidis Karalis, J. D. Joannopoulos, and Marin Soljacic, "Efficient wireless non-radiative mid-range energy transfer", *Annals of Physics*, vol.323, no.1, pp.34-48, Jan. 2008.

[3] Thierry Bieler, Marc Perrottet, Valerie Nguyen, and Yves Perriard, "Contactless power and information transmission", *IEEE Transactions on Industry Applications*, vol. 38, no. 5, Sep/Oct. 2002.

[4] C.R. Neagu, H.V. Jansen, A. Smith, J.G.E. Gardeniers, and M.C. Elwenspoek, "Characterization of a planar microcoil for implantable microsystems", *A: Physical Sensors and Actuators*, vol. 62, no. 1-3, pp. 599-611, July 1997.

[5] Christian Peters and Yiannos Manoli, "Inductance calculation of planar multi-layer and multi-wire coils: An analytical approach", *A: Physical Sensors and Actuators*, vol. 145-146, pp. 394-404, Jul-Aug. 2008.

[6] T. Akin, B. Ziaie, K. Najafi, "RF telemetry powering and control of hermetically sealed integrated sensors and actuators", *IEEE Solid-State Sensor and Actuator Workshop*, pp. 145–148, June 1990.

[7] W.J. Heetderks, "RF powering of millimeter- and submillimeter- sized neural prosthetic implants", *IEEE Transactions* on *Biomedical Engineering*, vol. 35, no. 5, pp. 323-327, May 1988.

[8] S. Smith, T.B. Tang, J.T.M. Stevenson, B.W Flynn,. H.M. Reekie, A.F. Murray, A.M. Gundlach, D. Renshaw, B. Dhillon, A. Ohtori, Y. Inoue, and A.J. Walton, "Miniaturized drug delivery system with wireless power transfer and communication", *The Institution of Engineering and Technology Seminar on MEMS Sensors and Actuators*, pp. 155-162, Apr. 2006.

[9] W. Liu, K. Vichienchom, M. Clements, S.C. DeMarco, C. Hughes, E. McGucken, M.S. Humayun, E. De Juan, J.D. Weiland, and R. Greenberg, "A neuro-stimulus chip with telemetry unit for retinal prosthetic device", *IEEE Journal of Solid-State Circuits*, vol. 35, no. 10, pp. 1487-1497, Oct. 2000.

[10] K. Finkenzeller, *RFID Handbook, Fundamentals and Applications in Contactless Smart Cards and Identifications*, 2nd edition, John wiley & sons, Ch. 4, 2003.

[11] S. Esko, K. Jouni, P. Juha, Y. Arto and K. Ilkka, "Application of near field communication for health monitoring in daily life", *IEEE International Conference on Engineering in Medicine and Biology*, pp.3246-3249, Aug. 2006.

[12] H. G. Schantz, "A real time location system using near field electromagnetic ranging", *IEEE Antenna and Propagation Society International Symposium*, pp. 3792-3795, Jun. 2007.

[13] J. G. Bolger, F. A. Kirsten and L. S. Ng, "Inductive power coupling for an electric highway system", *IEEE Vehicular Technology Conference*, vol. 28, pp. 137-144, March 1978.

[14] John J. Sojdehei, Paul N. Wrathall and Donald F. Dinn, "Magneto-Inductive (MI) communications", *MTS/IEEE Conference and Exhibition: Oceans*, vol. 1, pp. 513-519, 2001.

[15] Zhi Sun, I.F. Akyildiz, "Magnetic induction communications for wireless underground sensor networks", *IEEE Transactions on Antennas and Propagation*, vol. 58, no. 7, pp. 2526-2435, July 2010.

[16] H. Schantz, "A near-field propagation law and a novel fundamental limit to antenna gain versus size", *IEEE Antenna & Propagation Society International Symposium*, vol. 3A, pp. 134-137, July 2005.

[17] Yong-Hae Kim, Seung-Youl Kang, Myung-Lae Lee, Byung-Gon Yu, Taehyoung Zyung, "Optimization of wireless power transmission through resonant coupling", *International Conference-Workshop on Compatibility and Power Electronics*, pp. 426-431, May 2009.

[18] A.P. Sample, D.A. Meyer, and J.R. Smith, "Analysis, experimental results, and range adaptation of magnetically coupled resonators for wireless power transfer", *IEEE Transactions on Industrial Electronics*, vol. 58, no. 2, pp. 544-554, Mar 2010.

[19] Mehdi Kiani, and Maysam Ghovanloo, "The circuit theory behind coupled-mode magnetic resonance-based wireless power transmission", *IEEE Transactions on Circuits and Systems*, vol. 59, no. 9, September 2012.

[20] Hengzhen Crystal Jing and Yuanxun Ethan Wang, "Capacity performance of an inductively coupled near field communication system", *IEEE International Symposium of Antenna and Propagation Society*, pp. 1-4, July 2008.

[21] Umar Azad, and Y.E. Wang, "Analysis and experimental results for an inductively coupled near-field power transmission system", *IEEE International Workshop on Antenna Technology (IWAT),* pp. 157-160, March 2012.

[22] Umar Azad, H.C. Jing, and Y.E. Wang, "Link budget and capacity performance of inductively coupled resonant loops", *IEEE Transactions on Antennas and Propagations,* vol. 60, no. 5, pp. 2453-2461, May 2012.

[23] C.E. Shannon, "A mathematical theory of communication", *The Bell System Technical Journal 27*, pp. 379-423, July 1948.

[24] E.L. Maxwell and D.L. Stone, "Natural Noise fields 1cps to 100kc", *IEEE Transactions on Antennas and Propagation*, vol. 11, no. 3, pp 339-43, May 1963.

[25] John Meloy, "What and where is the natural noise floor?", Aj6LS, Jan. 2003.

[26] J. I. Agbinya, "A magneto-inductive link budget for wireless power transfer and inductive communication systems," *Progress in Electromagnetics Research C*, vol. 37, pp. 15-28, 2013.

[27] Z. Sun and I. F. Akyildiz, "On capacity of magnetic induction-based wireless underground sensor networks," *in Proc. of IEEE Infocom*, Orlando, USA, March 2012.

[28] Mari Carmen Domingo, "Magnetic induction for underwater wireless communication networks", *IEEE Transactions on Antennas and Propagation,* vol. 60, no. 9, June 2012.

[29] Burhan Gulbahar, and Oagur B. Akan, "A communication theoretical modeling and analysis of under-water magneto-inductive wireless channels", *IEEE Transactions on Wireless Communications*, vol. 11, no. 9, September 2012.

[30] S. Kim, Y.E. Wang, "Theory of switched RF resonators", *IEEE Transactions on Circuits and Systems*, vol. 53, no. 12, pp 2521-2528, Dec. 2006.

[31] Xiaojing Xu, H. C. Jing and Y. E. Wang, "High speed pulse radiation from switched electrically small antennas", *IEEE Antenna and Propagation Symposium*, pp.167-170, July 2006.

[32] Xiaojing Xu and Y. E. Wang, "Wideband pulse transmission from switched electrically small antennas", *IEEE Radio and Wireless Symposium*, pp.483-486, January 2007.

[33] Xiaojing Xu and Y. E. Wang, "Beyond the efficiency bandwidth limit with switched electrically small antennas", *IEEE Antenna and Propagation Symposium*, pp.2261-2264, June 2007.

[34] *IEEE Standards for safety levels with respect to human exposure to radio frequency electromagnetic fields, 3 kHz to 300 GHz*, IEEE Standard C95.1, 1999.

[35] G. Lazzi, "Thermal effects of bioimplants", *IEEE Engineering in Medicine and Biology magazine*, vol. 24, no. 5, pp. 75-81, Sept. 2005.

[36] N. Shinohara, "Power without wires", *IEEE Microwave Magazine*, vol. 12, no. 7, Dec. 2011.

[37] JaeChun Lee, Sangwook Nam, "Fundamental aspects of near-field coupling small antennas for wireless power transfer", *IEEE Transactions on Antennas and Propagation*, vol. 58, no. 11, pp. 3442-3449, Nov. 2010.

[38] Qiaowei Yuan, Qiang Chen, Long Li, and K. Sawaya, "Numerical analysis on transmission efficiency of evanescent resonant coupling wireless power transfer system", *IEEE Transactions on Antennas and Propagation*, vol. 58, no. 5, pp. 1751-1758, May 2010.

[39] Tech ChuanBeh, T. Imura, M. Kat, and Y. Hori, "Basic study of improving efficiency of wireless power transfer via magnetic resonance coupling based on impedance matching", *IEEE International Symposium on Industrial Electronics*, pp. 2011-2016, July 2010.

[40] Jongmin Park, YoundoTak, Yoongoo Kim, Youngwook Kim, and Sangwook Nam, "Investigation of adaptive matching methods for near-Field wireless power transfer", *IEEE Transactions on Antennas and Propagation*, vol. 59, no. 5, pp. 1769.1773, May 2011.

[41] SanghoonCheon, Yong-Hae Kim, Seung-Youl Kang, MyungLae Lee, Jong-Moo Lee, TaehyoungZyung, "Circuit-model-based analysis of a wireless energy-transfer system via

coupled magnetic resonances", *IEEE Transactions on Industrial Electronics*, vol. 58, no. 7, pp. 2906-2914, July 2011.

[42] Thuc Phi Duang, Jong-Wook Lee, "Experimental results of high-efficiency resonant coupling wireless power transfer system using a variable couplingm", *IEEE Microwave and Components Wireless Letters*, vol. 21, no. 8, pp. 442-444, August 2011.

[43] M. Zargham, P.G. Gulak, "Maximum achievable efficiency in Near-field coupled power-transfer systems", *IEEE Transactions on Bio-Medical Circuits and Systems*, vol. 6, no. 3, pp 228-245, June 2012.

[44] B. Cannon, J. Hoburg, D. Stancil, and S. Goldstein, "Magnetic resonant coupling as potential means for wireless power transfer to multiple small receivers", *IEEE Transactions on Power Electronics*, vol. 24, no. 7, pp. 1819-1825, July 2009.

[45] W. Zhong, C. Lee, and R. Hui, "General Analysis on the Use of Tesla's Resonators in Domino Forms for Wireless Power Transfer", *IEEE Transactions on Industrial Electronics*, vol. 60, no. 1, pp. 261-270, Jan. 2013.

[46] C. Snow, "Mutual inductance of any two circles", *Bureau of Standards Journal of Research*, vol. 1, no. 4, pp. 531-542, Oct. 1928.

[47] F. C. Flack, E. D. James, and D. M. Schlapp, "Mutual inductance of air-cored coils: Effect on design of radio-frequency coupled implants", *Medical and Biological Engineering and Computing*, vol. 9, no. 2, pp. 79-85, 1971.

[48] S. Babic, C. Akyel, "Improvement in calculation of the self- and mutual inductance of thin-wall solenoids and disk coils", *IEEE Transaction on Magnetics*, vol. 36, no. 4, pp. 1970-1975, July 2000.

[49] C. Akyel, S. Babic, and S. Kincic, "New and fast procedures for calculating the mutual inductance of coaxial circular coils (disk coil-circular coil)", *IEEE Transactions on Magnetics*, vol. 38, no. 5, pp. 1367–1369, 2002.

[50] S. Babic, C. Akyel, and S. J. Salon, "New procedures for calculating the mutual inductance of the system: Filamentary circular coil-massive circular solenoid", *IEEE Transactions on Magnetics*, vol. 38, no. 5, pp. 1131–1134, 2003.

[51] J. T. Conway, "Inductance calculations for noncoaxial coils using bessel functions", *IEEE Transactions on Magnetics*, vol. 43, no. 3, pp. 1023– 1034, Mar. 2007.

[52] J. T Conway, “Noncoaxial inductance calculations without the vector potential for axisymmetric coils and planar coils”, *IEEE Transactions on Magnetics*, vol. 44, no. 4, pp. 453–462, Apr. 2008.

[53] R.S. Elliott, “The history of electromagnetics as Hertz would have known it”, *IEEE Transactions on Microwave Theory and Techniques*, vol. 36, no. 5, pp. 806-823, May 1988.

[54] H. Hertz, *Dictionary of scientific biography*, vol. 6, New York: Scribner, pp. 340-349.

[55] D. Schneider, “Wireless power at a distance is still far away”, *IEEE Spectrum*, vol. 47, no. 5, pp. 34-39, May 2010.

[56] John J. O’Neill, *Prodigal genius – the life of Nikola Tesla*, New York: Washburn, 1944.

[57] W.C. Brown, “The history of power transmission by radio waves”, *IEEE Transactions on Microwave Theory and Techniques*, vol. 32, no. 9, pp. 1230-1242, Sep. 1984.

[58] James O. McSpadden, John C. Mankins, “Space solar power programs and microwave wireless power transmission technology”, *IEEE Microwave Magazine*, vol. 3, no. 4, pp. 46-57, Dec. 2002.

[59] Constantine A. Balanis, *Antenna Theory: Analysis and Design*, 2nd edition, John Wiley & Sons, pp. 204-208.

[60] Christian Peters and Yiannos Manoli, “Inductance calculation of planar multi-layer and multi-wire coils: An analytical approach” , *International Conference on Sensors and Actuators*, vol. 145-146, pp. 394-404, July-August 2008.

[61] Frederick Emmons Terman, *Radio Engineers Handbook*, 1st edition, McGraw Hill, NY, pp. 65-73, 1932.

[62] J.H. Morecroft, *Principles of Radio Communication*, 3rd edition, John Wiley & Sons, NY, pp. 235-239, 1933.

[63] William R. Smythe, *Static and Dynamic Electricity*, 2nd edition, McGraw Hill, NY, pp. 270-271, 1950.

[64] Ki-Bong Kim, E. Levi, Z. Zabar, L. Birenbaum, "Mutual inductance of noncoaxial circular coils with constant current density" , *IEEE Transaction on Magnetics*, vol. 33, no. 5, pp. 4303-4309, Sep. 1997.

[65] Roger F. Harrington, *Time-Harmonic Electromagnetic Fields*, John Wiley & Sons, NY, 2001.

[66] David M. Pozar, *Microwave Engineering*, 3rd Edition, New York: John Wiley and Sons, pp77-79.

[67] Matthew N.O. Sadiku, *Elements of Electromagnetics*, 4th edition, Oxford university press, pp. 350-351.